EFFECT OF TRANSVERSE ISOTROPY ON TIME DEPENDENT PROPERTIES OF MAHA SARAKHAM SALT

KANYA KRAIPRU

A Thesis Submitted in Partial Fulfillment of the Requirements for the Degree of
Doctor of Philosophy in Civil, Transportation and Geo-resources Engineering
Suranaree University of Technology
Academic Year 2023

ผลกระทบของทรานซ์เวอร์สไอโซทรอปีต่อสมบัติที่ขึ้นกับเวลาของเกลือหินชุดมหาสารคาม

นางสาวกัญญา ไกรปรุ

วิทยานิพนธ์นี้เป็นส่วนหนึ่งของการศึกษาตามหลักสูตรปริญญาวิศวกรรมศาสตรดุษฎีบัณฑิต
สาขาวิชาวิศวกรรมโยธา ขนส่ง และทรัพยากรธรณี
มหาวิทยาลัยเทคโนโลยีสุรนารี
ปีการศึกษา 2566

EFFECT OF TRANSVERSE ISOTROPY ON TIME DEPENDENT PROPERTIES OF MAHA SARAKHAM SALT

Suranaree University of Technology has approved this thesis submitted in partial fulfillment of the requirements for the Degree of Doctor of Philosophy.

Thesis Examining Committee

.....

(Assoc. Prof. Dr. Pornkasem Jongpradist)
Chairperson

.....

(Dr. Thanittha Thongprapha)
Member (Thesis Advisor)

.....

(Emeritus Prof. Dr. Kittitep Fuenkajorn)
Member

.....

(Asst. Prof. Dr. Prachya Tepnarong)
Member

.....

(Asst. Prof. Dr. Decho Phueakphum)
Member

.....

(Assoc. Prof. Dr. Yupaporn Ruksakulpiwat)
Vice Rector for Academic Affairs and Quality Assurance

.....

(Assoc. Prof. Dr. Pornsiri Jongkol)
Dean of Institute of Engineering

กัญญา ไกรปรุ : ผลกระทบของทรานซ์เวอร์สไอโซทรอปีต่อสมบัติที่ขึ้นกับเวลาของเกลือหินชุดมหาสารคาม (EFFECT OF TRANSVERSE ISOTROPY ON TIME DEPENDENT PROPERTIES OF MAHA SARAKHAM SALT)
อาจารย์ที่ปรึกษา : อาจารย์ ดร.ธนิษฐา ทองประภา, 147 หน้า.

คำสำคัญ: การคืบช่วงทรานส์เชียนต์/ การคืบช่วงคงตัว/ ความหนืดเชิงพลาสติก/ แบบจำลองเบอเกอร์/ ไอโซทรอปิก

วัตถุประสงค์ของการศึกษานี้ คือ เพื่อหาผลกระทบของทรานซ์เวอร์สไอโซทรอปีต่อการเปลี่ยนแปลงรูปร่างเชิงเวลาของเกลือหินชุดมหาสารคาม การทดสอบการคืบแบบแกนเดียวและแบบสามแกนได้ถูกดำเนินการบนตัวอย่างทรงปริซึมขนาด 54x54x108 ลูกบาศก์มิลลิเมตร ที่มีมุมระหว่างแนวตั้งฉากของระนาบชั้นหิน (ทรานซ์เวอร์สไอโซทรอปี) กับแนวแกนหลักแตกต่างกัน (β) ภายในระยะเวลาทดสอบ 10 วัน ผลการทดสอบระบุว่าการเปลี่ยนแปลงรูปร่างแบบทันทีทันใดและแบบคืบมีค่าสูงสุดเมื่อมุม β เท่ากับ 0 องศา และมีค่าต่ำสุดเมื่อมุม β เท่ากับ 90 องศา ความแตกต่างเหล่านี้มีค่าลดลงเมื่อความดันล้อมรอบเพิ่มขึ้น ตัวอย่างเกลือหินที่มีมุมทรานซ์เวอร์สไอโซทรอปีต่ำจะแสดงการคืบช่วงทรานส์เชียนต์มาก ก่อนการเข้าสู่ช่วงคงตัว เมื่อเปรียบเทียบกับตัวอย่างเกลือหินที่มีมุมทรานซ์เวอร์สไอโซทรอปีสูงกว่า ผลกระทบของความดันล้อมรอบและทรานซ์เวอร์สไอโซทรอปีสามารถอธิบายได้ด้วยพารามิเตอร์ของเบอเกอร์ ระดับแอนไอโซทรอปีของพารามิเตอร์ของเบอเกอร์มีค่าลดลงเมื่อความดันล้อมรอบเพิ่มขึ้น กล่าวได้ว่าเกลือหินไม่เพียงมีความเป็นไอโซโทรปีมากขึ้นแต่ยังแสดงพฤติกรรมแบบแมกซ์เวลล์ภายใต้ความดันล้อมรอบสูง สมการเชิงประจักษ์ถูกสร้างขึ้นเพื่อแสดงพารามิเตอร์ของเบอเกอร์ในฟังก์ชันของการวางตัวของระนาบชั้นหิน ระยะเวลาของการให้แรง ความเค้นเฉือนรวมหกด้านที่ถูกใช้และความดันล้อมรอบ ซึ่งสามารถใช้กับการคืบของเกลือหินภายใต้สภาวะจริงได้

สาขาวิชา เทคโนโลยีธรณี
ปีการศึกษา 2566

ลายมือชื่อนักศึกษา .....กัญญา.....
ลายมือชื่ออาจารย์ที่ปรึกษา .....

KANYA KRAIPRU: EFFECT OF TRANSVERSE ISOTROPY ON TIME DEPENDENT PROPERTIES OF MAHA SARAKHAM SALT. THESIS ADVISOR: THANITTHA THONGPRAPHA, Ph.D., 147 PP.

Keyword: Transient creep/ Steady-state creep/ Visco-plastic/ Burgers model/ Isotropic

The objective of this study is to determine the effect of transverse isotropy on time-dependent deformation of bedded Maha Sarakham salt. Uniaxial and triaxial creep tests are performed on prismatic specimens (54×54×100 mm^3) having normal to bedding plane making various (transverse isotropic) angles (β) with the major principal direction within the test duration of 10 days. Results indicate that instantaneous and creep deformations are highest for $\beta = 0°$ and lowest at $\beta = 90°$. Their differences become smaller as the confining pressure increases. Salt specimens with lower transverse isotropic angles show larger transient creep before reaching steady-state phase, as compared to those with higher angles. The effect of confining pressure and transverse isotropy can be described by Burgers parameters. The anisotropy degrees of the Burgers parameters decrease with increasing confining pressures, suggesting that salt not only becomes more isotropic, but also behaves as Maxwell material under high confinements. Empirical equations are derived to represent the Burgers parameters as a function of bedding plane orientation, loading duration, applied octahedral shear stress and confining pressure, which can be used to describe salt creep under in-situ conditions.

School of Geotechnology
Academic Year 2023

Student's Signature .....
Advisor's Signature .....

ACKNOWLEDGEMENT

I wish to acknowledge the funding supported by Royal Golden Jubilee Ph.D. scholarship awarded by the Thailand Research Fund under the office of the Prime Minister, the Royal Thai Government.

I would like to express my sincere thanks to Dr. Thanittha Thongprapha for her valuable guidance and efficient supervision. I appreciate her strong support, encouragement, suggestions and comments during the research period. My heartiness thanks to Assoc. Prof. Dr. Pornkasem Jongpradist, Emeritus Prof. Dr. Kittitep Fuenkajorn, Asst. Prof. Dr. Prachya Tepnarong and Asst. Prof. Dr. Decho Phueakphum for their constructive advice, valuable suggestions and comments on my research works as thesis committee members. Grateful thanks are given to all staffs of Geomechanics Research Unit, Institute of Engineering who supported my work.

Finally, I most gratefully acknowledge my parents for all their support and encouragement throughout the period of this study.

KANYA KRAIPRU

TABLE OF CONTENTS

Page

TABLE OF CONTENTS (Continued)

Page

TABLE OF CONTENTS (Continued)

Page

LIST OF TABLES

Table **Page**

LIST OF FIGURES

Figure **Page**

LIST OF FIGURES (Continued)

Figure **Page**

LIST OF FIGURES (Continued)

Figure **Page**

LIST OF FIGURES (Continued)

Figure **Page**

SYMBOLS AND ABBREVIATIONS

β	=	The angle between the normal of bedding planes and the major principal stress
τ_{oct}	=	Octahedral shear stress
σ_1	=	Major principal stresses
$\sigma_2 = \sigma_3$	=	Minor principal stresses
E_x	=	Elastic moduli in x-direction (lateral)
E_y	=	Elastic moduli in y-direction (axial)
E_z	=	Elastic moduli in z-direction (lateral)
ν_{xy}	=	Poisson's ratios in x-y coordinate system
ν_{yz}	=	Poisson's ratios in y-z coordinate system
ν_{xz}	=	Poisson's ratios in x-z coordinate system
G_{xy}	=	Shear modulus in x-y coordinate system
G_{yz}	=	Shear modulus in y-z coordinate system
G_{xz}	=	Shear modulus in x-z coordinate system
ε_1	=	Axial strain
ε_{3P}	=	Strains measured parallel to the strike of bedding planes
ε_{3O}	=	Strains measured normal to the strike of bedding planes
s	=	Mean stresses
s_i	=	Stress deviations along principal axes
e	=	Mean strains
e_i	=	Strain deviations
E_I	=	Elastic modulus
E_V	=	Spring constant in transient phase
η_v	=	Viscosity coefficient in steady-state phase
η_P	=	Viscosity coefficient in steady-state phase
$E_{I,1}$	=	Elastic modulus in axial direction
$E_{V,1}$	=	Spring constant in transient phase in axial direction
$\eta_{v,1}$	=	Viscosity coefficient in steady-state phase in axial direction

SYMBOLS AND ABBREVIATIONS (Continued)

$\eta_{P,1}$	=	Viscosity coefficient in steady-state phase in axial direction
$E_{I.3O}$	=	Elastic modulus normal to bedding plane strike direction (lateral)
$E_{V,3O}$	=	Spring constant in transient phase normal to bedding plane strike direction (lateral)
$\eta_{v,3O}$	=	Viscosity coefficient in steady-state phase normal to bedding plane strike direction (lateral)
$\eta_{P,3O}$	=	Viscosity coefficient in steady-state phase normal to bedding plane strike direction (lateral)
$E_{I.3P}$	=	Elastic modulus parallel to bedding plane strike direction (lateral)
$E_{V,3P}$	=	Spring constant in transient phase parallel to bedding plane strike direction (lateral)
$\eta_{v,3P}$	=	Viscosity coefficient in steady-state phase parallel to bedding plane strike direction (lateral)
$\eta_{P,3P}$	=	Viscosity coefficient in steady-state phase parallel to bedding plane strike direction (lateral)
t	=	Testing time
$e_1(t)$	=	Strain deviations as a function of time along the major principal stress
$e_O(t)$	=	Strain deviations as a function of time along the minor principal axes normal to bedding planes
$e_P(t)$	=	Strain deviations as a function of time along the minor principal axes parallel to bedding planes
$E_{I,\ 0°}$	=	Elastic modulus from specimens with β = 0°
$E_{I,\ 90°}$	=	Elastic modulus from specimens with β = 90°
$\eta_{P,\ 0°}$	=	Viscosity coefficient in steady-state phase from specimens with β = 0°
$\eta_{P,\ 90°}$	=	Viscosity coefficient in steady-state phase from specimens with β = 90°

SYMBOLS AND ABBREVIATIONS (Continued)

$E_V^*{}_{,0°}$	=	Viscoelastic phase from specimens with β = 0°
$E_V^*{}_{,0°}$	=	Viscoelastic phase from specimens with β = 90°
ε_v	=	Volumetric strains
$\gamma_{oct,\,V}$	=	Octahedral shear strains at the transition point from instantaneous phase into transient phase
$\gamma_{oct,\,P}$	=	Octahedral shear strains at the transition point from transient phase into steady-state creep phase
$\overline{\gamma}_{oct}$	=	Range of transient creep phase
$\overline{\gamma}_{oct,0^\circ}$	=	Range of transient creep phase for β = 0°
$\overline{\gamma}_{oct,90^\circ}$	=	Range of transient creep phase for β = 90°

CHAPTER I
INTRODUCTION

1.1 Background and rationale

Time-dependent properties of rock salt are major factors which has to be taken into consideration in the design and stability analysis of underground structures. The major research efforts, particularly, in the US and European countries, are aimed at developing safe storage facility in rock salt for nuclear waste disposal (e.g., Hunter, 1979; Senseny et al., 1992; Munson, 1997; Hunsche and Hampel, 1999; Langer, 1999), for energy storage (e.g. Langer, 1993; Staudtmeister and Rokahr, 1997; Ehgartner and Sobolik, 2006; Wang et al., 2016; Khaledi et al., 2016; Wang et al., 2018), and for salt and potash mines (e.g., Holcomb and Hannum, 1982; Dawson and Munson, 1983; Jeramic, 1994; Daemen and Fuenkajorn, 1996; Hansen, 1997; Khamrat et al., 2018). Several investigators have focused their efforts on the strength, deformation characteristics and creep properties of rock salt (e.g. Sriapai et al., 2011; Zhang et al., 2012; Fuenkajorn et al., 2012; Sartkaew and Fuenkajorn, 2013; Aditya et al., 2018; Phatthaisong et al., 2018). Results from studying creep properties of salt rock show that creep is complicated and related to the loading (Hamami et al., 1999; Fuenkajorn and Phueakphum, 2010), loading rate (Liang et al., 2011), temperature (Senseny, 1986; Moslehy and Alshibli, 2023; Dong et al., 2023), stress level and loading path (Hampel et al., 1998; Wang et al., 2014; Mansouri and Ajalloeian, 2018; Rouabhi et al., 2019). Several constitutive creep models have been derived to describe the time-dependent behavior of rock salt under various environmental conditions (e.g. confining pressures, loading rates, temperatures and moisture contents). These include rheological models (Lindner and Brady, 1984; Hardy and Sun, 1986; Wang et al., 2014), empirical models (Nair et al., 1974; Langer, 1984; Motta and Pinto, 2014), and physical theory models (Oksenkrug and Shafarenko, 1974; Senseny, 1983).

Rock salt in the northeast of Thailand and associated mineral deposits in the Maha Sarakham formation are widely spread in enormous quantities. Most of rock salt exhibits transverse isotropic structures due to the layers of crystallization and

inclusions (e.g. anhydrite, potash, gypsum and clay minerals) (Warren, 1999). The properties of rock salt depend not only on the factors mentioned above but also on the transverse isotropic characteristics (Dubey et al., 1999; Dubey and Gairola, 2000, 2008; Dubey, 2018). Jeremic (1994) reports that rock salt from Poland shows the transverse isotropic effect on uniaxial compressive strength where the minimum strength is obtained when normal to bedding plane makes an angle (β) of 45° with the loading direction. Thongprapha et al. (2022) find that the minimum compressive strength of salt from Thailand is obtained when β is 60° under confining pressures from 2 to 40 MPa. The intrinsic elastic moduli are highest when loading is parallel to bedding plane ($\beta = 90°$), and lowest when it is normal to the beds ($\beta = 0°$). The apparent elastic moduli and Poisson's ratios for $0° < \beta < 90°$ can be described by Amadei's solution (Amadei, 1996). The solution has been widely applied to describe the evolution of the apparent elastic moduli and Poisson's ratios for other strong and brittle rocks (e.g. Nasseri et al., 2003; Miller et al., 2013; Gholami and Rasouli, 2014; Nejati et al., 2019).

The effect of transverse isotropy on salt creep has however rarely been investigated. Dubey and Gairola (2008) perform uniaxial creep tests on transverse isotropic salt from India under three bedding orientations (0°, 45°, and 90°), and find that steady-state creep rate is highest when $\beta = 45°$ and lowest for $\beta = 0°$. Most salt researchers have studied the effect of transverse isotropy on salt only under unconfined condition. In addition, governing equations for describing the salt creep as affected by transverse isotropic characteristics have never been derived for practical use.

1.2 Research objectives

The objective of this study is to experimentally investigate the effect of transverse isotropy on time-dependent properties of Maha Sarakham salt. The tasks involve performing uniaxial and triaxial creep tests on prismatic salt specimens containing various bedding plane orientations with respect to the major principal axis. The elastic, visco-plastic and visco-elastic parameters are calibrated from these results by using stress-strain deviations as a function of time based on the Burgers model. The governing equations are proposed to describe creep deformation of transverse

isotropic medium. The findings can be used to predict the salt behavior with bedding plane orientation, confining pressure and octahedral shear stress.

1.3 Research methodology

The research methodology of this study comprises 8 steps, including 1) literature review, 2) preparation of salt sample, 3) laboratory testing methods and results (uniaxial and triaxial creep test), 4) determination of creep parameters under transversely isotropic condition, 5) derivation of governing equations to describe creep deformation of transverse isotropic medium, 6) discussions and conclusions, and 7) thesis writing, as shown in Figure 1.1.

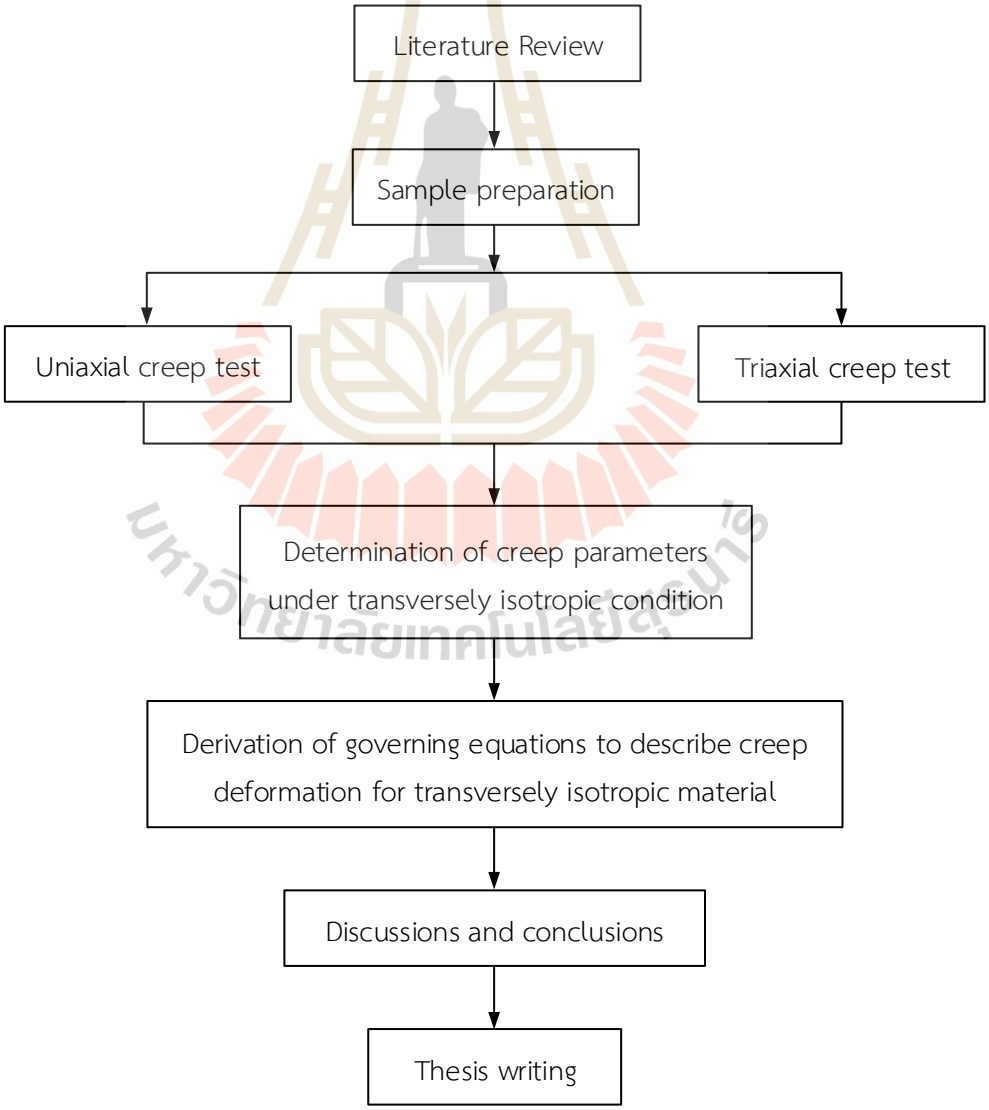

Figure 1.1 Methodology of this research.

1.3.1 Literature review

Literature review is carried out to study previous research on the occurrence and characteristics of transversely isotropic on rock salt, time-dependent testing, and the transverse isotropic effect on the properties of rocks, especially those related to time-dependent behavior and creep behavior analysis of transverse isotropic medium. Journals, conference papers, and technical reports are the sources of information. The literature review is summarized as given in Chapter II thesis.

1.3.2 Sample preparation

Rock salt samples have been obtained from Thaikali Co., Ltd., underground openings in the northeast of Thailand. They are part of the Lower Salt member of the Maha Sarakham formation. Sample preparation is carried out at Suranaree University of Technology laboratory. The specimens are prepared to obtain rectangular blocks with nominal dimensions of 54×54×108 mm^3 (L/D=2). Each sample contained salt beds that can be observed by alteration of dark and light bands of halite. Salt specimens are prepared with nominal angles (β) between specimen main axis and the normal to bedding planes varying from 0°, 45°, 65°, 75° and 90° for uniaxial creep test and varying from 0°, 25°, 45°, 65° and 90° for triaxial creep test.

1.3.3 Laboratory testing methods and results

Uniaxial and triaxial creep tests are conducted following ASTM D7070-08 standard practice on rock salt specimens, except the specimen shape. Five specimens are performed the uniaxial creep test under applied constant axial stress (σ_1) of 10 MPa. The total of 17 specimens are performed the triaxial creep test under constant octahedral shear stress (τ_{oct}) of 9 MPa, varying confining pressures (lateral stresses) range from 3, 6, 12 and 24 MPa. All specimens are tested for up to 10 days. The axial and lateral deformations are measured by installed digital displacement gages. The time-related deformations are recorded. The results can be used to determine the creep strains of rock salt with various bedding plane orientations from uniaxial and triaxial creep tests.

1.3.4 Determination of creep parameters under transversely isotropic condition

The relations of stress-strain deviation as a function of time are derived from the constitutive relation under linear-viscoelastic conditions. The elastic, visco-

elastic and visco-plastic parameters are calibrated from uniaxial and triaxial creep test results using these relations. Assuming the salt behavior here can be described by the Burgers model. The regression analysis is conducted utilizing the SPSS statistical software (Wendai, 2000). These Burger parameters exhibit the effect of transverse isotropy on creep behavior. The effect of confining pressure and transverse isotropy on these parameters is described by elliptical theory.

1.3.5 Derivation of governing equations to describe creep deformation of transverse isotropic medium

The relations between octahedral shear strain and volumetric strain are used to describe the transition zone of salt creep behavior (transient creep phase) between instantaneous and steady state phases under different bedding plane orientations. The governing equations are proposed to predict the evolution of transient zones with bedding plane orientation, confining pressure and octahedral shear stress. The condition at which salt becomes isotropic and changes behavior are determined.

1.3.6 Discussions and conclusions

The adequacy and reliability of the test data including the correctness of the interpretation and analysis are described in discussions. The results obtained here and those obtained elsewhere are compared to analyze in terms of similarity and discrepancy. Conclusions from the research study are drawn to summarize the overall of this research. Future research needs are identified to confirm the validity and enhance comprehension.

1.3.7 Thesis Writing

All study activities, methods, and results are documented and compiled in the thesis.

1.4 Scope and limitations

1) Uniaxial and triaxial creep tests are performed on rock salt specimens obtained from the Maha Sarakham formation. (Thaikali Co., Ltd., northeast of Thailand)

2) All specimens are prepared to have different bedding plane orientations including normal, parallel and incline to the major principal stress.

3) The rock salt specimen for uniaxial creep test are prepared to obtain nominal dimensions of rectangular specimens are 54×54×108 mm^3 with bedding plane orientation respect to the major principal stress (β) of 0°, 45°, 65°, 75° and90°. For triaxial creep test, β angles varying from 0°, 25°, 45°, 65° and 90°.

4) Uniaxial creep tests are performed under applied constant axial stress of 10 MPa for 10 days.

5) Triaxial creep tests are performed under constant octahedral stress (γ_{oct}) of 9 MPa with varying confining pressures (lateral stresses) range from 3, 6, 12 and 24 MPa.

6) Testing procedure will follow the relevant ASTM standard practice, as much as, practical.

7) All tests are performed under ambient temperature (°C).

8) The research findings are published in international journal.

1.5 Thesis contents

This thesis comprises eight chapters. Chapter 1 explains the background and rationale, the objectives, the methodology and scope and limitations of the research. Chapter 2 summarizes the literature review results to enhance the comprehension on the transversely isotropic rock and time-dependent properties of rocks. Chapter 3 describes the preparation of salt sample. Chapter 4 describes the procedure and results of the laboratory testing (uniaxial and triaxial creep testing). Chapter 5 shows the derivation of stress-strain deviations as a function of time and calibrations of Burgers parameters. Chapter 6 describes the transverse isotropic effect on time-dependent properties of rock salt under confinement. Chapter 7 presents the derivation of governing equations to describe and predict the creep behavior under transverse isotropic medium. Chapter 8 gives the discussions, conclusions, and recommendations for future studies.

CHAPTER II
LITERATURE REVIEW

2.1 Introduction

Previous studies are reviewed to enhance an understanding of the relationship between transverse isotropic rock and time-dependent properties of rock. These include the rock characteristics, time-dependent behavior of Maha Sarakham salt and transverse isotropic effect on time-dependent properties. The constitutive models used to describe the time-dependent behavior of transverse isotropic rock are investigated.

2.2 Definition of rock characteristics

The definition characteristic under linear elasticity yields is described by the relation of strains in terms of the stresses that inverts from the generalized Hook's law in cartesian coordinate (x, y, z). The anisotropic elasticity equations can be presented in matrix form called **compliance matrix**, as shown in Equation (2.1). The component of strains depends on the component of stresses. The new notation has only one subscript for the strain and stress by numbered from 1 to 6. The 36 S_{ij} are material constants called **stiffness component**. When considering the strain energy in an elastic material, the stiffness matrix is symmetry. There are only 21 independent elastic constants.

2.2.1 Isotropic rock

Isotropic rock has the same rock properties (such as strength, stiffness) in all directions, as shown in Figure 2.1a. There are two independent constants and 12 nonzero terms in compliance matrix in the terms of Young's moduli (E), Poisson's ratio (ν) and shear moduli (G). The Young's moduli and Poisson's ratio in different directions are equal ($E_x = E_y = E_z$ and $\nu_{xy}=\nu_{yz}=\nu_{xz}$) and shear moduli are calculated by these single E and ν values ($G_{xy} = G_{yz} = G_{xz}$). Barla (1974) states that this behavior cannot describe the exact stresses and deformations in a rock mass.

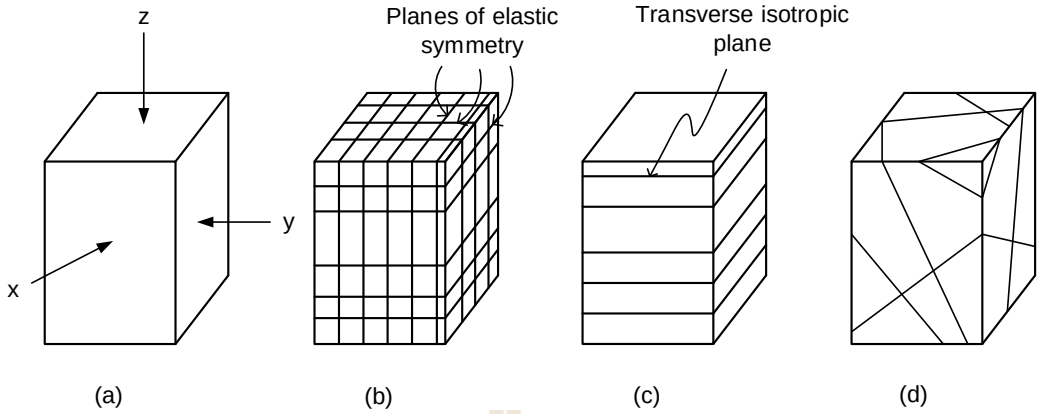

Figure 2.1 Illustration of rock characteristics: Isotropic (a), Transverse isotropic (b), Orthotropic (c), Completely anisotropic (d) rocks (Harrison and Hudson, 2000).

$$\begin{bmatrix} \varepsilon_x \\ \varepsilon_y \\ \varepsilon_z \\ \varepsilon_{yz} \\ \varepsilon_{xz} \\ \varepsilon_{xy} \end{bmatrix} = \begin{bmatrix} \frac{1}{E_x} & \frac{-\nu_{xy}}{E_y} & \frac{-\nu_{xz}}{E_z} & 0 & 0 & 0 \\ \frac{-\nu_{yx}}{E_x} & \frac{1}{E_y} & \frac{-\nu_{yz}}{E_z} & 0 & 0 & 0 \\ \frac{-\nu_{zx}}{E_x} & \frac{-\nu_{zy}}{E_y} & \frac{1}{E_z} & 0 & 0 & 0 \\ & & & \frac{1}{2G_{yz}} & 0 & 0 \\ & & & & \frac{1}{2G_{xz}} & 0 \\ & & & & & \frac{1}{2G_{xy}} \end{bmatrix} \begin{bmatrix} \sigma_x \\ \sigma_y \\ \sigma_z \\ \sigma_{yz} \\ \sigma_{xz} \\ \sigma_{xy} \end{bmatrix} \quad (2.1)$$

2.2.2 Anisotropic rock

Many rocks near the Earth's surface exhibit distinct fabric elements, such as stratification, bedding, layering, jointing, foliation, or fissuring, leading to a variation of anisotropic rock properties.

Amadei (1996) states that cleavage and foliation are the characteristics of anisotropic rock in the metamorphic rocks such as schist, phyllites, gneisses and slates. Slates and phyllites have closely spaced fractures called cleavages that are formed by parallel orientated microscopic grains of chlorite, mica or another platy mineral cause split into planes. The fabric of schists is formed by the sub-parallel to parallel arrangement of large platy minerals such as chlorite, mica and talc. Foliated metamorphic rocks such as in gneisses express the foliation that alternating layers of different mineral composition. Non-foliated metamorphic rocks such as marble, the orientation of calcite grains also shows some anisotropy. The intact laminated, stratified, bedded and layered rock are the characteristics of anisotropy in sedimentary rock such as sandstones, siltstones, shales, coal and limestones. In addition, the anisotropic rock mass can be found in volcanic formations such as basalt and tuff.

Rock masses that are discontinuous and intersected by one or multiple spaced joint sets also exhibit anisotropic behavior. In the most practical case, orthotropic and transverse isotropic materials are the patterns of anisotropic rocks, as in a co-ordinate system that attach to directions of symmetry or their apparent structure.

(1) Orthotropic rock

Orthotropy (ortho-rhombic symmetry) has three mutually perpendicular fracture sets as shown in Figure 2.1b. The properties along each three principal directions are different. There are only 9 independent elastic constants: three elastic moduli (E_x, E_y, E_z), three Poisson's ratios (ν_{xy}, ν_{xz}, ν_{yz}) and three shear moduli (G_{xy}, G_{xz}, G_{yz}). The orthotropic formulation used to describe the deformability of rocks has three mutually perpendicular sets of joints in the principal symmetry direction (Goodman, 1989). For example, the rocks that have orthotropic behavior are slates, schists, sandstones, coal, gneisses and granites, assuming the bedding planes and cleat of coal often be planes of elastic symmetry.

(2) Transverse isotropic rock

Transverse isotropic rock has an axis of symmetry of rotation in z-fold (normal to the bedding planes). Let x and y are two perpendicular directions in the plane normal to the axis of symmetry (bedding plane). This plane has isotropic properties that called transverse isotropic plane as shown in Figure 2.1c. The properties

are the same in this plane but different perpendicular to the plane. Transverse isotropy has only 5 independent elastic constants: two elastic moduli ($E_x = E_y$, E_z), two Poisson's ratios ($\nu_{xy} = \nu_{yz}$, ν_{xz}) and one shear modulus (G_{xy}). Amadei (1996) states that in rocks such as phyllites, schists, siltstones, sandstones, mudstones, shales, basalts and gneisses often use the formulation of transverse isotropy to characterize the deformability. For these rocks, foliation, schistosity, or bedding planes are assumed to be the transverse isotropic plane.

Anisotropic rock can be classified by using degrees of anisotropy. There are three methods to define these values: point load strength, strength and elastic modulus. Tsidzi (1990) proposes the classification by point load index to classify the degree of anisotropy for foliated rocks. Ramamurthy (1993) defines the anisotropy strength (R_c) from ratio between maximum-to-minimum strength. Table 2.1 shows the degrees of anisotropy classification based on R_c. The strength of anisotropy primarily relies on the uniaxial compressive strength of the rock. Nonetheless, according to Zhang (2006), degree of anisotropy for a particular rock is not constant when subjected to confinement.

Amadei et al. (1987) determine the degrees of anisotropy of rock by calculating ratio of maximum-to-minimum elastic modulus (E_{max}/E_{min}). They find that the ratio for intact transverse isotropic rock vary between 1 and 4. The anisotropy elastic modulus in four groups of anisotropic rock classified by Worotnicki (1993) are presented in Table 2.2.

Table 2.1 Anisotropy strength range and rock classes (Ramamurthy, 1993).

Anisotropic ratio	Class	Rock Types
$1.0 < R_c < 1.1$	Isotropic	Sandstone
$1.1 < R_c < 2.0$	Low anisotropy	Sandstone, Shale
$2.0 < R_c < 4.0$	Medium anisotropy	Shale, Slate
$4.0 < R_c < 6.0$	High anisotropy	Slate, Phyllite
$6.0 < R_c$	Very high anisotropy	Slate, Phyllite

Table 2.2 Ranges of anisotropy elastic modulus (Amadei et al., 1987).

Anisotropic rock group	Example rock	Degree of anisotropy
Quartzofeldspathic rocks	Quartz and arkose sandstones, Granites, Granulites and Gneisses	$1.5 < E_{max}/E_{min} < 3.5$
Basic/lithic rocks	Igneous rock, Amphibolites, Lithic and greywacke sandstones,	$1.5 < E_{max}/E_{min} < 3.5$
Pelitic (clay) and pelitic (micas) rocks	Mudstones, Phyllites, Schists and Slates	$1.5 < E_{max}/E_{min} < 6$ (Highest anisotropy)
Carbonate rocks	Limestones, Marbles and Dolomites	$E_{max}/E_{min} < 1.7$ (Medium anisotropy)

2.3 Analysis of transverse isotropic effect on elastic property of materials

Transverse isotropy (bedding plane orientation) affects the properties of rock varying with direction (Goodman, 1989). Several investigators study the effect of transverse isotropy on strength and deformation of rock. Sukjaroen et al. (2021) find that the minimum compressive strength of rock salt obtained when bed inclination makes an angle of 60° with the loading direction. This agrees with the test results obtained by McLamore and Gray (1967) on slate, Al-Harthi (1998) and Colak and Unlu (2004) on sandstone, siltstone and claystone, and Saeidi et al. (2014) on limestone, granite and schist. However, Jeremic (1994) indicates that rock salt from Poland has the minimum strength when the bed inclination makes an angle of 45°. When the bedding plane orientation increases, the elastic modulus increases (Figure 2.2) but Poisson's ratio slightly decreases. (Yun-si et al., 2012; Kim et al., 2012; Heng et al., 2015; Wang et al., 2016; Hu et al., 2017; Cheng et al., 2017; Meng et al., 2018; Thongprapha et al., 2022). The minimum elastic modulus is obtained when loading direction normal to bedding plane orientation (β = 0°). Several investigators have observed that both intrinsic and apparent elastic moduli increase with increasing confining pressures (Nasseri et al., 2003; Miller et al., 2013; Fereidooni et al., 2016; Xu et al., 2018).

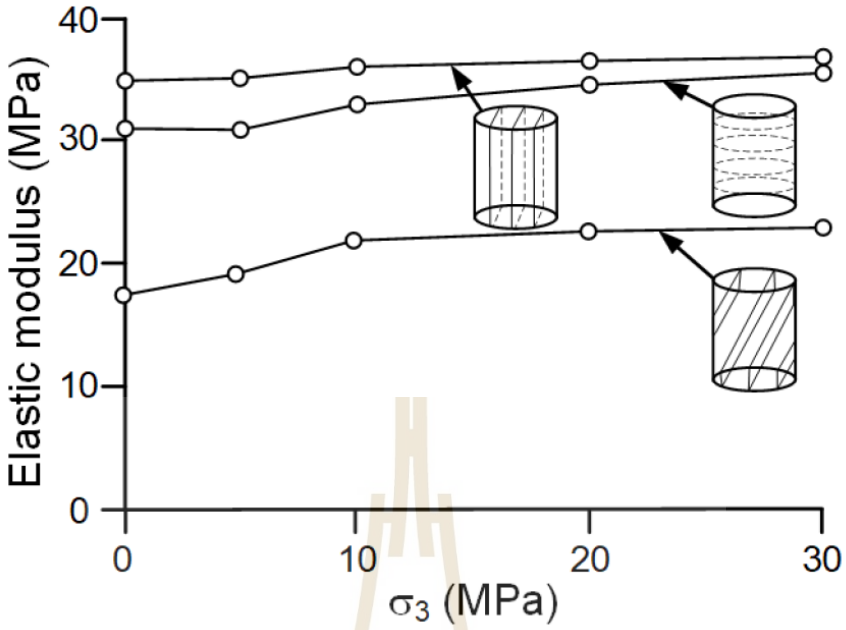

Figure 2.2 Young's modulus as a function of confining pressures and bedding planes (Hu et al., 2017).

Nasseri et al. (2003) perform compression test on schist, and find that the degrees of rock anisotropy in terms of strength ($\sigma_{90°}/\sigma_{0°}$) and elastic moduli ($E_{90°}/E_{0°}$) decrease with increasing confining pressure. This agrees with the experimental results obtained by Miller et al. (2013) on mudstone, by Xu et al. (2018) on phyllite, and by Fereidooni et al. (2016) on phyllite, slate, hornfels and schist. Thongprapha et al. (2022) state that the increment of confining pressures reduces the degree of salt anisotropy by stiffening the soft layers and tightening the inter crystalline boundaries along bedding planes. The intrinsic and apparent elastic and shear moduli normal to bedding plane strike rapidly increases, and they reach those parallel to the bedding planes. And rock salt has the transition from transverse isotropic to isotropic behaviour (degree of anisotropy equals 1) under the confining pressure up to 30 MPa, as shown in Figure 2.3.

Amadei (1996) proposes the equations that determine the deformability properties of transverse isotropic rock by assuming uniform stresses. Hakala et al. (2007) estimate and interpret the anisotropic elastic parameters by comparing the elastic parameters obtained from Amadei's solution with test results. They indicate that the apparent Young's modulus and Poisson's ratio are barely different with test results.

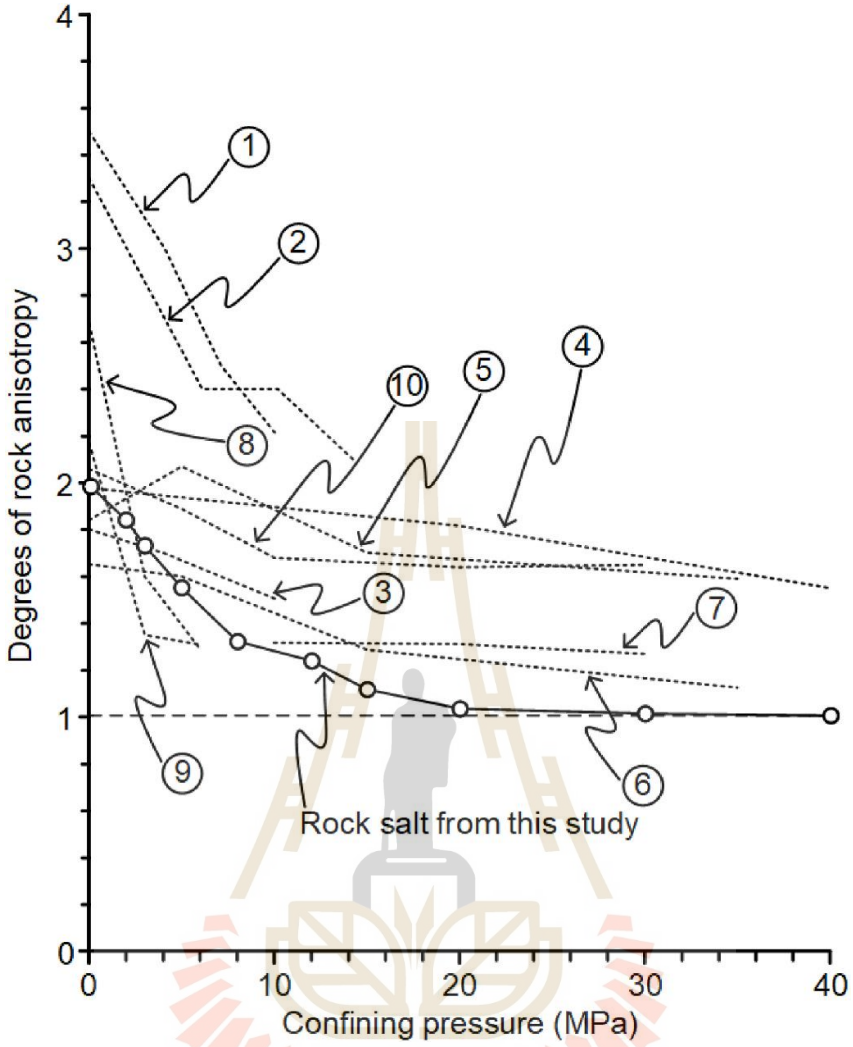

Figure 2.3 Degrees of rock anisotropy (E90°/E0°) under different confining pressures (Thongprapha et al., 2022).

Hwu and Ting (1989) use the two-dimensional elliptic inclusion to analyse anisotropic materials. The hoop stress expresses elliptic hole shape that is controlled by the real constant in major and minor axes of elliptic hole. The elliptic inclusion has the major axis (2a) and minor axis (2b), as shown in Figure 2.4. This solution is as well as the analysis of general anisotropic elastic materials by matrix.

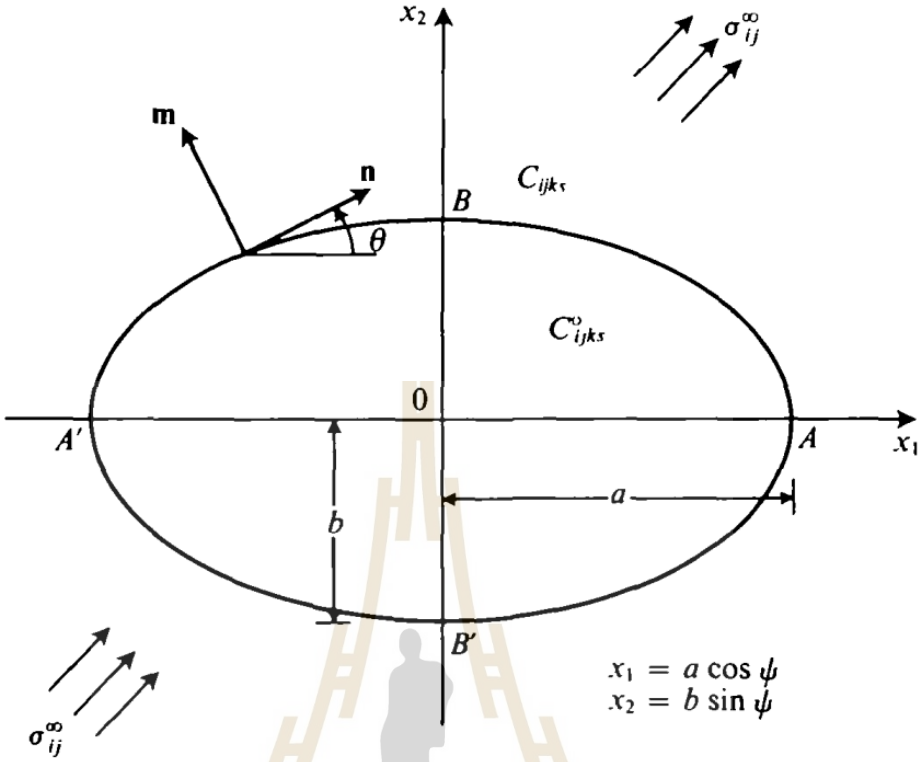

Figure 2.4 Boundary of elliptic inclusion in an infinite anisotropic elastic material (Hwu and Ting, 1989)

2.4 Time-dependent properties of Maha Sarakham Salt and Constitutive laws of salt

Time-dependent deformation, also known as creep, refers to the behaviour in which rocks can undergo continuous deformation without altering the applied stress. The American Society for Testing and Materials (ASTM) provides a standardized test method for creep, outlined in ASTM D7070 – 08. When loads are removed, creep strain seldom can be recovery fully, and hence it is largely plastic deformation. The creep deformation includes three different characteristic sections; the primary, secondary and tertiary phases, as shown in Figure 2.5.

Primary creep occurs shortly after the initial loading and is characterized by a gradually decreasing rate of strain. In Region I shows a primary or transient strain behaviour. The secondary or steady-state creep is Region II. This phase is almost constant slope which corresponds to tertiary or accelerating creep leading to rather a sudden failure, as shown in Region III. The two main mechanisms governing the creep

behaviour of rock salt are (Fuenkajorn and Daemen, 1988; Cristescu and Hunsche, 1996; Senseny et al., 1992):

(1) Dislocation climb mechanism: inter-crystalline boundaries sliding

(2) Dislocation glide mechanism: cleavage planes sliding

Phase I is controlled only by dislocation climb mechanism exclusively, while both dislocation climb and dislocation glide mechanisms are observed in phases II and III. Notably, phase III occurs primary microcracks. Time-dependent materials require constitutive equations to represent their behavior, which replace the elastic and plastic equations. Rheological models are used extensively to assist in visualizing the mechanisms that govern the constitutive equation, and to help in formulating the equation themselves.

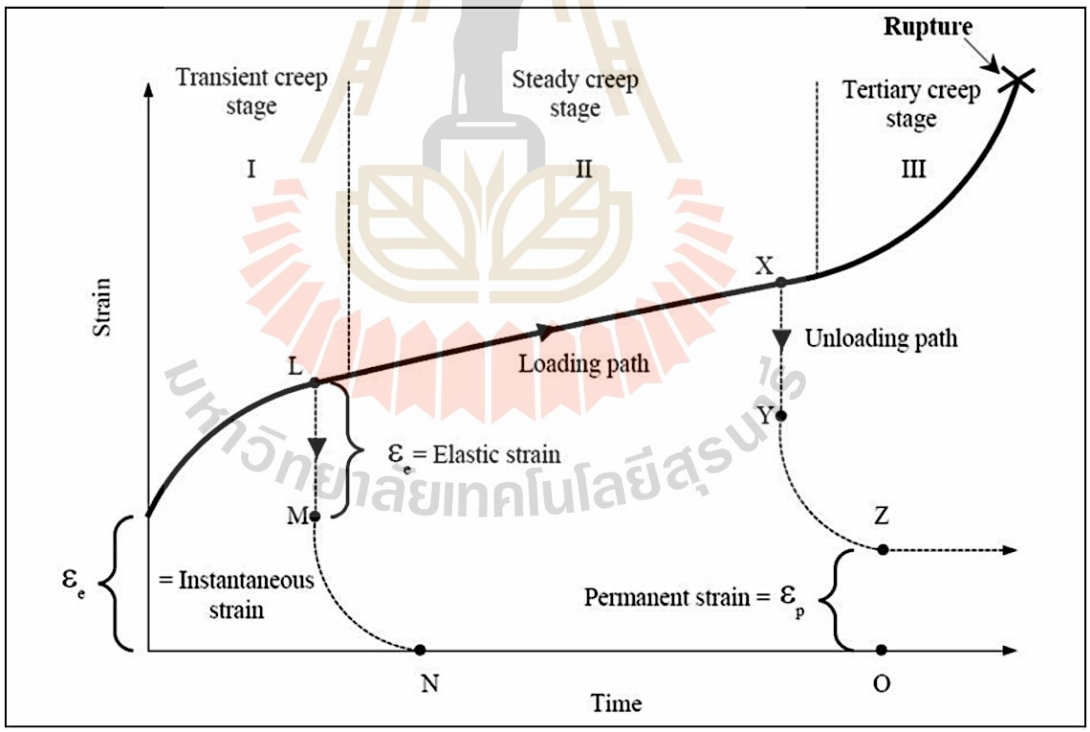

Figure 2.5 Creep strain as a function of time (modified from Jeremic, 1994).

The constitutive laws of creep behaviour of rock salt can be divided into two categories, namely the empirical model, which is summarized by experimental

phenomena and the non-linear rheological model (Aydan et al., 2012, 2015). Many models have been proposed for describing each stage of rock salt creep behaviour. Ling et al. (2007) construct the constitutive equation for instantaneous creep of salt cavern based on stress level. Wu et al. (2015, 2019) propose the creep model for the triaxial compression behaviour by using a variable-order fractional derivative and fitting the rock salt creep in transient and steady creep stages. Besides that, Zhang et al. (2012) establish equation to simulate transient creep stage from test data. Several investigators propose constitutive model to describe the steady stage of salt rock creep to carry out uniaxial and triaxial compression creep test (Wang et al., 2014; Wang et al., 2018) with deviatoric stress (Munson, 1997; Hunsche and Hampel, 1999; Liu et al., 2006), temperature (Wawersik, 1988; Raj and Pharr, 1992), stress history (Gunther et al., 2015). For a whole creep process, Zhou et al. (2013) replace Abel dashpot in the traditional Nishihara model and propose a constitutive creep model by using a time-fractional derivative providing a precise description.

Linear visco elastic model which is one of constitutive laws is used to analyze the time-dependent properties of rock salt in this study. Linear viscoelastic model includes four basic models: the Maxwell, Kelvin, generalized Kelvin, and Burgers model. Each model has a different arrangement of several mechanical elements (springs, dashpots, friction resistance to movement) as shown in Figure 2.6. The combination of each basic element has a unique and readily defined stress-strain-time law (Franklin and Dusseault, 1989).

The Burgers model is one of linear visco-elastic models that are widely used to analyze the creep behavior of rock salt. The reason for this preference is its simplicity and its ability to describe the elastic, visco-elastic, and visco-plastic phases separately (Handin et al., 1984; Gnirk and Johnson, 1964; Langer, 1984; Hardy and Sun, 1986; Senseny et al., 1992). The constitutive equation of Burgers model as follows (Jeremic, 1994):

$$\sigma+\left(\frac{\eta_1}{E_1}+\frac{\eta_2}{E_2}+\frac{\eta_1}{E_2}\right)\dot{\sigma}+\frac{\eta_1\eta_2\ddot{\sigma}}{E_1E_2}=\eta_1\dot{\varepsilon}+\frac{\eta_1\eta_2\ddot{\varepsilon}}{E_2} \tag{2.2}$$

$$\varepsilon(t)=\sigma_0\left\{\frac{1}{E_1}+\frac{t}{\eta_1}+\frac{1}{E_2}\left[1-\exp\left(-E_2t/\eta_2\right)\right]\right\} \tag{2.3}$$

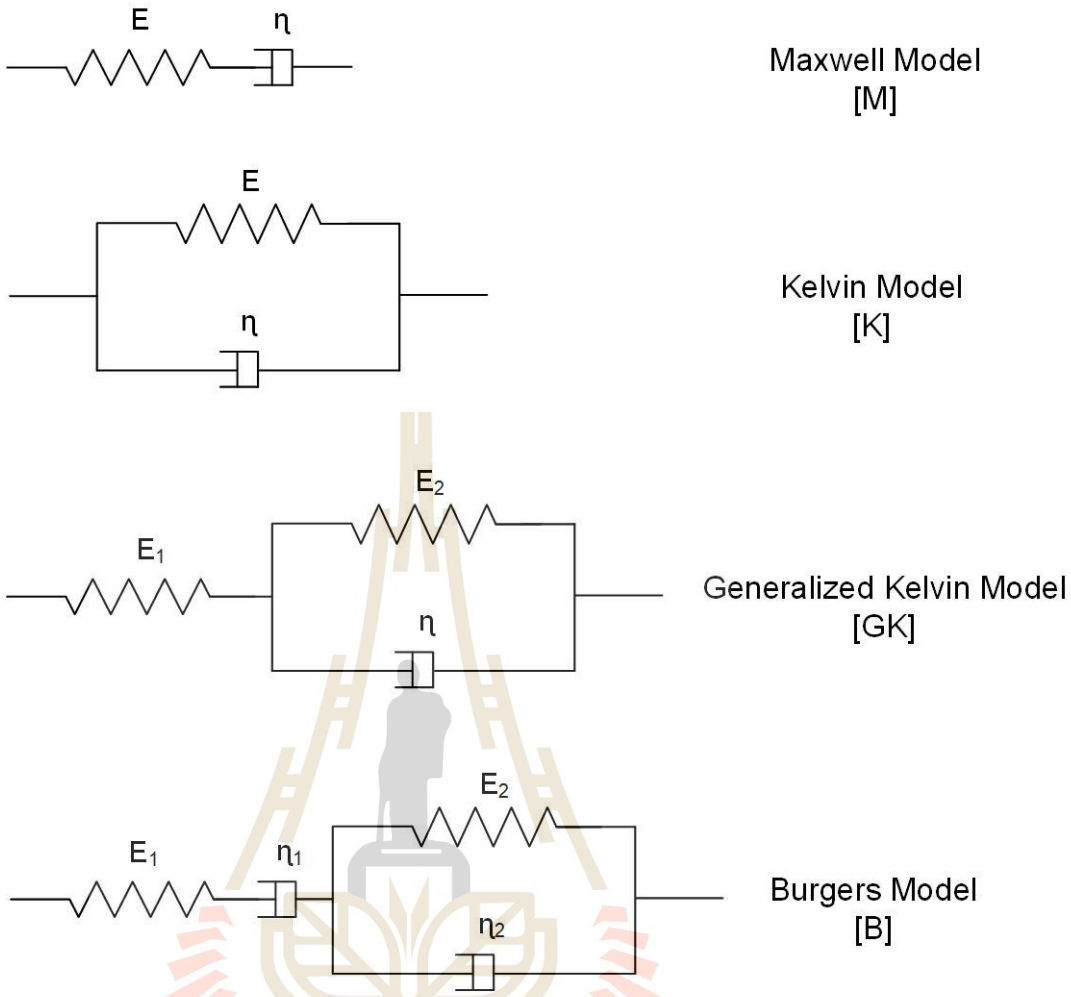

Figure 2.6 Arrangement of linear springs and dashpots of linear viscoelastic models (Franklin and Dusseault, 1989).

where σ and ε are stress and strain (which are a function of time), $\dot{\sigma}$ and $\dot{\varepsilon}$ are stress rate ($\partial\sigma/\partial t$) and strain rate ($\partial\varepsilon/\partial t$), $\ddot{\sigma}$ and $\ddot{\varepsilon}$ are stress acceleration ($\partial^2\sigma/\partial t^2$) and strain acceleration ($\partial^2\varepsilon/\partial t^2$), t is time, E_1 is the elastic modulus, E_2 is the spring constant in visco-elastic phase, η_1 is the viscosity coefficient in steady-state phase, and η_2 is the viscosity coefficient in transient phase.

The time-dependent behaviour of rock salt is intricate and influenced by various factors, including grain size, bonding between grains, loading conditions, temperature, time, humidity, inclusions, and others. Only relevant factors are included in this study and commonly shown by the effect on deformation and creep properties.

The intermediate principal stress effect on the time-dependent behaviour of Maha Sarakha salt are investigated by Samsri et al. (2010) and Sriapai et al. (2013). They perform polyaxial creep under constant mean stress (σ_m) of 15 MPa with varying loading conditions ranging from the triaxial ($\sigma_1 \neq \sigma_2 = \sigma_3$) to the polyaxial ($\sigma_1 \neq \sigma_2 \neq \sigma_3$ and $\sigma_1 = \sigma_2 \neq \sigma_3$) stress. The elastic, visco-elastic (transient) and visco-plastic (steady-state) behaviour of the salt are determined by using Burgers model. The salt elastic modulus is independent with intermediate principal stress (σ_2) but tends to increase as the applied τ_{oct} increases. The visco-elastic and visco-plastic parameters increase when σ_2 increases from the $\sigma_2 = \sigma_3$ condition to the $\sigma_2 = \sigma_1$ condition under the same magnitude of τ_{oct}. Khamrat and Fuenkajorn (2016) determine the effect of σ_2 on the long-term closure of salt storage caverns. The Burgers parameters are defined as a function of Lode parameter. Their findings propose that calculating time-dependent deformation from conventional creep test results might lead to an overestimation of actual closure for cylindrical caverns by as much as 16% and for spherical caverns by 35%. The results of Archeeploha et al. (2017) may overestimate as much as 15% and 35%, respectively.

Yang et al. (1999) study the effect of axial and confining pressures on stress-strain behaviour of salt rock. The steady-state creep rates of the rock under uniaxial and triaxial creep tests are described by an exponential equation:

$$\dot{\varepsilon} = \dot{\varepsilon}_{ss} + A \times \exp\left[\left(t_0 - t\right) / \beta\right] \tag{2.4}$$

where $\dot{\varepsilon}$ is total creep strain rate, $\dot{\varepsilon}_{ss}$ is steady-state creep strain rate, t_0 is reference time and A and β are material constants.

The results indicate that the creep strain rate relates with the stress/strain state but does not relate to the loading history. The steady-state creep strain rate increases with increasing deviatoric stress and decreasing confining pressure. Wang et al. (2015) indicate that the deviatoric stress level affects to the lateral deformation than the axial deformation in tertiary creep stage. The correlation between deviatoric stress and steady creep strain rate can be describe by an exponential equation.

The presence of impurities and inclusions influences the creep deformation and creep properties of salt. The inclusions often appear as thin seams or beds. Salt impurities comprise ferruginous inclusions and thin clay seams between bedding planes or grain boundaries. These factors may cause the decreasing of creep deformation of rock salt, as reported by Franssen and Spiers (1990), Senseny et al. (1992) and Raj and Pharr (1992). Kensakoo (2006) studies the effect of anhydrite and clay minerals thin seams that perpendicular to the core axis salt specimens on the elastic modulus and visco-plasticity coefficient. Anhydrite seam effect causes the elasticity of specimen increases from 22 GPa to as high as 36 GPa. However, the effect of clay in the salt specimens remains unclear.

The intrinsic variability of Middle and Lower members of the Maha Sarakham salt is studied by Fuenkajorn et al. (2011). They vary the contents of anhydrite from 0% to 100% (by weight). Visco-plasticity exponentially increases with crystal size. Dislocation glide becomes main mechanism for the specimen comprising large crystals. Fine crystals are deformed by dislocation climb mechanism affecting the visco-plasticity of specimen reduces.

The influence of carnallite contents occurring by potash ore deposit at the salt basin on the time-dependent parameters of rock salt is determined by Luangthip et al. (2017). Salt specimens are varied with carnallite content (C%). As the C% increases, the elastic, visco-elastic, and visco-plastic parameters of the creep test specimens rapidly decrease. While pure halite exhibits the characteristic of a Burgers material, pure carnallite behaves a Maxwell material.

2.5 Effect of transverse isotropy on time-dependent properties of rock

Many previous studies have been investigated the effects of transverse isotropy on the time-dependent behavior of rock that can divide in 4 categories:

(1) The axial and lateral strains that occur over time.

Liu et al. (2015) study the effect of deviatoric stress level and transverse isotropy of a clayey rock on the triaxial compressive creep test. The findings suggest that perpendicular samples exhibit higher axial and lateral strains compared to parallel

samples at the same deviatoric stress level. This agrees well with the result obtained by Luo et al. (2021) on interlayer rock.

Xiong et al. (2014) state that the loading orientations and the bedding planes affect to the time dependent properties under biaxial creep test. Under the same stress level and specimen type, the axial loading parallel to the bedding plane, and the lateral loading perpendicular to the bedding plane are lower than that with the axial strain with the both loading orientations parallel to the bedding plane.

(2) Three stages of creep deformation of rocks under constant stress: instantaneous and transient creep (primary stage), steady-stage creep (secondary stage), and accelerating creep (tertiary stage).

Dubey and Gairola (2008) perform the uniaxial creep test in rock salt with β angles of 0, 30 and 90°. The result states that the β effect of all creep stages of rock salt, this effect decreases when the loading rate increases.

Wu et al. (2018) study the effect of transverse isotropy on time-dependent behavior of foliated metamorphic greenschists. The result indicates that instantaneous, transient and steady-state strains are affected by structural anisotropy. The instantaneous and transient creep of specimens with bedding plane perpendicular and parallel to axial loading are higher than that of oblique 45 and 60 degrees to the axial loading at any stress level. The instantaneous and transient creep of specimens with bedding plane perpendicular and parallel to axial loading obvious to closure or open of the inherent void and crack along the bedding plane to unfavorably oriented induced compression or tensile stress (act parallel to bedding) than specimen that oblique 45 and 60 degrees to the axial loading. The instantaneous strain and transient creep duration decrease with increasing of creep stress level, as shown in Figure 2.7. Figure 2.8 shows the slope of steady-state rate increment, the least steady-state rate occurs at IA0 (bedding plane perpendicular to axial loading) while the greatest occurs at IA45 (oblique 45 degrees to the axial loading) mainly due to the shear displacement.

Naumann et al. (2007) state that elastic straining and inelastic compaction are the causes of initial deformation. The transient creep strain for perpendicular sample is higher than for parallel samples due to the effect of shearing along the

bedding plane. Transient creep is more influenced by the bedding plane compared to steady-state creep.

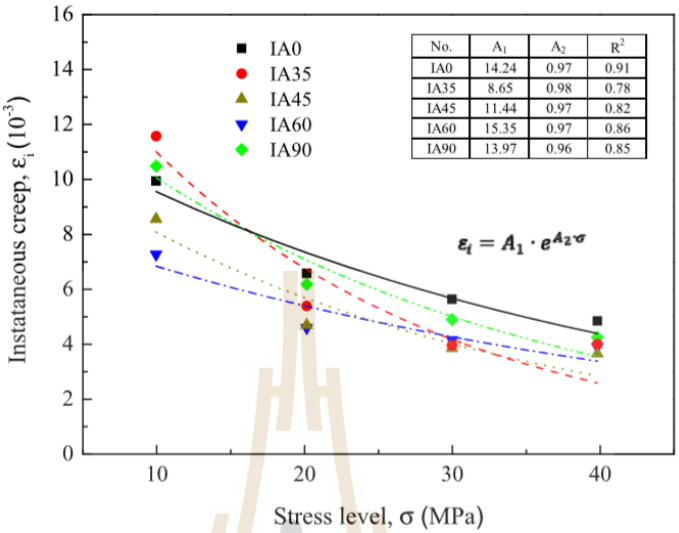

No.	A_1	A_2	R^2
IA0	14.24	0.97	0.91
IA35	8.65	0.98	0.78
IA45	11.44	0.97	0.82
IA60	15.35	0.97	0.86
IA90	13.97	0.96	0.85

(a)

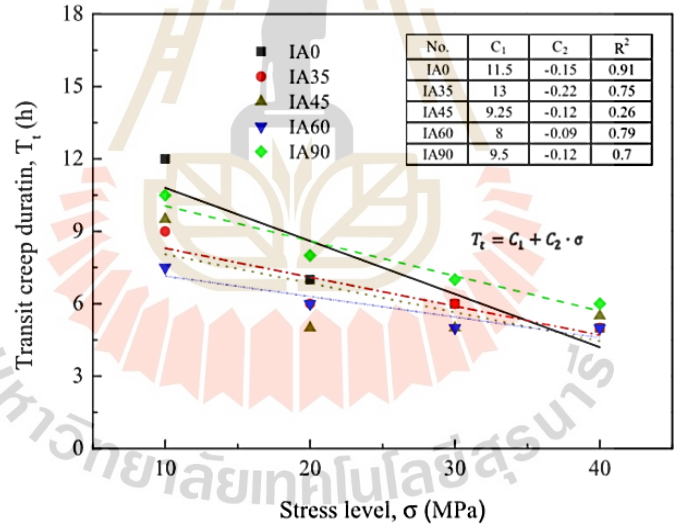

No.	C_1	C_2	R^2
IA0	11.5	-0.15	0.91
IA35	13	-0.22	0.75
IA45	9.25	-0.12	0.26
IA60	8	-0.09	0.79
IA90	9.5	-0.12	0.7

(b)

Figure 2.7 Instantaneous strain (a) and creep duration (b) as a function of stress (Wu et al., 2018).

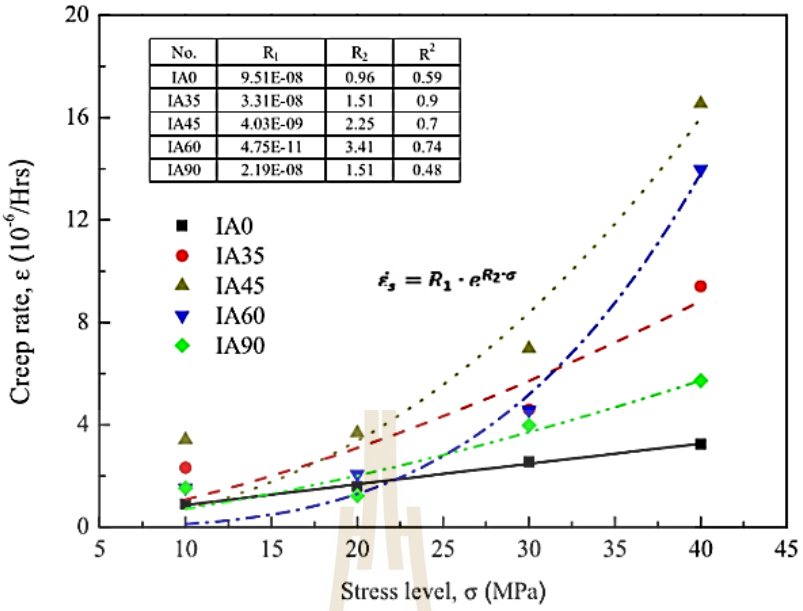

(a)

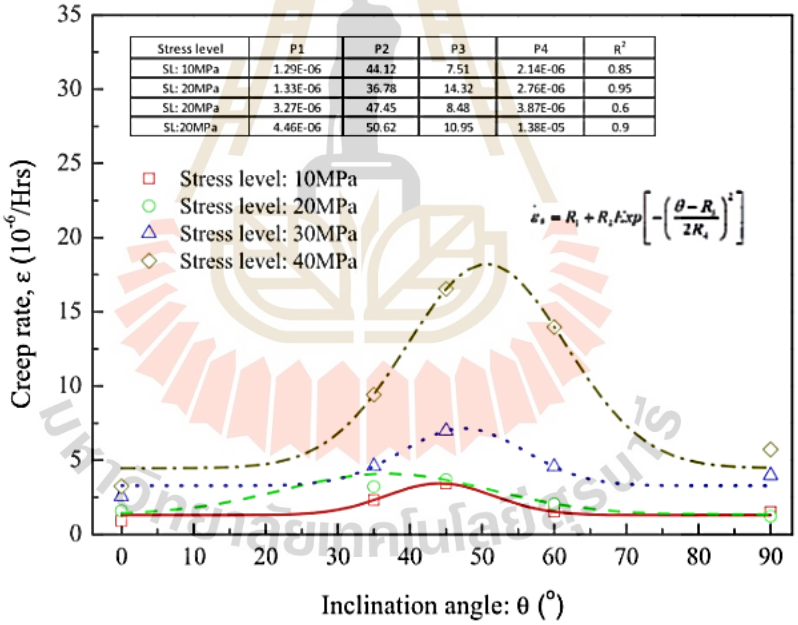

(b)

Figure 2.8 Steady-state creep rate with varying applied stress (a), and bedding plane orientation (b) (Wu et al., 2018).

In addition, Li et al. (2020) state that strain during instantaneous stage decreases with the orientation of the shale plane as a result of the apparent elastic modulus (E_β) increases with the shale plane. Several studies have depicted the strain-time relationship during deformation under compression creep tests, primarily focusing

on soft rocks at shallow depths. Wu et al. (2016) investigate the effect of transverse isotropy on rheological properties of hard rock at deep depth. The strain-time curves of the hard rock show instantaneous and steady-state creep, without the accelerated creep phase. The transverse isotropy strongly affects rheological behaviors, including the instantaneous modulus, duration of transient creep, steady-state creep rate, contraction ratio and volumetric strain.

(3) The strain rate on the creep deformation

Liu et al. (2015) study the effect of transverse isotropy on creep rate of clayey rock. The axial creep rates of both parallel and perpendicular specimens are similar during the initial creep stage. At the steady creep stage, the axial creep rate of perpendicular specimen is slightly lower than those of parallel specimen, as shown in Figure 2.9.

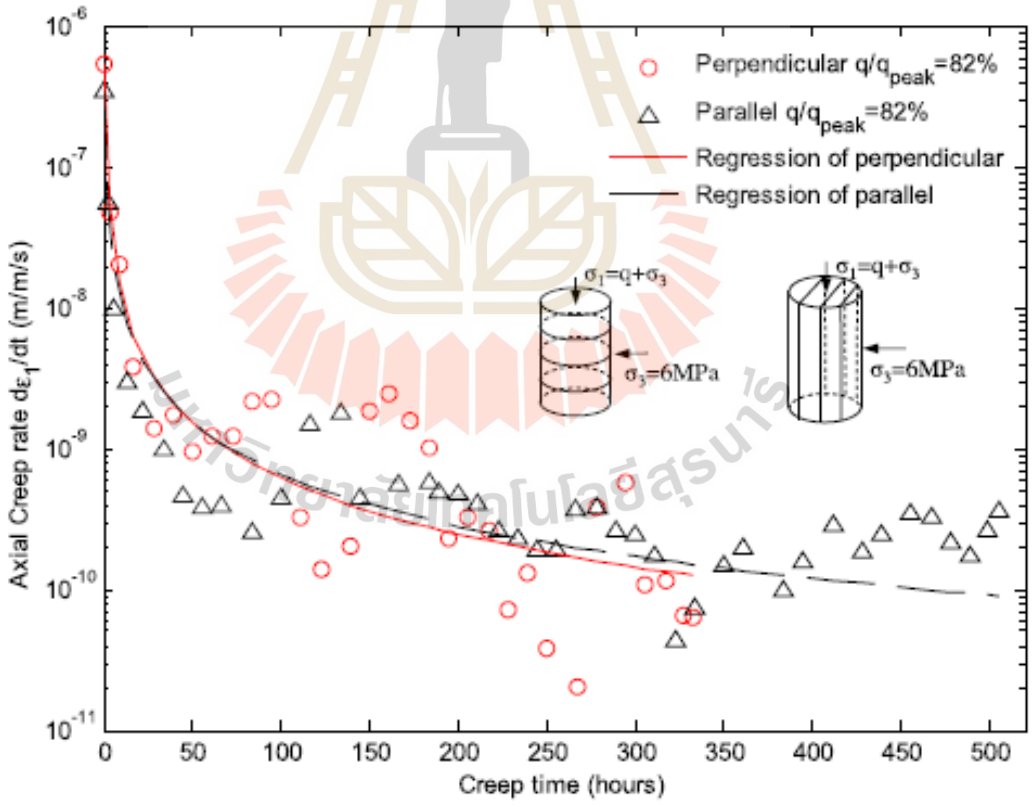

Figure 2.9 Axial creep strain rate with different deviatoric creep stress at q/q_{peak}= 82 % (Liu et al., 2015)

Wu et al. (2018) and Zhang et al. (2022) state that highest steady creep rate is β = 45°. Wang et al. (2018) apply the general power model in Equation (2.5) to analyze the effect of transverse isotropy from creep rate.

$$\dot{\varepsilon}(t) = \dot{\varepsilon}_0 \cdot t^b \tag{2.5}$$

(4) Creep parameters include elastic modulus (E_1), spring constant in visco-elastic phase (E_2), viscosity coefficient in steady-state phase (η_1) and viscosity coefficient in transient phase (η_2).

Zhang et al. (2022) perform the uniaxial creep test to study the transverse isotropic creep behavior of layered phyllite. Creep deformation on these specimens occurs in four stages: instantaneous elastic deformation, deceleration, steady-stage and accelerated creep stage. The result finds that creep parameters (elastic modulus (E_1, E_2) and viscosity coefficients (η_2, η_3)) initially decrease and then increase with the bedding angle (Figure 2.10). Therefore, the creep characteristics of the layered rock are governed by the presence of natural weakness planes and a considerable transverse isotropic effect.

From the reviewed studies, it shows the effect of transverse isotropy on the creep characteristics of rock. In addition, many studies have found that there are some factors decreasing this effect. Wang et al. (2018) state that the anisotropic ratios (axial strain rate ratios in the creep stage) show the influence of bedding planes. The anisotropic ratios decrease with increasing deviatoric stress and confining pressure. This agrees with the experimental results obtained by Naumann et al. (2007). Wu et al. (2018) state that the effect of transverse isotropy is slowly weakened with the stress level increases.

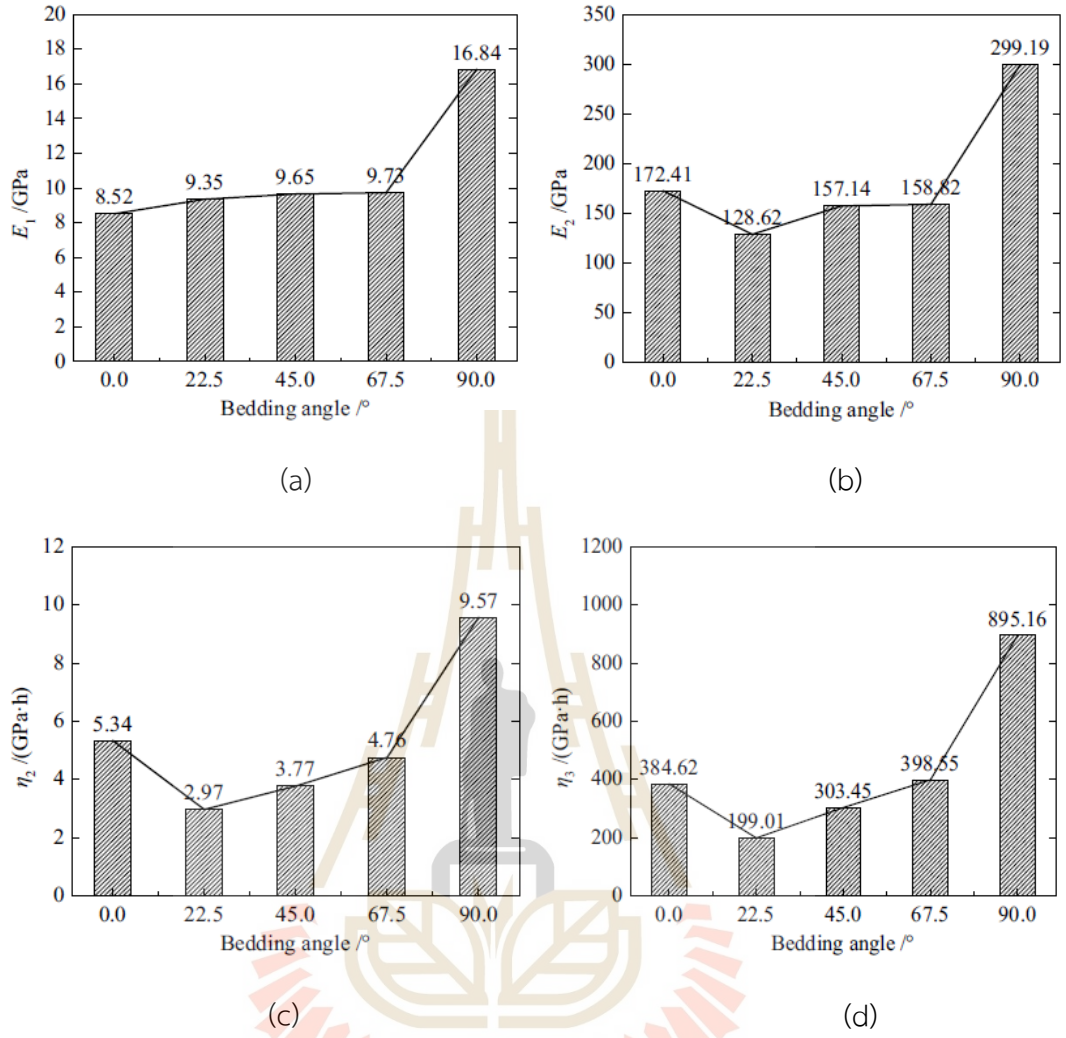

Figure 2.10 Correlation between bedding angle and creep parameters: elastic modulus, E_1 (a), elastic modulus, E_2 (b), viscosity coefficients, η_2 (c), and viscosity coefficients, η_3 (d) (Zhang et al., 2022).

2.6 Constitutive models of transverse isotropy on time-dependent properties of rock

The importance of describing the creep characteristic of transverse isotropic rock is to construct a reasonable creep constitutive model. The creep models of transverse isotropic materials can be divided into two categories, namely the empirical model which is summarized by experimental phenomena and the theoretical model which is obtained by viscoelastic plastic element model.

Hatzor and Heyman (1997) establish the new empirical model for describing compression-dilation behavior of anisotropic rock salt. The predicted result shows that

the dilation stress decreases with decreasing confining pressure and with increasing value of β.

Xu et al. (2019) and Zhang et al. (2022) propose the new creep model combining a Maxwell body, a Kelvin body, and a nonlinear visco-plastic body in 2D and 3D to describe all creep processes of transverse isotropic rocks. These models are called ubhm model. The three-dimensional forms of the creep model can be expressed as:

$$\varepsilon_{11}(t)=\begin{cases}\dfrac{S_{ij}}{2G_1}+\dfrac{\sigma_m\delta_{ij}}{3K}+\dfrac{S_{ij}}{2H_1}t+\dfrac{S_{ij}}{2G_2}\left(1-e^{-\frac{G_2}{H_2}t}\right) & S_{ij}<S_S\\ \dfrac{S_{ij}}{2G_1}+\dfrac{\sigma_m\delta_{ij}}{3K}+\dfrac{S_{ij}}{2H_1}t+\dfrac{S_{ij}}{2G_2}\left(1-e^{-\frac{G_2}{H_2}t}\right)+\dfrac{S_{ij}-S_S}{2H_3}\dfrac{at^n+b}{t} & S_{ij}\geq S_S\end{cases} \tag{2.6}$$

where σ_m and S_{ij} are the spherical stress tensor and deviatoric stress tensor, S_s is the three-dimensional creep strength of the rock, G_1 and G_2 are shear moduli of the elastic body and Kelvin body, K is bulk modulus of the elastic body, H_1, H_2 and H_3 are the three-dimensional viscosity coefficients of the viscous body, the Kelvin body and nonlinear body. The validation results demonstrate that the creep model effectively represents the entire creep stage in the transverse isotropic rock.

Luo et al. (2021) derive the viscoelastic equations for three interlayered rock conditions: soft-hard, soft-soft and hard-hard interlayered for rock specimens. The loading is applied parallel to or perpendicular with bedding plane. In this study, they define the creep properties of hard rock behaves the generalized Kelvin model and soft rock behaves the Burgers model. A sum form of creep models on each rock type is described the specimen with loading perpendicular to the bedding plane. A dividing form of creep models of each rock type is described the specimen with loading parallel to the bedding plane. The three-dimension creep equation of hard soft interlayered rock for the loading parallel to the bedding plane can be expressed in Equation (2.7) and the loading parallel to the bedding plane can be expressed in Equation (2.8). The theoretical model fits well with the measure values that error within 5%.

$$\varepsilon(t)=\sigma_0\alpha_K\left(\frac{1}{3G_1}+\frac{1}{9K_1}-\frac{e^{-\frac{G_2}{\eta_1}t}}{3G_2}+\frac{1}{3G_2}\right)+\sigma_0\alpha_B\left(\frac{1}{3G_3}+\frac{1}{9K_3}-\frac{e^{-\frac{G_4}{\eta_2}t}}{3G_4}+\frac{1}{3G_4}+\frac{t}{3\eta_3}\right) \quad (2.7)$$

$$\varepsilon(t)=\frac{\left(\frac{1}{3G_1}+\frac{1}{9K_1}-\frac{e^{-\frac{G_2}{\eta_1}t}}{3G_2}+\frac{1}{3G_2}\right)\left(\frac{1}{3G_3}+\frac{1}{9K_3}-\frac{e^{-\frac{G_4}{\eta_2}t}}{3G_4}+\frac{1}{3G_4}+\frac{t}{3\eta_3}\right)}{\left(\frac{1}{3G_1}+\frac{1}{9K_1}-\frac{e^{-\frac{G_2}{\eta_1}t}}{3G_2}+\frac{1}{3G_2}\right)\beta_B+\left(\frac{1}{3G_3}+\frac{1}{9K_3}-\frac{e^{-\frac{G_4}{\eta_2}t}}{3G_4}+\frac{1}{3G_4}+\frac{t}{3\eta_3}\right)\beta_K}\sigma_0 \quad (2.8)$$

Wu et al. (2018) propose the creep models to describe the transverse isotropic effect on creep behavior of greenschists by combining the effect of bedding plane and rock matrix. Rock matrix is described by Burgers model, and bedding plane described by Maxwell model. Figure 2.11 shows the 1-D Mathematic representations of creep model. The Burger model fit well with test result as shown in Figure 2.12. The anisotropy induced by the bedding plane is modeled using an anisotropic strength criterion, which exhibits a characteristic U-shaped curve with the minimum value occurring at 45 + 1/2 (friction angle). Figure 2.12(a) demonstrates that fitting with the Burgers model eliminates the use of the Maxwell model for bedding planes.

Based on the assumption of constant Poisson's ratio, Li et al. (2020) derive a 3-D creep constitutive equation of transverse isotropic rock between specimens with horizontally and vertically oriented bedding through different operator methods. Kou et al. (2023) establish the nonlinear damage creep model for describing the entire creep characteristics for phyllite specimens with various bedding plane orientations. They indicate that their model is more accurate than the Nishihara and modified Nishihara model.

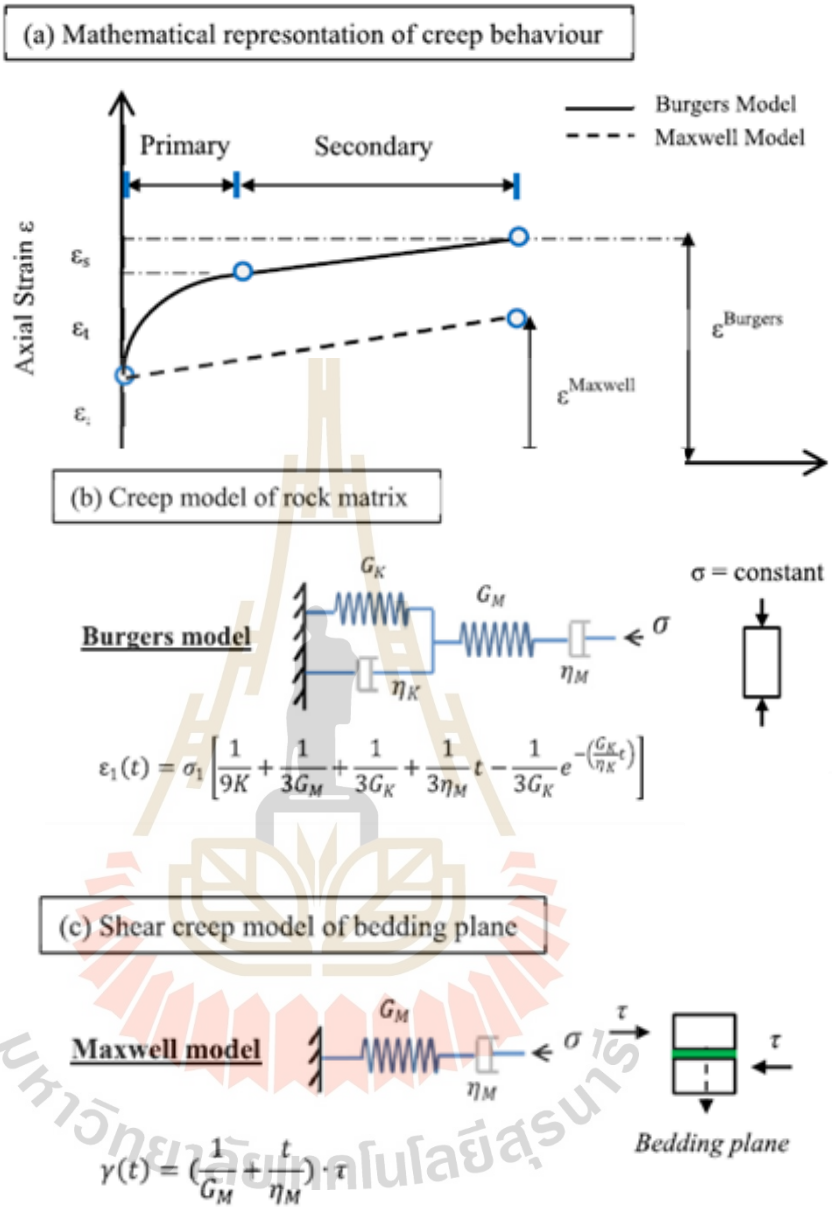

Figure 2.11 Mathematical representations of creep model of greenschist: Strain-time curve of Burgers and Maxwell model, (b) Rock matrix creep model (Burgers model), and (c) Shear creep model of bedding plane (Maxwell model) (Wu et al., 2018)

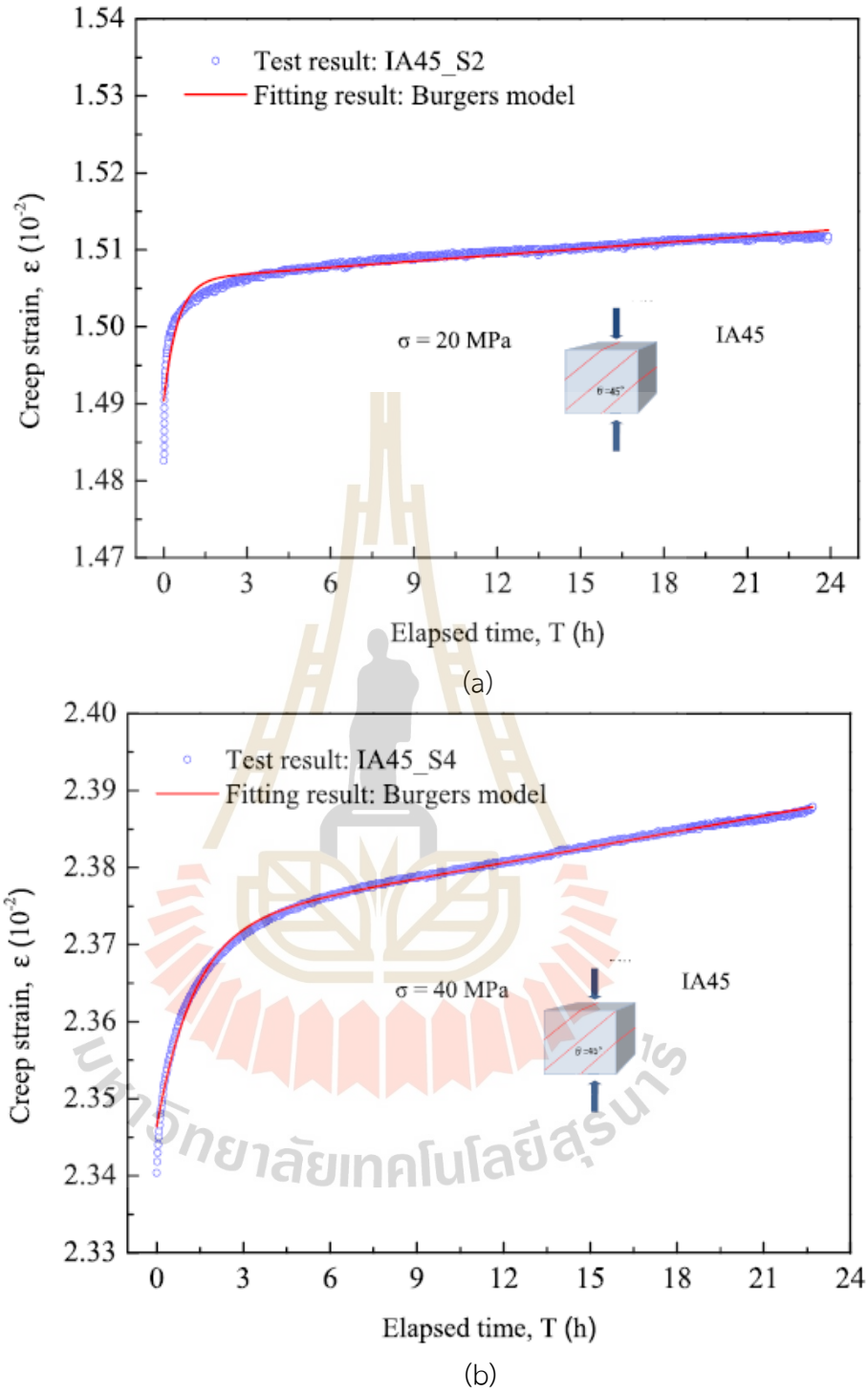

Figure 2.12 Results of fitting with Burgers model for specimen with β = 45° under compression stress of 20 MPa (a) and 40 MPa (b) (Wu et al., 2018).

CHAPTER III
SAMPLE PREPARATION

3.1 Introduction

This chapter describes the sources and characteristics of rock salt samples used in this study. The rock salt preparation and specifications for uniaxial and triaxial creep tests are also presented. The physical and chemical properties using X-ray diffraction analysis are determined.

3.2 Sample preparation

The salt specimens tested here are obtained from the potash mine opening at depths of 200-300 m of Thai Kali Co., Ltd., Nakhon Ratchasima province. Salt blocks are collected from Lower Members of Maha Sarakham formation (Figure 3.1). The origin and geology of Maha Sarakham formation are described by Warren (1999). Sample preparation is carried out in the laboratory at Suranaree University of Technology. The salt blocks are cut by using organic oil as lubricant to obtain rectangular specimens with nominal dimensions of 54×54×108 mm^3. Each sample contained salt beds that can be observed by alteration of light and dark bands of halite. For uniaxial creep test, the salt samples have nominal angles (β) between specimen main axis and the normal to bedding planes varying from 0°, 45°, 65°, 75° and 90°, as shown in Figure 3.2. Five specimens are prepared for uniaxial creep test. Figure 3.3 shows some salt samples for triaxial creep test that have β angles varying from 0°, 25°, 45°, 65° and 90°. Each angle β is prepared to here three specimens, except β = 0° and 90° which are prepared four specimens each, with a total of 17 specimens for triaxial creep test. The bedding plane strike is parallel to one of the specimen side surfaces, as shown in Figure 3.4. The dimensions, physical properties and bedding plane orientations of the salt specimens for uniaxial and triaxial creep tests are summarized in Tables 3.1 and 3.2.

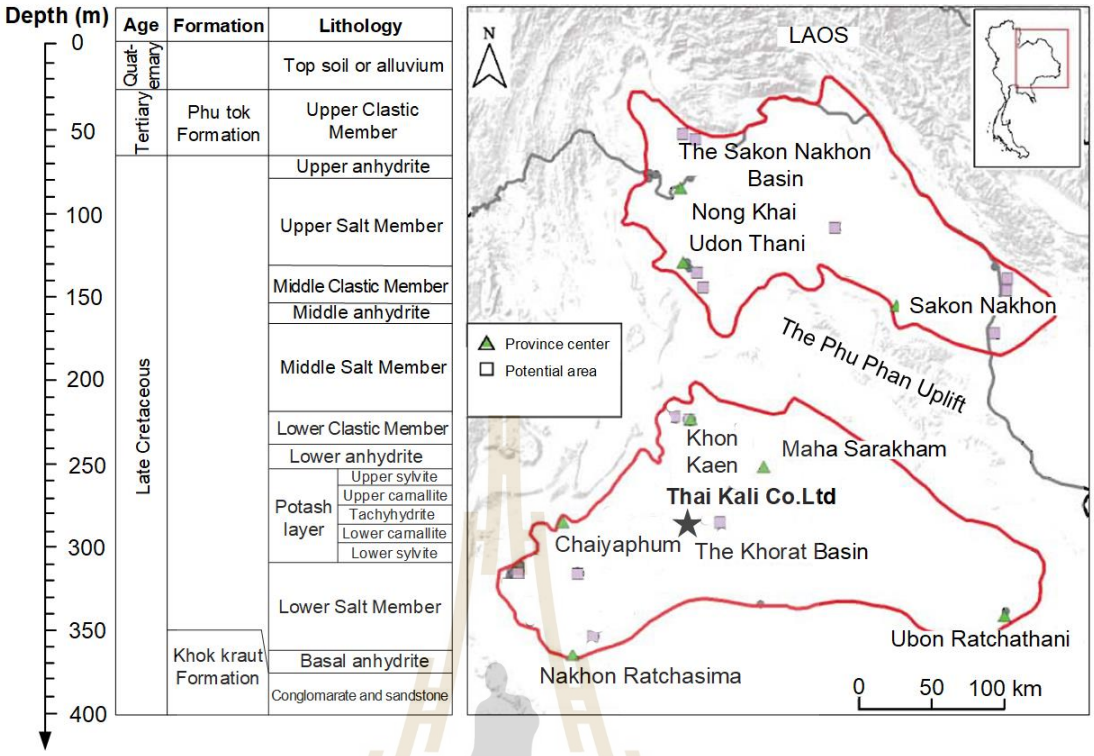

Figure 3.1 Stratigraphy of Maha Sarakham formation and location of Thai Kali Co.,Ltd. in Khorat salt basin. (Shen and Siritongkham, 2020)

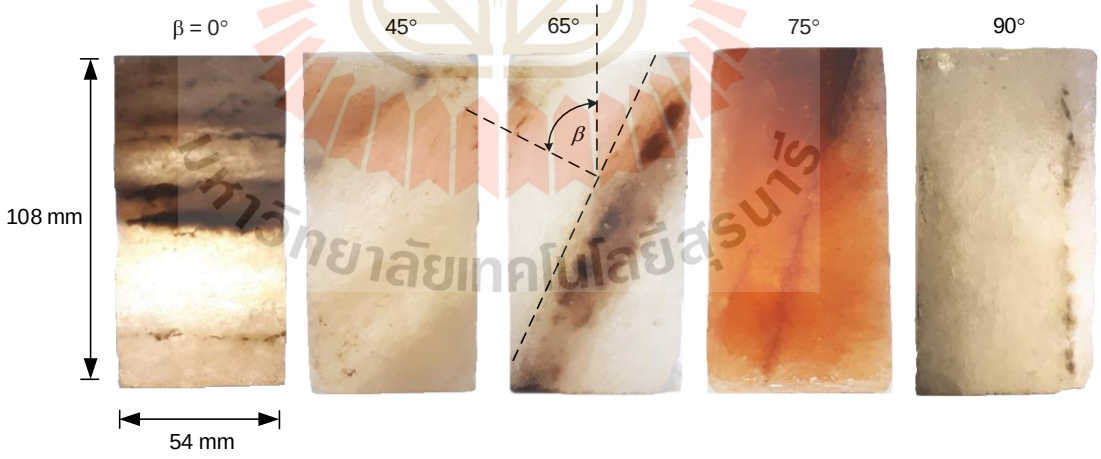

Figure 3.2 Salt specimens prepared for uniaxial creep test.

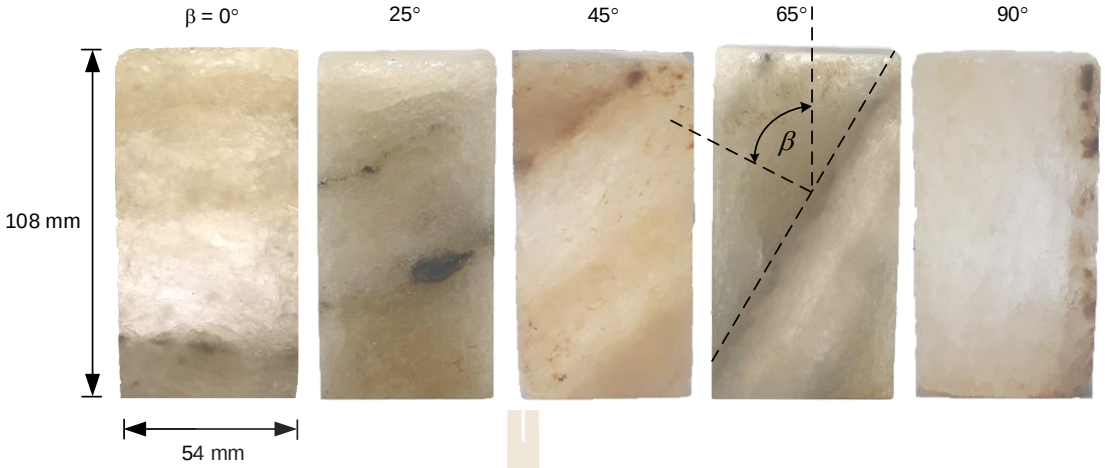

Figure 3.3 Some salt specimens prepared for triaxial compression creep test.

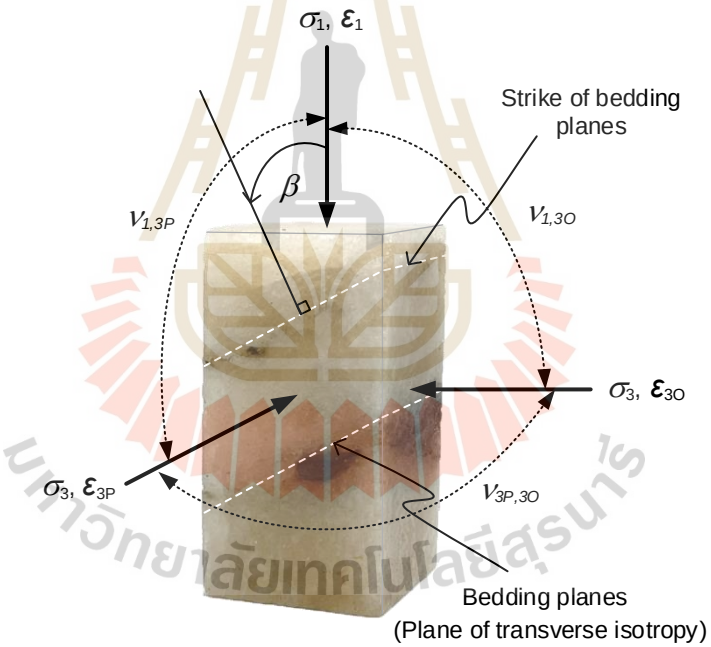

Figure 3.4 Notation showing bedding plane orientation used in this study.

Table 3.1 Salt specimens prepared for uniaxial creep tests.

Specimen No.	β (degrees)	Width (mm)	Length (mm)	Height (mm)	Weight (g)	Density (g/cm^3)
UC-0-0	0	55.33	51.88	106.84	643.51	2.10
UC-45-0	45	53.81	53.37	107.24	638.82	2.07
UC-65-0	65	54.77	52.7	107.05	638.69	2.07
UC-75-0	75	54.74	55.17	107.64	680.68	2.09
UC-90-0	90	53.75	53.14	107.97	658.29	2.13

Table 3.2 Salt specimens prepared for triaxial creep tests.

Specimen No.	β (degrees)	Width (mm)	Length (mm)	Height (mm)	Weight (g)	Density (g/cm^3)
TC-0-3	0	54.36	55.79	107.84	686.64	2.10
TC-0-6	0	52.94	53.81	108.69	656	2.12
TC-0-12	0	55.26	55.26	105.94	685.4	2.12
TC-0-24	0	55.74	55.14	54.54	353.44	2.11
TC-25-3	25	55.34	54.66	105.78	697.36	2.18
TC-25-6	25	54.54	54.22	104.22	668.66	2.17
TC-25-12	25	52.06	52.90	100.82	579.24	2.09
TC-45-3	45	55.78	53.90	100.40	632.6	2.10
TC-45-6	45	56.06	56.60	111.24	755.64	2.14
TC-45-12	45	55.04	54.10	103.44	652.04	2.12
TC-65-3	65	54.38	55.38	109.76	695.07	2.10
TC-65-6	65	55.40	55.16	107.16	721.36	2.20
TC-65-12	65	53.24	51.54	101.78	605.35	2.17
TC-90-3	90	56.84	56.81	110.4	752.72	2.11
TC-90-6	90	54.79	56.04	110.93	723.63	2.12
TC-90-12	90	57.68	57.26	110.60	772.16	2.11
TC-90-24	90	53.82	55.64	56.36	363.05	2.15

3.3 X-ray diffraction (XRD) analysis

The XRD analysis uses finely ground specimen powder with particle sizes less than 0. 25 mm (mesh #60) to determine the mineral compositions of specimens using the X-ray diffraction (Bruker, D2 Phaser). The results from X-ray diffraction analysis of salt specimens are shown in Table 3.3.

The results of X-ray diffraction analysis show that the salt consists mainly of halite 95.48% and slight amount of trace minerals 4.52% by weight. These trace minerals include anhydrite, sylvite, dickite, tachyhydrite, gypsum and clay mineral disseminating between halite crystals.

Table 3.3 Mineral compositions of salt specimens obtained from XRD analysis.

Mineral Name	Mineral compositions (%)	
	Sample No.1	Sample No.1
Halite	95.48	95.52
Anhydrite	0.31	0.24
Sylvite	0.36	0.26
Gypsum	1.69	1.96
Dickite	0.31	0.01
Montmorillonite	0.64	0.97
Illite	0.79	0.55
Tachyhydrite	0.42	0.49

CHAPTER IV
LABORATORY TEST METHODS AND RESULTS

4.1 Introduction

The objective of this chapter is to describe the method to determine the creep behavior of rock salt and results of the laboratory experiments. The laboratory tests are divided into two testing; 1) uniaxial creep test under applied constant axial stress (σ_1) 10 MPa 2) triaxial creep test under constant octahedral shear stress (τ_{oct}) 9 MPa. The results have been used to determine the effect of transverse isotropic on creep behavior of rock salt.

4.2 Uniaxial creep test

A consolidation load frame (Jandakaew, 2007) has been used to apply constant axial stress for the uniaxial creep test. The uniaxial creep tests are conducted following ASTM D7070-08 standard practice except the specimen shape. Before testing, the cantilever beam with dead load is calibrated to obtain truly constant axial stress to specimens. The samples are performed under constant axial stress of 10 MPa from pre-calculated dead weight and cantilever beam for up to 10 days. Neoprene sheets are placed at the interfaces between top and bottom of specimen surfaces and the loading platens. The displacement dial gages are installed to measure the axial and lateral deformations that parallel and normal to the strike of bedding planes (Figure 4.1). During the test, the time and deformation are recorded to the nearest 0.001 mm. The reading intervals are made once every minute for the first 10 minutes of testing and increased to every 2 min for 10 minutes later, every 5 min until 1 hour, and every 30 min until the end of the test. All bedding plane orientations have been tested.

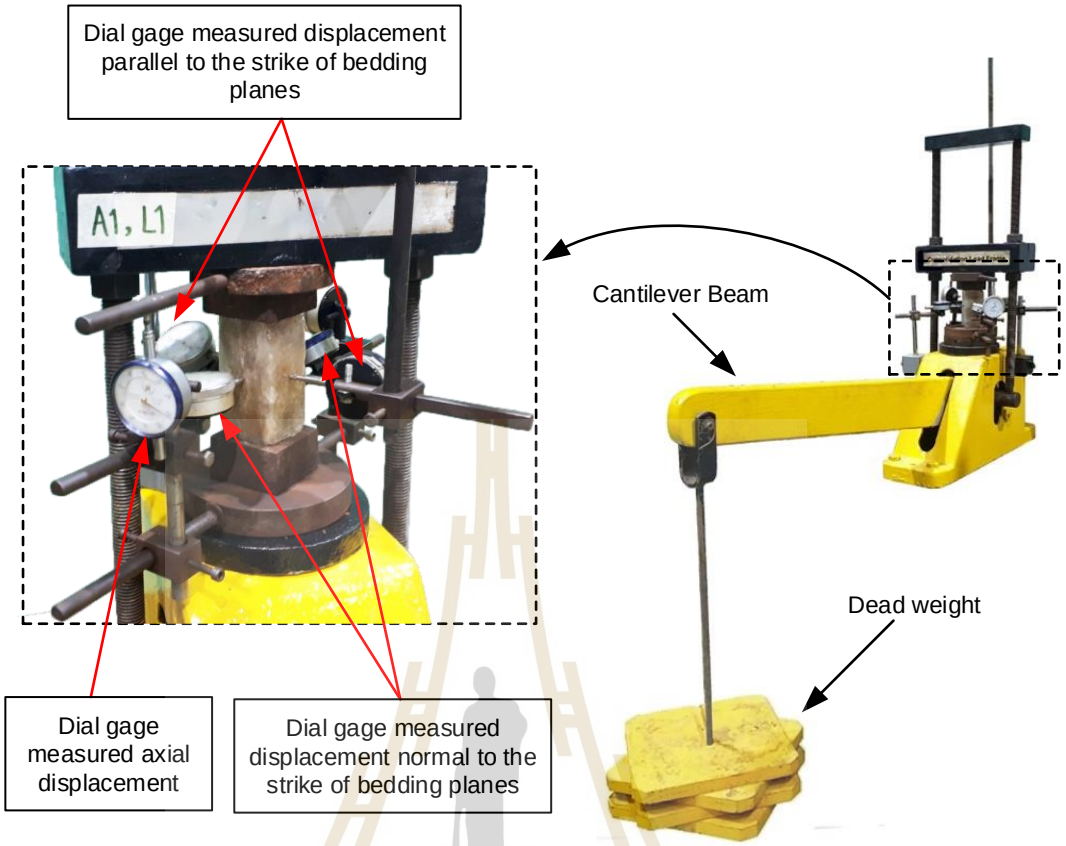

Figure 4.1 Laboratory arrangement for uniaxial creep test

4.3 Triaxial creep test

The test procedure and calculation follow the ASTM D7070-08 standard practice, except the specimen shape. All specimens are tested under the same constant octahedral shear stress (τ_{oct}) of 9 MPa. This shear stress magnitude is selected based on previous studies (Archeeploha et al., 2017 and Fuenkajorn et al., 2012) on the same salt. It is sufficiently high to induce plastic creep to the specimens, but not too excessive to cause failure. The constant axial stress (σ_1) and lateral stresses ($\sigma_2 = \sigma_3$) to salt specimens are applied by polyaxial load frame (Fuenkajorn et al., 2012 and Sriapai et al., 2013) as shown in Figure 4.2. The axial stress is applied by a hydraulic pump. The test frame utilizes two pairs (N-S direction and E-W direction) of cantilever beams to apply lateral stresses to the specimen. Before testing, the two pairs of cantilever beam with dead load is calibrated to obtain truly constant axial stress to specimens. The salt specimen is installed into the center of the load frame by six loading platens arranged in three mutually perpendicular directions and strike of

bedding plane parallel to N-S cantilever beams, as show in Figure 4.3. To minimize friction, neoprene sheets are placed at the interfaces between specimen surfaces and the platens. The test is performed under 2 stage: hydrostatic stress and pre-defined octahedral shear stress stage. The test frame utilizes two mutually perpendicular cantilever beams and dead load to apply confining pressures (lateral stresses) range from 3, 6, 12 and 24 MPa. The axial stress is applied by hydraulic cylinder connected to a hydraulic pump first and then maintained for a minimum of one hour primarily to ensure that the salt specimen is under hydrostatic condition. Then adjusted to obtain the pre-defined octahedral shear stress. The applied stresses for triaxial creep test are calculated from the three principal stresses as (Jaeger et al., 2007)

$$\tau_{oct} = (1/3)\{(\sigma_1 - \sigma_2)^2 + (\sigma_2 - \sigma_3)^2 + (\sigma_3 - \sigma_1)^2\}^{1/2} \quad (4.1)$$

Table 4.1 shows the summary of loading conditions for triaxial creep test. One salt specimen is used for each confining pressure and bedding plane orientation. All bedding plane orientations have been subjected to confining pressures from 3 to 12 MPa. Except under confining pressures of 24 MPa, the specimens are tested only β = 0° and 90°. Each specimen is tested for 10 days. The displacement dial gages are installed to measure the axial and lateral deformations that parallel and normal to the strike of bedding planes. During the test, the salt deformations are recorded to the nearest 0.001 mm. The reading intervals are made once every minute for the first 10 minutes of testing and increased to every 3 minutes for 15 minutes later, every 15 minutes until 1 hour, and every 30 minutes until the end of the test. All tests are conducted under ambient temperature (25° ± 2° Celsius).

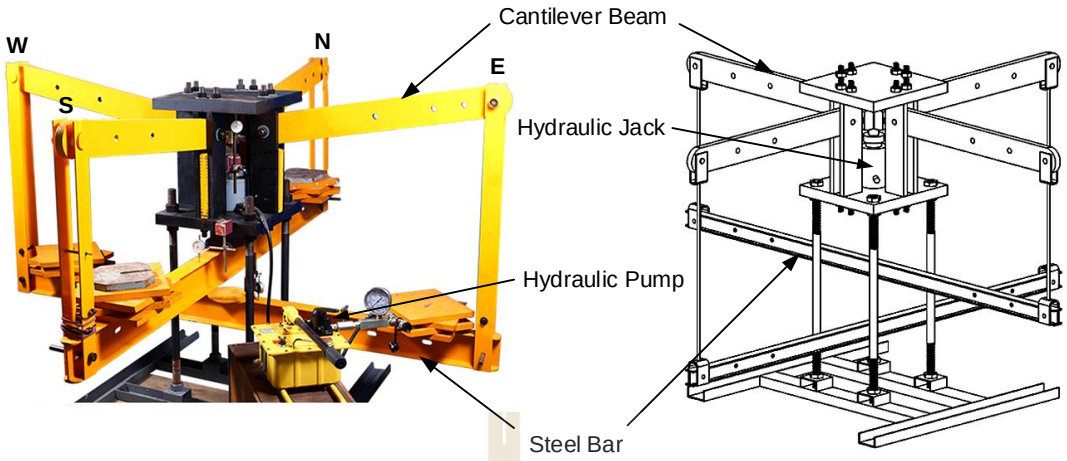

Figure 4.2 Polyaxial load fame (Fuenkajorn et al., 2012)

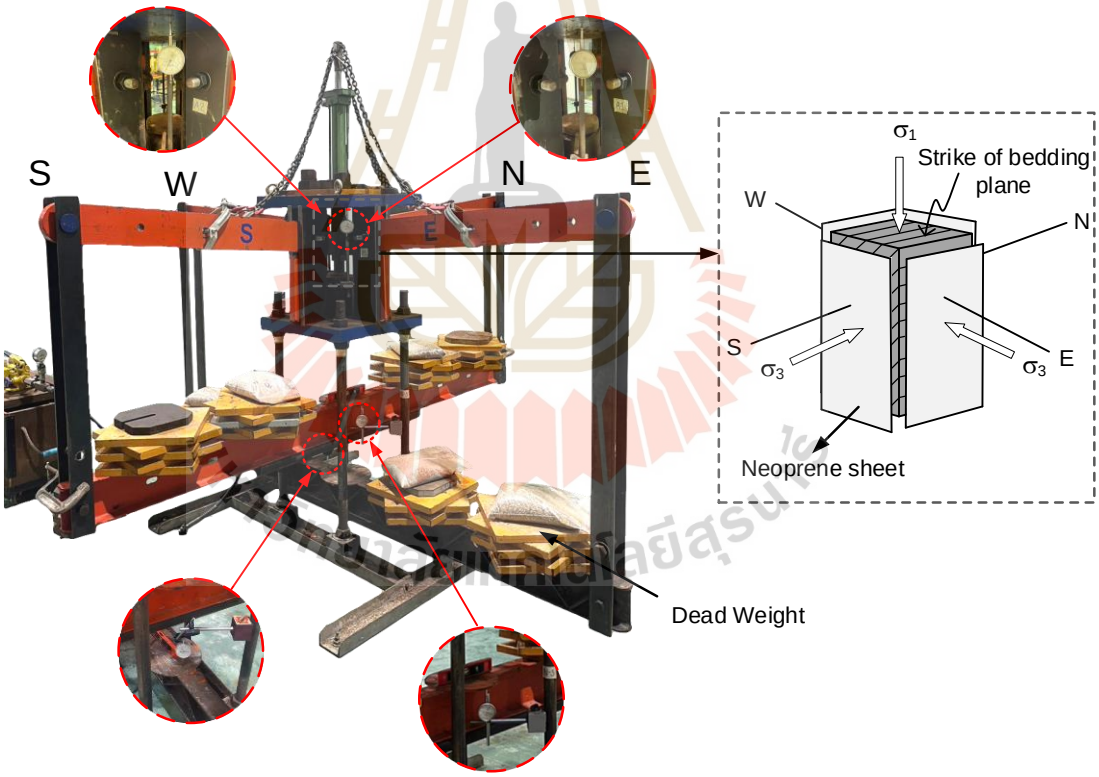

Figure 4.3 Direction of salt specimen arrangement and displacement dial gages installation.

Table 4.1 Loading conditions for triaxial creep test

σ_3 (MPa)	σ_1 @Hydrostatic (MPa)	σ_1 @τ_{oct} 9 MPa (MPa)
3	2	22
6	5	25
12	9	31
24	18	43

4.4 Test results

4.4.1 Uniaxial creep test

The strain-time curves obtained from the uniaxial creep testing as shows in Figure 4.4, where ε_1 represents axial strain, and ε_{3P} and ε_{3O} are lateral strains parallel and normal to the strike of bedding planes. Symbols of measured strain directions are given in this figure. The curves exhibit a non-linear trend and show three creep phases with the instantaneous, transient and steady-state creep phases of the rock salt deformation. Rock salt specimens first undergo instantaneous elastic deformation after each load condition is applied and enters the transient phase. Then, the creep rate gradually decreases with increasing time after that the creep tends to be in the steady-state creep phase when the creep rate becomes constant. The ε_1, ε_{3P} and ε_{3O} decrease with the β angle increases. The ε_{3O} are higher than ε_{3P} for $\beta > 0°$, but quite close for specimens with $\beta = 0°$.

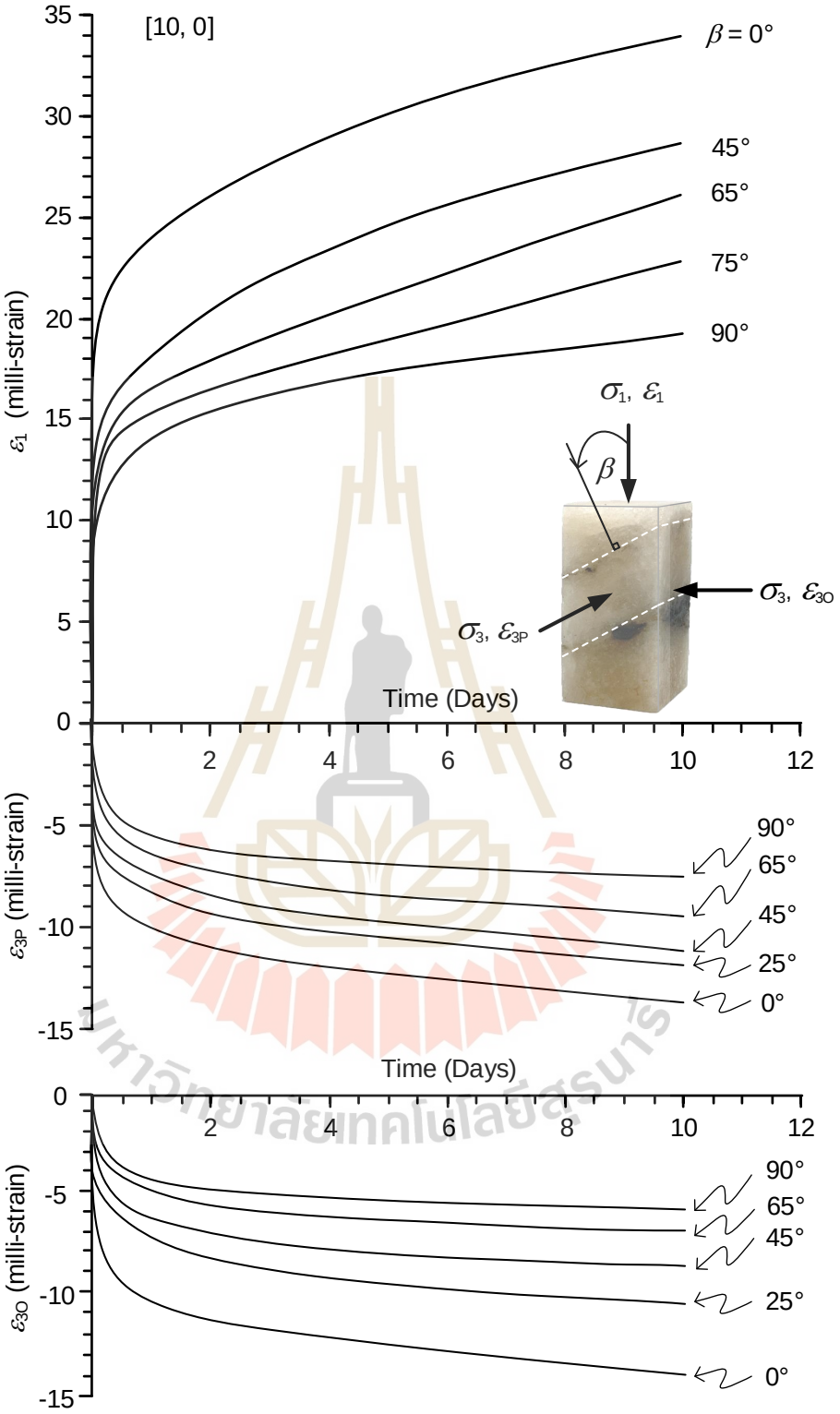

Figure 4.4 Strain-time curves of salt specimen with angles β for uniaxial creep test. Number in bracket indicate applied stresses in MPa [σ_1, σ_3]

4.4.2 Triaxial creep test

The strain-time curves with angles β obtained from the triaxial creep testing under confining pressures of 3, 6, 12 and 24 MPa as show in Figures 4.5 to 4.8, respectively. Instantaneous, transient and steady-state creep phases can be observed for the three strains measured from all angles β. The axial strains obtained from $\beta = 0°$ (normal to bedding plane) are always greater than these from $\beta = 90°$ (parallel to bedding plane). The axial strain (ε_1) decreases with the β angle increases. This is also true for both lateral strains (ε_{3P} and ε_{3O}) obtained under the same confining pressure. The differences between ε_{3P} and ε_{3O} magnitudes are greatest at $\beta = 90°$ ($\varepsilon_{3P} > \varepsilon_{3O}$). They reduce when angles β reduce toward 0 degree. The differences between the creep strains measured from the specimen with $\beta = 0°$ and with $\beta = 90°$ significantly decrease as the confining pressures increase, suggesting that under high confinement test time-dependent deformation of the salt specimens become more isotropic.

Figure 4.9 shows the close-up image of all post-test specimens for triaxial creep test. The deformation pattern that observed from the salt specimens subjecting to creep testing is controlled by two main mechanisms: dislocation climb (sliding between inter-crystalline boundaries) and dislocation glide (sliding between cleavage planes). Under low confinement, the salt crystals tend to be deformed along the bedding plane direction. Under high confinement, salt crystals are dense and have laterally elongated deformation that hardly relates to bedding plane direction.

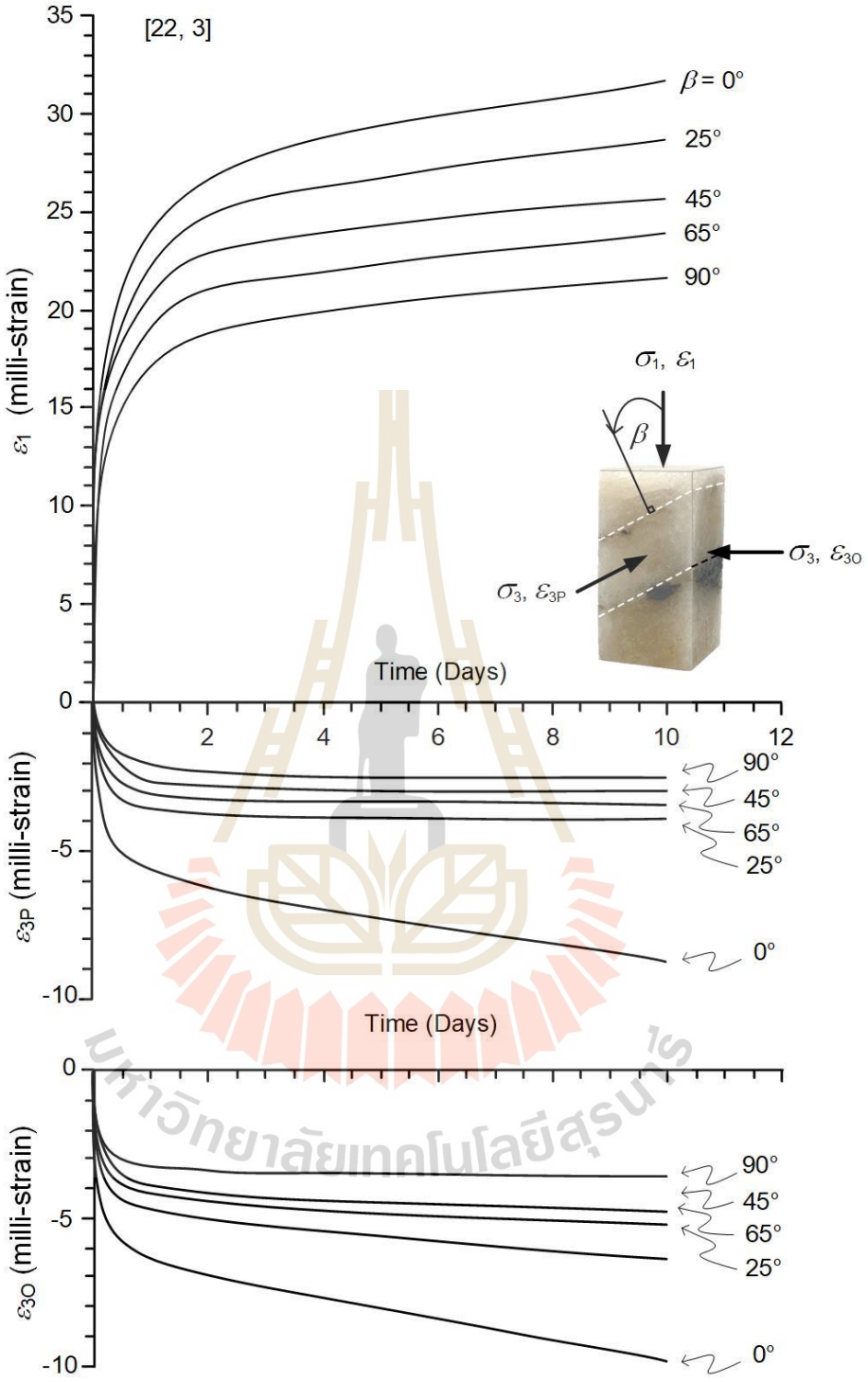

Figure 4.5 Strain-time curves of salt specimen with angles β for triaxial creep test under confining pressure 3 MPa. Number in bracket indicate applied stresses in MPa [σ_1, σ_3]

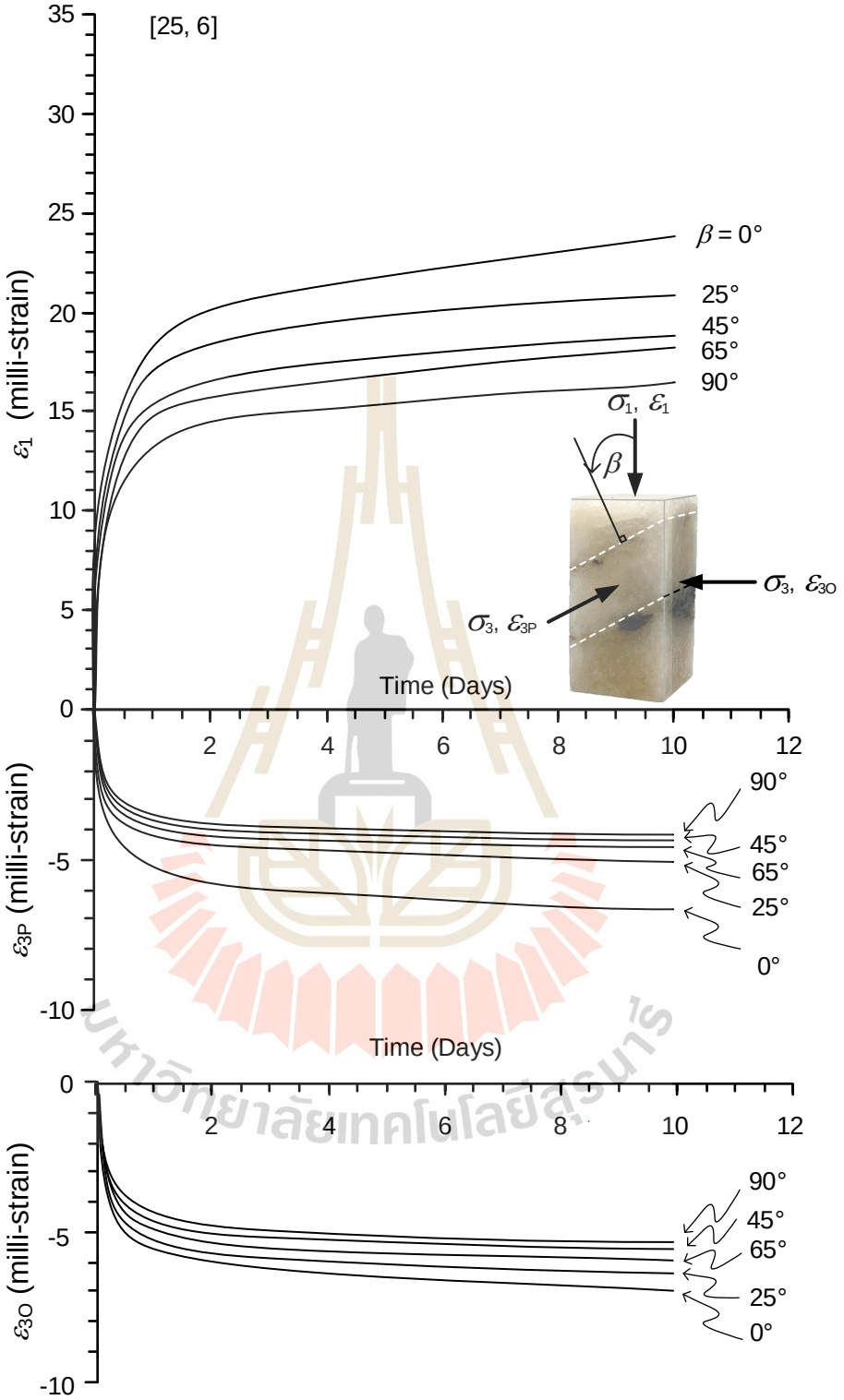

Figure 4.6 Strain-time curves of salt specimen with angles β for triaxial creep test under confining pressure 6 MPa. Number in bracket indicate applied stresses in MPa [σ_1, σ_3]

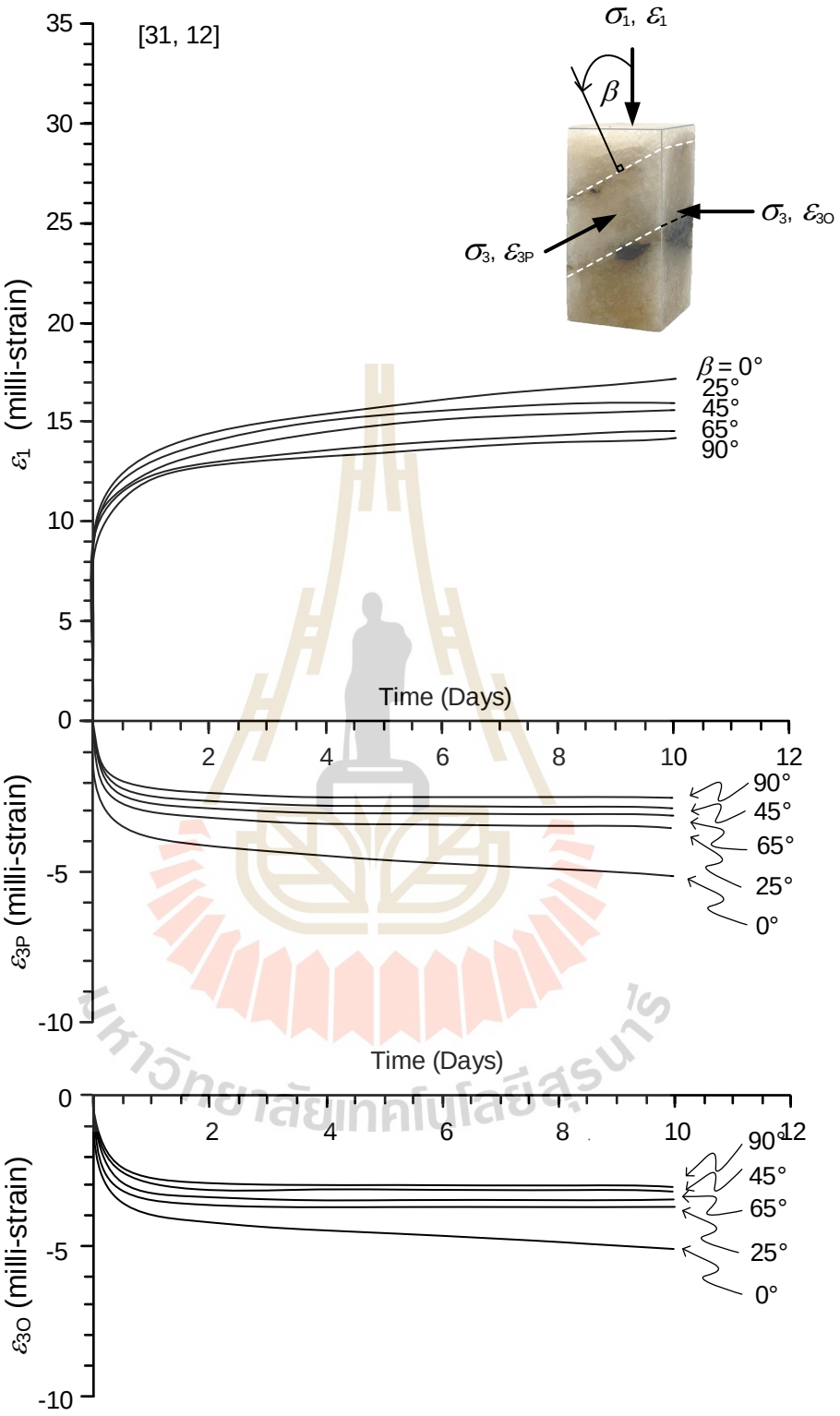

Figure 4.7 Strain-time curves of salt specimen with angles β for triaxial creep test under confining pressure 12 MPa. Number in bracket indicate applied stresses in MPa [σ_1, σ_3]

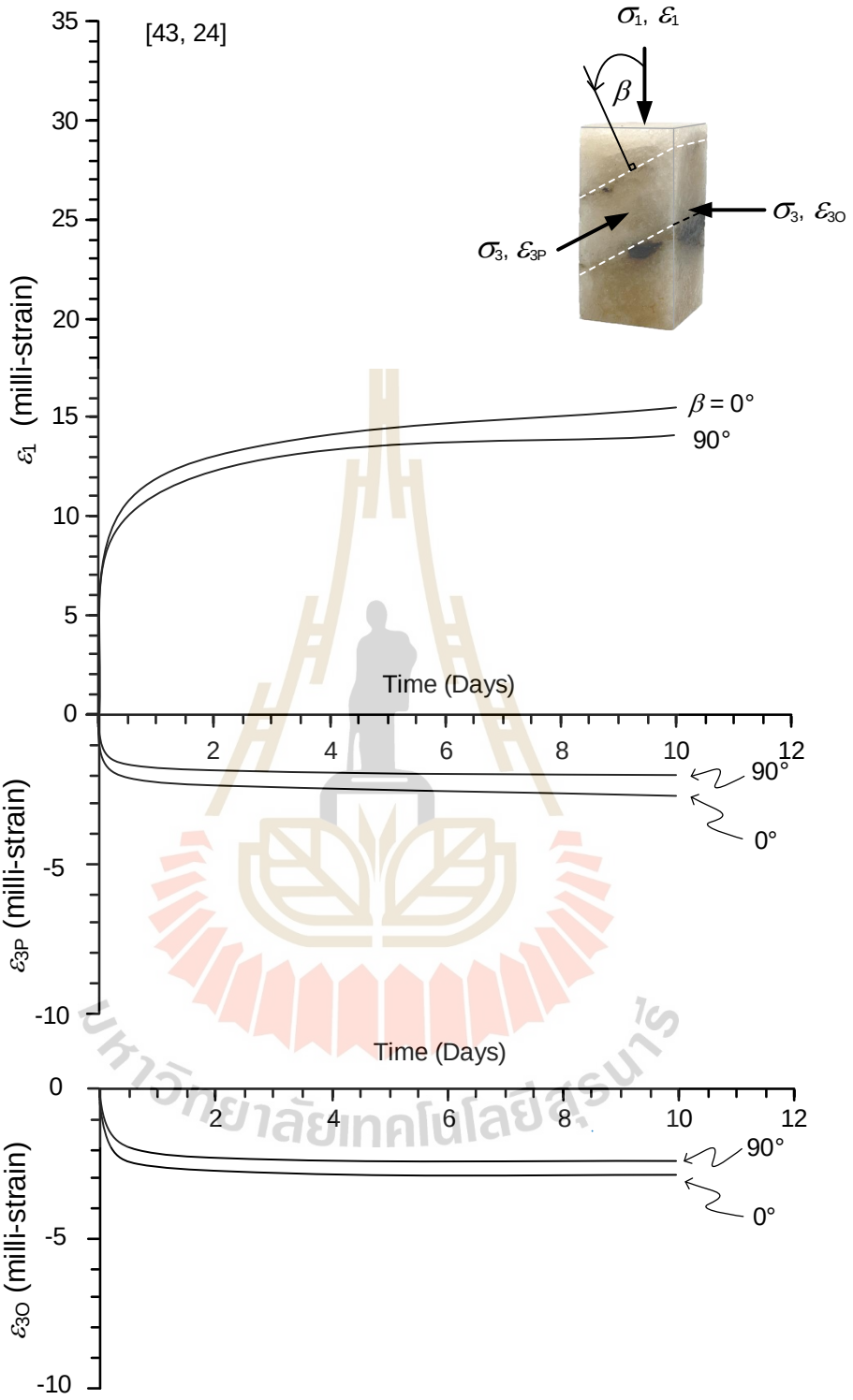

Figure 4.8 Strain-time curves of salt specimen with angles β for triaxial creep test under confining pressure 24 MPa. Number in bracket indicate applied stresses in MPa [σ_1, σ_3]

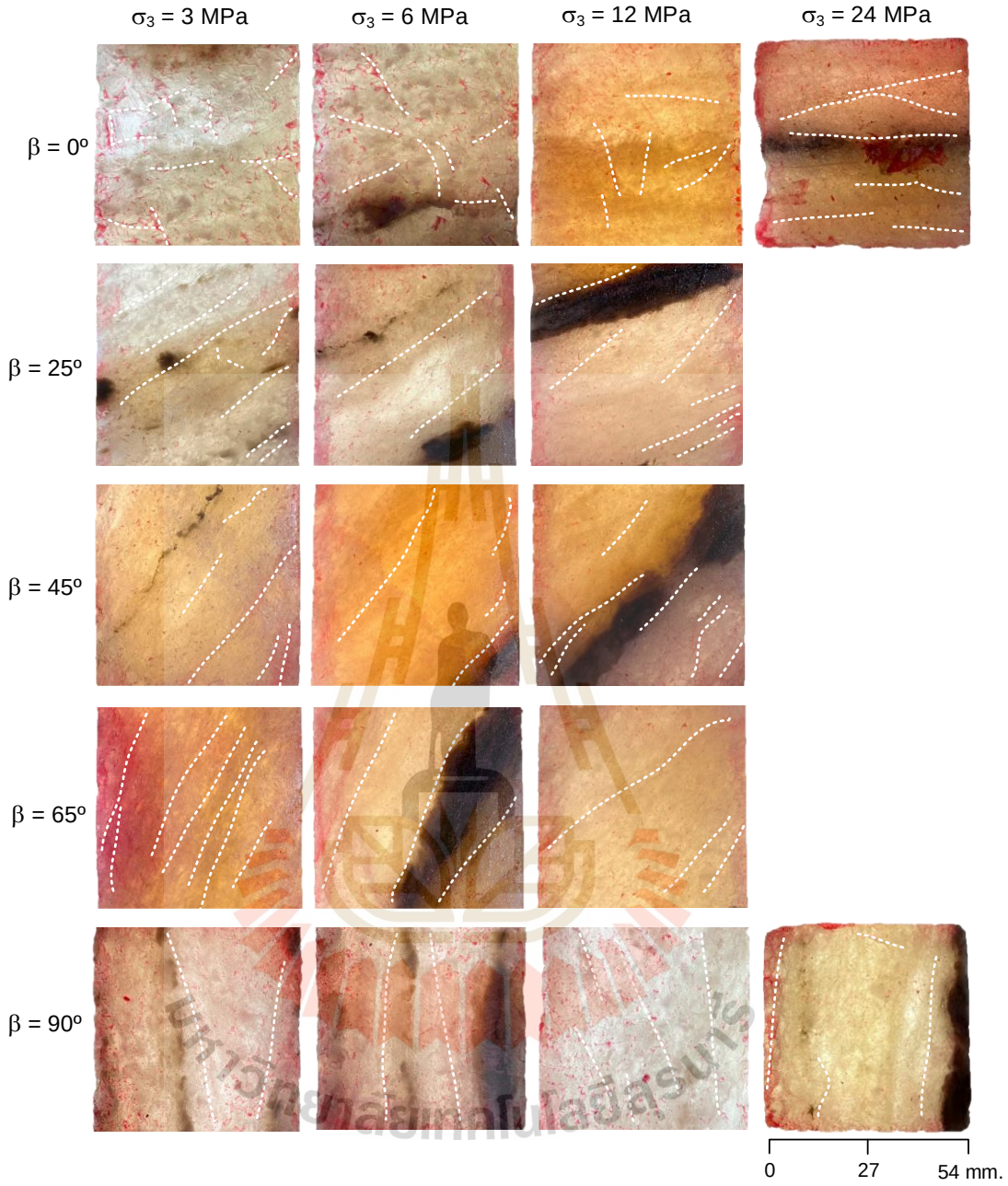

Figure 4.9 Close-up image of salt crystals after testing under confining pressures of 3, 6, 9, 12 and 24 MPa with difference angles β. White dash lines indicate dislocation planes induced after testing.

CHAPTER V
CALIBRATION OF BURGERS PARAMETERS

5.1 Introduction

The propose of this chapter is to describe the derivation of stress-strain deviations as a function of time based on the Burgers model. Burgers parameters are calibrated by these equations from the creep test result, as described in Chapter IV. The objective is to help explain the creep behavior of rock salt with various bedding plane orientations.

5.2 Stress-strain deviation as a function of time

Stress-strain deviation is used here to describe the salt deformation because it considers both mean stress-strain and deviatoric stress-strain. The mean stresses (s) and stress deviations (s_i) along principal axes can be calculated by using the following equations (Jaeger et al., 2007):

$$s_i = \sigma_i - s \tag{5.1}$$

$$s = (1/3)\cdot(\sigma_1 + 2\sigma_3) \tag{5.2}$$

where i represents notation along principal axes. i = 1, 3P and 3O represent directions along major principal axis, parallel to bedding plane and normal to bedding plane, respectively.

The mean strains (e) and strain deviations (e_i) of each specimen are calculated by using the following equations:

$$e_i = \varepsilon_i - e \tag{5.3}$$

$$e = (1/3)\cdot(\varepsilon_1 + \varepsilon_{3O} + \varepsilon_{3P}) \tag{5.4}$$

where ε_1 is the major principal strain, ε_{3O} and ε_{3P} are principal strains measured normal and parallel to the strike of bedding planes.

The strain deviation - time curves from uniaxial creep test are shown in Figure 5.1 and for triaxial creep test in Figure 5.2.

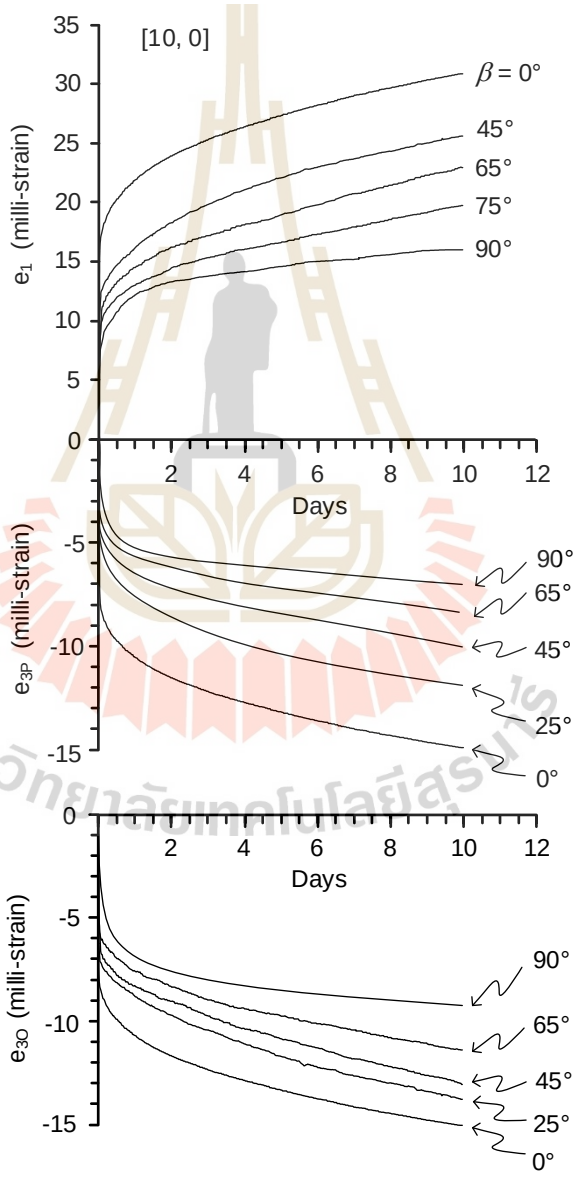

Figure 5.1 Strain deviation-time curves of salt specimens with angles β for uniaxial creep test under axial stress of 10 MPa. Numbers in bracket represent [σ_1, σ_3].

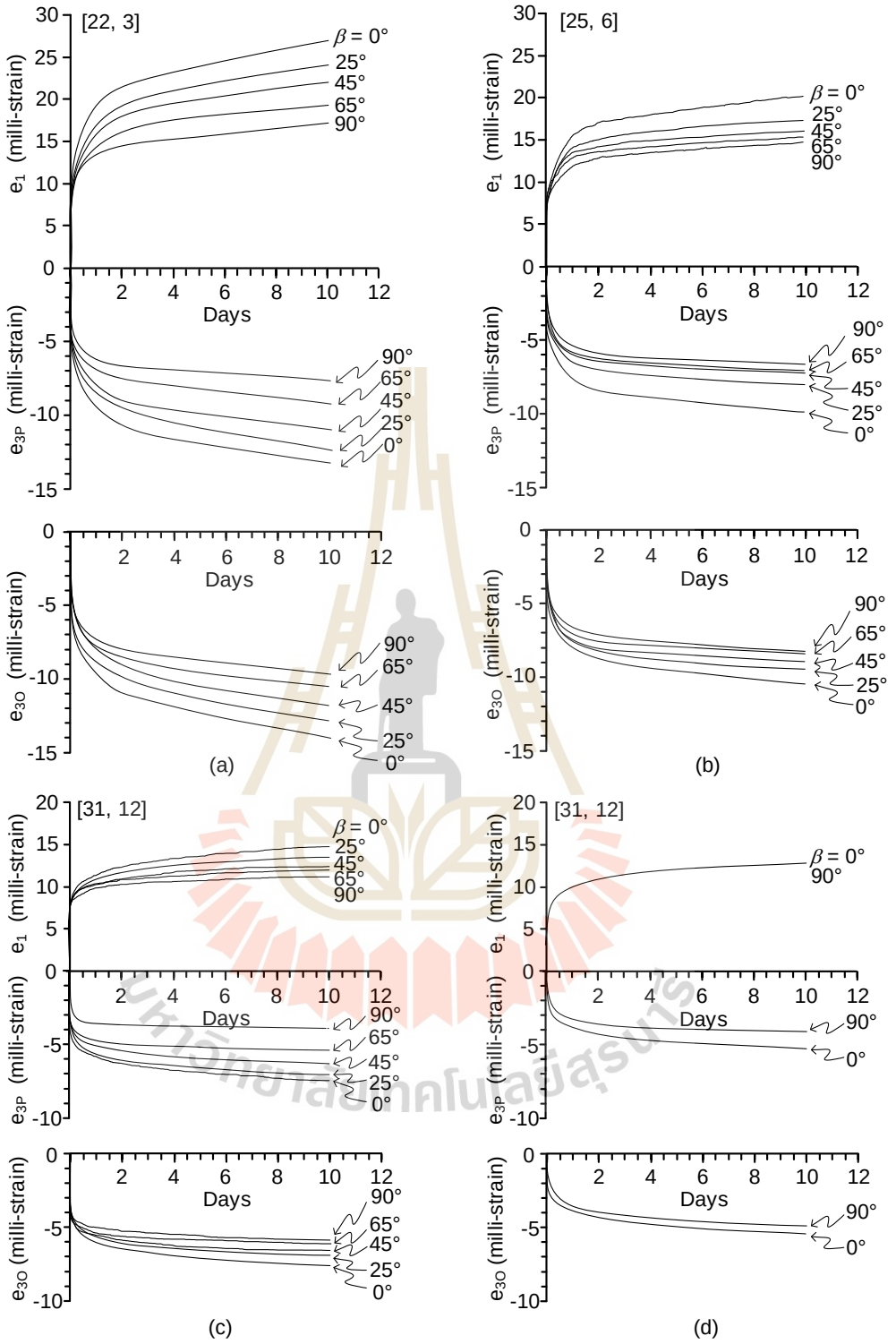

Figure 5.2 Strain deviation-time curves of salt specimens with angles β for triaxial creep test under the confining pressure of 3 MPa (a), 6 MPa (b), 12 MPa (c), and 24 MPa (d). Numbers in bracket represent [σ_1, σ_3].

5.3 Burgers creep model

Derivation of governing equations for stress-strain deviation based on the Burgers model (Richard, 1993) is described in this section. It is recognized that the Burgers model has been widely used to describe the time-dependent behavior of rock salt (e.g., Gnirk and Johnson, 1964; Handin et al., 1984; Langer, 1984; Hardy and Sun, 1986; Senseny et al., 1992). This is because it is simple and can describe the elastic, visco-elastic and visco-plastic phases separately. The arrangement of physical components in the Burgers model is shown in Figure 5.3. The Burgers model includes the elastic component (E_I) representing the characteristics of instantaneous phase, a parallel combination of elastic and viscous components (E_V and η_v) representing the transient phase, and viscous component (η_P) representing steady-state phase of creep deformation.

Relation of stress-strain deviation can be written as (Jaeger et al., 2007):

$$e_i = \frac{s_i}{2G} \tag{5.5}$$

$$\text{where } G = \frac{E}{2(1+\nu)} \tag{5.6}$$

where G is shear modulus, E is the elastic modulus and ν is the Poisson's ratios.

Substituting Equations (5.6) into (5.5), the stress-strain deviation in term of elastic modulus and Poisson's ratio can be written as:

$$e_i = \left(\frac{1}{E}\right)s_i + \left(\frac{\nu}{E}\right)s_i; \tag{5.7}$$

The stress-strain deviation is derived using Laplace transformation and time operators of the Burgers model. From the Equation (5.7):

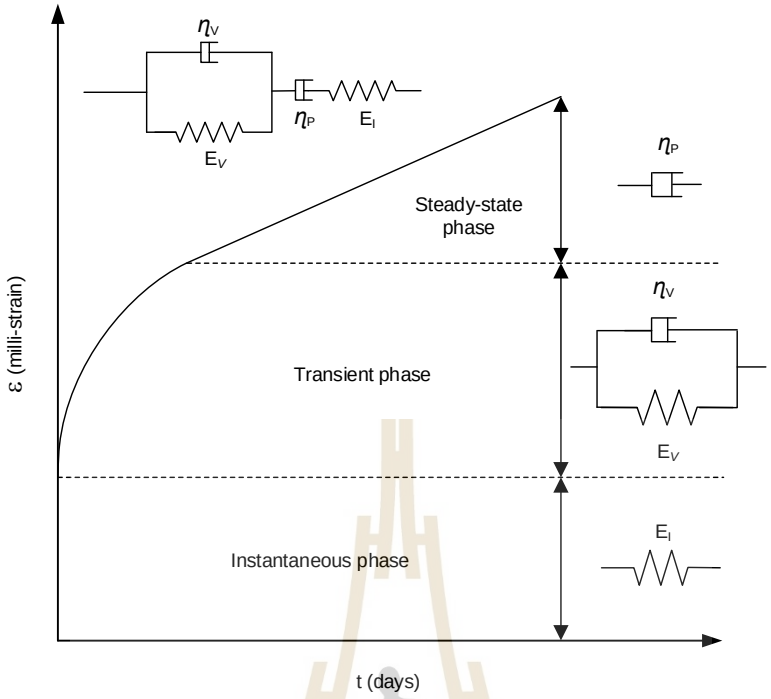

Figure 5.3 Modular components of Burgers model.

$$\hat{e}_i(s) = \left(\frac{1}{\hat{E}(s)}\right)\hat{s}_i(s) + \left(\frac{\hat{\nu}(s)}{\hat{E}(s)}\right)\hat{s}_i(s) \tag{5.8}$$

Substituting $\hat{s}_i(s) = \frac{s_i}{s}$; $\hat{E}(s) = \frac{9K\hat{Q}_1}{(\hat{Q}_1 + 6K\hat{P}_1)}$; $\hat{\nu}(s) = \frac{3K\hat{P}_1 - \hat{Q}_1}{(\hat{Q}_1 + 6K\hat{P}_1)}$, and performing inverse Laplace transformation, the relation of stress – strain deviations as a function of time can be expressed as:

$$e_i(t) = \left(\frac{1}{E_{I,i}} + \frac{t}{\eta_{P,i}} + \frac{1}{E_{V,i}}\left(1 - \exp\left(\frac{-E_{V,i}t}{\eta_{V,i}}\right)\right)\right)s_i \tag{5.9}$$

where $E_{I,i}$ is elastic modulus (GPa), $E_{V,i}$ is the spring constant in transient phase (GPa), $\eta_{P,i}$ is the viscosity coefficient in steady-state phase (GPa·Day), $\eta_{V,i}$ is the viscosity coefficient in transient phase (GPa·Day) and t is the testing time (day).

The relation of stress – strain deviations as a function of time along the major principal stress ($e_1(t)$) can be expressed as:

$$e_1(t)=\left(\frac{1}{E_{I,1}}+\frac{t}{\eta_{P,1}}+\frac{1}{E_{V,1}}\left(1-\exp\left(\frac{-E_{V,1}t}{\eta_{V,1}}\right)\right)\right)s_1 \tag{5.10}$$

The relation of stress – strain deviations as a function of time along the minor principal axes normal ($e_{3O}(t)$) and parallel ($e_{3P}(t)$) to bedding planes:

$$e_{3O}(t)=\left(\frac{1}{E_{I,3O}}+\frac{t}{\eta_{P,3O}}+\frac{1}{E_{V,3O}}\left(1-\exp\left(\frac{-E_{V,3O}t}{\eta_{V,3O}}\right)\right)\right)s_{3O} \tag{5.11}$$

$$e_{3P}(t)=\left(\frac{1}{E_{I,3P}}+\frac{t}{\eta_{P,3P}}+\frac{1}{E_{V,3P}}\left(1-\exp\left(\frac{-E_{V,3P}t}{\eta_{V,3P}}\right)\right)\right)s_{3P} \tag{5.12}$$

Regression analyses with multiple variables and constants are performed to determine the Burgers parameters for all principal strain deviations for each salt specimen using the SPSS statistical software (Wendai, 2000). The comparison between test result and curves fitting with Burgers model are shown in Appendix A. The model fits well to the test results for all different bedding plane orientations and confining pressures, which is evidenced by the coefficient of correlations values (R^2) greater than 0.9. The calibrated Burgers parameters are shown in Tables 5.1, 5.2 and 5.3 respectively.

The parameters obtained from the major principal direction for unconfined and confined condition of 3, 6, 12 and 24 MPa are plotted as a function of bedding plane orientation in Figure 5.4. The diagrams show that the parameters (E_I, E_V, η_P and η_V) tend to increase linearly with bedding plane orientation. This is also true for all confining pressures. The instantaneous creep phase representing by E_I, the transient

creep phase representing by E_V and η_V tend to increase. The steady-state creep phase representing by η_P tend to decrease with increasing confining pressure. The differences between the Burgers parameters obtained from the specimen with $\beta = 0°$ and with $\beta = 90°$ notably decrease as the confining pressures increase, suggesting that the salt specimens become more isotropic under high confinement.

Table 5.1. Burgers parameters calibrated from major principal strain deviation-time curves for each specimen.

β (°)	σ_3 (MPa)	σ_1 (MPa)	Burgers parameters in axial direction				R^2
			$E_{I,1}$ (GPa)	$E_{V,1}$ (GPa)	$\eta_{P,1}$ (GPa·Day)	$\eta_{V,1}$ (GPa·Day)	
0	0	10	0.589	0.836	10.223	1.264	0.946
	3	22	2.343	1.222	31.073	0.987	0.984
	6	25	2.889	1.856	42.080	0.707	0.986
	12	31	3.559	3.031	46.812	0.401	0.913
	24	43	4.041	4.466	49.121	0.364	0.923
25	3	22	2.525	1.416	33.328	1.006	0.935
	6	25	2.987	1.961	43.269	0.731	0.947
	12	31	3.642	3.124	47.265	0.411	0.926
45	0	10	0.746	1.096	12.488	1.464	0.960
	3	22	2.642	1.575	36.552	1.108	0.985
	6	25	3.122	2.253	46.684	0.741	0.938
	12	31	3.742	3.282	50.512	0.426	0.913
65	0	10	2.795	1.393	14.869	1.553	0.983
	3	22	3.298	1.768	41.263	1.134	0.968
	6	25	3.806	2.591	49.500	0.789	0.922
	12	31	2.795	3.395	52.790	0.438	0.931
75	0	10	1.275	1.624	15.856	1.633	0.952
90	0	10	1.502	1.825	16.802	1.677	0.933
	3	22	3.053	2.020	44.431	1.156	0.964
	6	25	3.431	2.711	52.265	0.806	0.968
	12	31	3.922	3.544	55.929	0.445	0.928
	24	43	4.352	4.685	56.632	0.370	0.946

Table 5.2. Burgers parameters calibrated from minor principal axes normal to bedding plane.

β (°)	σ_3 (MPa)	σ_1 (MPa)	Burgers parameters normal to bedding plane strike direction				R^2
			$E_{I,3O}$ (GPa)	$E_{V,3O}$ (GPa)	$\eta_{P,3O}$ (GPa·Day)	$\eta_{V,3O}$ (GPa·Day)	
0	3	22	1.363	1.308	32.071	0.761	0.986
	6	25	1.863	1.906	43.367	0.525	0.986
	12	31	3.861	3.113	48.017	0.311	0.929
	24	43	4.965	4.513	50.501	0.284	0.923
25	3	22	1.415	1.385	32.486	0.845	0.915
	6	25	1.909	1.926	44.179	0.534	0.941
	12	31	3.873	3.120	48.365	0.329	0.906
45	3	22	1.486	1.454	33.125	0.998	0.945
	6	25	1.982	1.934	45.181	0.657	0.921
	12	31	3.891	3.127	48.907	0.363	0.916
65	3	22	1.562	1.505	33.125	0.998	0.932
	6	25	1.996	2.944	45.181	0.657	0.936
	12	31	3.913	3.143	48.907	0.363	0.940
90	3	22	1.650	1.550	33.758	1.099	0.969
	6	25	2.070	1.952	45.401	0.666	0.968
	12	31	3.925	3.158	49.161	0.385	0.878
	24	43	4.222	4.564	51.397	0.302	0.942

Table 5.3. Burgers parameters calibrated from minor principal axes parallel to bedding plane.

β (°)	σ_3 (MPa)	σ_1 (MPa)	Burgers parameters parallel to bedding plane strike direction				R^2
			$E_{I,3P}$ (GPa)	$E_{V,3P}$ (GPa)	$\eta_{P,3P}$ (GPa·Day)	$\eta_{V,3P}$ (GPa·Day)	
0	3	22	1.361	1.306	32.019	0.763	0.982
	6	25	1.862	1.935	43.317	0.526	0.986
	12	31	3.863	3.118	48.178	0.309	0.944
	24	43	4.966	4.516	50.503	0.283	0.911
25	3	22	1.458	1.452	37.625	0.895	0.932
	6	25	1.878	2.073	44.854	0.575	0.954
	12	31	4.002	3.218	50.397	0.326	0.958
45	3	22	1.565	1.958	42.365	1.005	0.954
	6	25	1.981	2.473	50.502	0.764	0.916
	12	31	4.062	3.510	54.157	0.397	0.923
65	3	22	1.682	1.985	42.365	1.005	0.901
	6	25	2.008	2.473	50.502	0.764	0.902
	12	31	4.104	3.510	54.157	0.397	0.842
90	3	22	1.859	2.026	44.425	1.142	0.954
	6	25	2.257	2.708	52.285	0.802	0.969
	12	31	4.081	3.577	55.912	0.442	0.884
	24	43	4.328	4.672	56.645	0.364	0.908

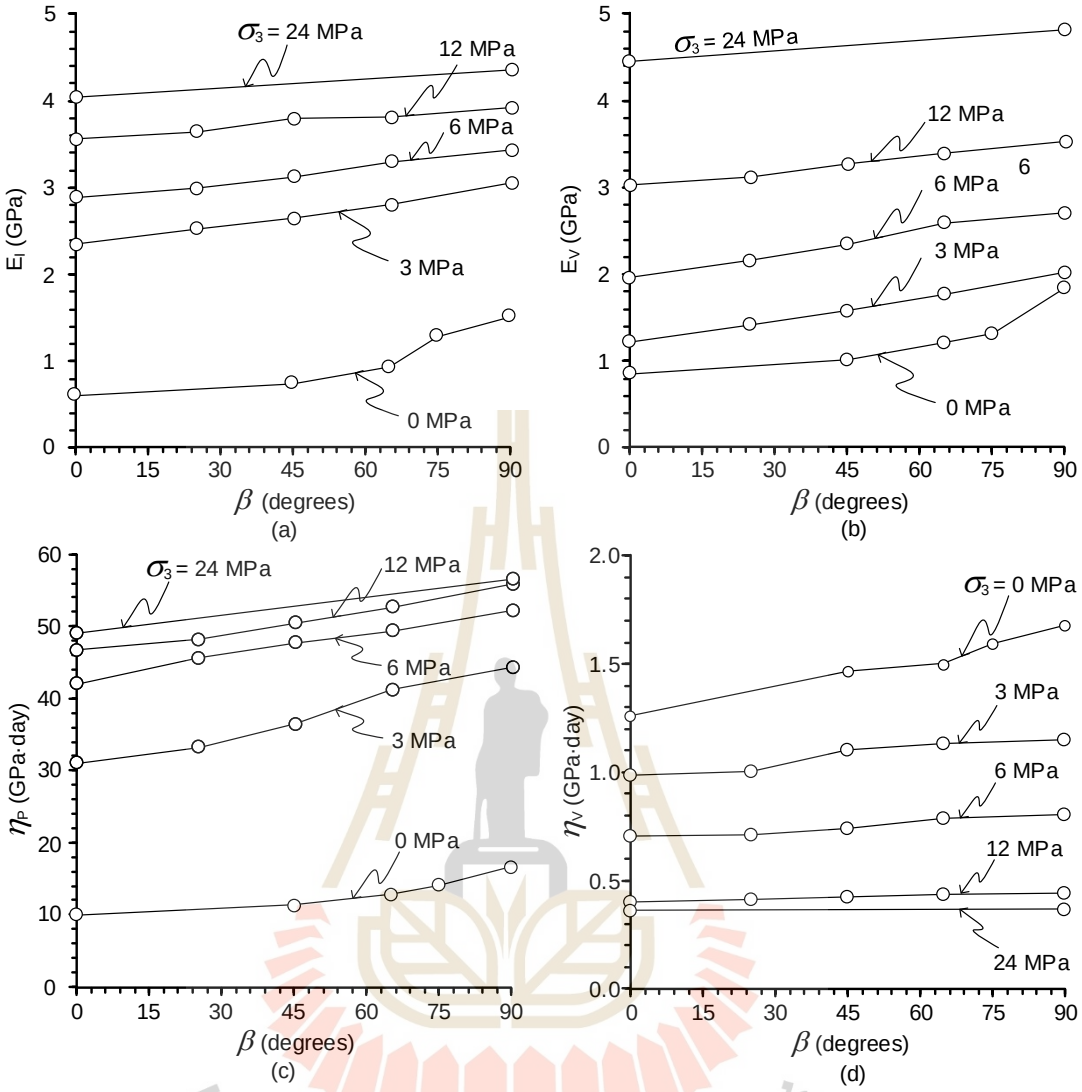

Figure 5.4 Burgers parameters, E_I (a), E_V (b), η_P (c) and η_V (d) with bedding plane orientation (β) for various confining pressure.

CHAPTER VI
ANALYSIS OF TEST RESULTS

6.1 Introduction

The propose of this chapter is to describe the effect of transverse isotropy on Burgers parameters under confinement for constant octahedral shear strains (γ_{oct}) of 9 MPa. The Burgers parameters with the transverse isotropic angle and confining pressure are described by elliptic equations. The Burgers creep parameters are used to represent instantaneous, visco-elastic, visco-plastic deformations of salt specimens. The degrees of anisotropy are determined in term of elastic, visco-elastic and visco-plastic deformations. Additionally, the confining pressures at which salt becomes isotropic are predicted. The relations of octahedral shear strains and volumetric strains are used to determine the transition zone (transient creep phase) between instantaneous and steady state phases under different bedding plane orientations. The creep phase evolution of transverse isotropic salt is presented.

6.2 Effect of transverse isotropy on creep properties under confinement

Creep properties described by the Burgers model can be separated into three phases: instantaneous deformation, visco-elastic, and visco-plastic creep phases, which can be represented here by $1/E_I$, $(1/E_V)$ $[1-\exp(-E_V/\eta_V)]$ and $1/\eta_P$, respectively. The visco-elastic term is, hereafter, represented in short by E_V^*. The relations between these parameters and bedding orientation as shown in Figure 6.1 follow an elliptical shape, reflecting the transverse isotropy. Elliptic equation is applied to represent the evolution of the three Burgers terms with the transverse isotropic angle β. Similar approach has been used by Hwu and Ting (1989) and Jiang (2016) who apply elliptic equation to describing apparent elastic moduli of anisotropic materials. The classical elliptic equation in the form of polar coordinate can be written as (Korn and Korn 1961; Polyanin and Manzhirov 2006):

$$r(\beta) = a / \{1 + [((a^2 - b^2) - 1) \cdot \cos^2 \beta]\} \quad (6.1)$$

where r is radius of ellipse, a and b are constants along x and y axes, and β is transverse isotropic angle measured clockwise from y-axis. Here, the parameters a and b represent the intrinsic deformation terms used in the Burgers model obtained from β = 90° and 0°.

From Equation (6.1) the Burgers parameters (E_I, η_P, E_V^*) can then be written as a function for transverse isotropic angle β in the forms of elliptic equations as:

$$E_I(\beta) = E_{I,90°} / \{1 + [((E_{I,90°} / E_{I,0°})^2 - 1) \cdot \cos^2 \beta]\}^{1/2} \quad (6.2)$$

$$\eta_P(\beta) = \eta_{P,90°} / \{1 + [((\eta_{P,90°} / \eta_{P,0°})^2 - 1) \cdot \cos^2 \beta]\}^{1/2} \quad (6.3)$$

$$E_V^*(\beta) = E_{V,90°}^* / \{1 + [((E_{V,90°}^* / E_{V,0°}^*)^2 - 1) \cdot \cos^2 \beta]\}^{1/2} \quad (6.4)$$

For β = 0° and 90°, $E_{I,0°}$ and $E_{I,90°}$ are intrinsic spring constants, $\eta_{P,0°}$ and $\eta_{P,90°}$ are intrinsic viscosity coefficients in steady-state creep phase, and $E_{V,0°}^*$ and $E_{V,90°}^*$ are intrinsic visco-elastic terms. Substituting the intrinsic parameters given in Table 6.1 into Equations (6.2) through (6.4), the E_I, E_V^*, η_P for 0°< β <90° under all confining pressure and bedding plane angles can be predicted. The comparisons of predictions (solid lines) and test results (point) are shown in Figure (6.1). The diagrams show that E_I and η_p (Figures. 6.1(a) and 6.1(c)) are greatest at β = 90° (axial stress parallel to bedding plane) and lowest at β = 0° (axial stress normal to bedding plane). Both parameters increase with confining pressure for all transverse isotropic angles β. The parameter E_V^* are lowest at β = 90° and greatest at β = 0° (Figure 6.1(b)). They become smaller as the confining pressure increases. The discrepancies of the Burgers parameters from all angles β also reduce with increasing the confining pressure, suggesting that salt specimens become more isotropic under high confinements.

Table 6.1. Intrinsic creep parameters.

σ_3 (MPa)	Creep parameters					
	$E_{I,\,0°}$ (GPa)	$E_{I,\,90°}$ (GPa)	$\eta_{P,\,0°}$ (GPa·Day)	$\eta_{P,\,90°}$ (GPa·Day)	$E_V^{*}{}_{,\,0°}$ (GPa)	$E_V^{*}{}_{,\,90°}$ (GPa)
0	0.589	1.502	10.223	16.802	0.762	0.447
3	2.343	3.053	31.073	44.431	0.581	0.409
6	2.889	3.431	42.080	52.265	0.500	0.356
12	3.559	3.922	46.812	55.929	0.330	0.282
24	4.041	4.352	49.121	56.632	0.224	0.213

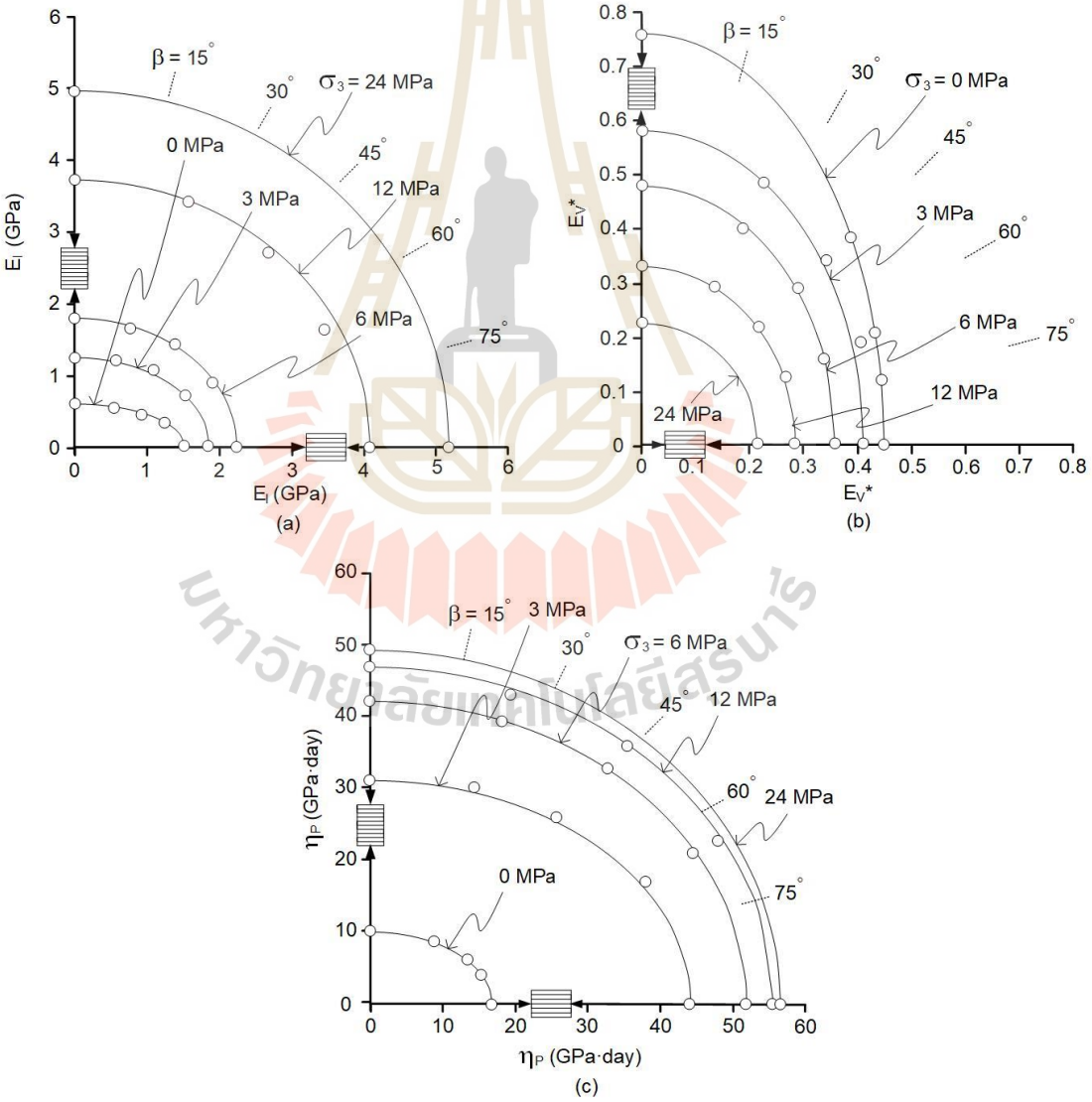

Figure 6.1 Polar plots of E_I (a), E_V^{*} (b) and η_P (c) for various angles β and confining pressures (σ_3). Points are test results and lines are elliptical equation.

The predictions agree well with the test results under all test conditions which can be evaluated by using the mean misfit (f). The mean fit can be calculated by (Riley et al., 1998):

$$f = (1/m)\sum_{i}^{m}\left[(1/n)\left(\sum_{j=1}^{n}(p_c - p_m)^2\right)\right]^{1/2} \quad (6.5)$$

where p_c and p_m are calculated and measured values, n is number of bedding plane angles (β) used for each confining pressure, and m is number of confining pressures. The mean misfits for the apparent E_I, η_P and E_V^* values are determined as 0.05 GPa, 0.84 GPa·Day and 0.02 GPa, respectively. These low values indicate good agreement between the elliptical calculations and measurements.

6.3 Degree of anisotropy

Anisotropic degrees are the values that characterize the anisotropy of rock (Ramamurthy et al., 1993). The degree of anisotropy for transverse isotropic materials is commonly expressed as the maximum-to-minimum Young's modulus ratios or the strength ratios as a function of confining pressures (Fereidooni et al., 2016; Hu et al., 2017; Xu et al., 2018). An attempt is made here to reveal the anisotropy degree of the creep behaviour of bedded salt under octahedral shear stress at 9 MPa. They are presented in the form of the maximum-to-minimum creep parameters on axial direction, ($E_{I,90°}/ E_{I,0°}$, $E_V^*{}_{,0°}/ E_V^*{}_{,90°}$ and $\eta_{P,90°}/ \eta_{P,0°}$). They are plotted in Figure 6.2. Table 6.1 gives their numerical values. The $E_{I,90°}/ E_{I,0°}$ and $E_V^*{}_{,0°}/ E_V^*{}_{,90°}$ considerably decrease, while $\eta_{VP,90°}/ \eta_{VP,0°}$ slightly decrease and become close to 1 (isotropic) as the confining pressure increases. This is probably due to tightening of pre-exist voids and inter-crystalline boundaries parallel to the bedding planes, and stiffening of the soft layers by confinement. They can be best described by power equations:

$$E_{I,90°}/ E_{I,0°} = 1.421\ \sigma_3^{-0.093} \quad (6.6)$$

$$\eta_{P,90°}/ \eta_{P,0°} = 1.544 \cdot \sigma_3^{-0.099} \quad (6.7)$$

$$E_V^*{}_{,0°}/ E_V^*{}_{,90°} = 1.678 \cdot \sigma_3^{-0.139} \quad (6.8)$$

The proposed equations fit well to the test results ($R^2 > 0.9$). Figure 6.3 presents the extrapolation of these empirical equations beyond the confining pressures used here (24 MPa) suggests that at σ_3 about 35-40 MPa instantaneous and visco-elastic creep phase would become isotropic ($E_{I,\,90°}/E_{I,\,0°}$ and $E_V^*{}_{,\,0°}/E_V^*{}_{,\,90°}$ equal to 1). Beyond 80 MPa the visco-plastic creep of salt also reaches an isotropic condition ($\eta_{P,\,90°}/\eta_{P,\,0°} = 1$). Note that the above postulation is true only if the salt is under 9 MPa octahedral shear stress. More discussions on this issue are given in chapter VII.

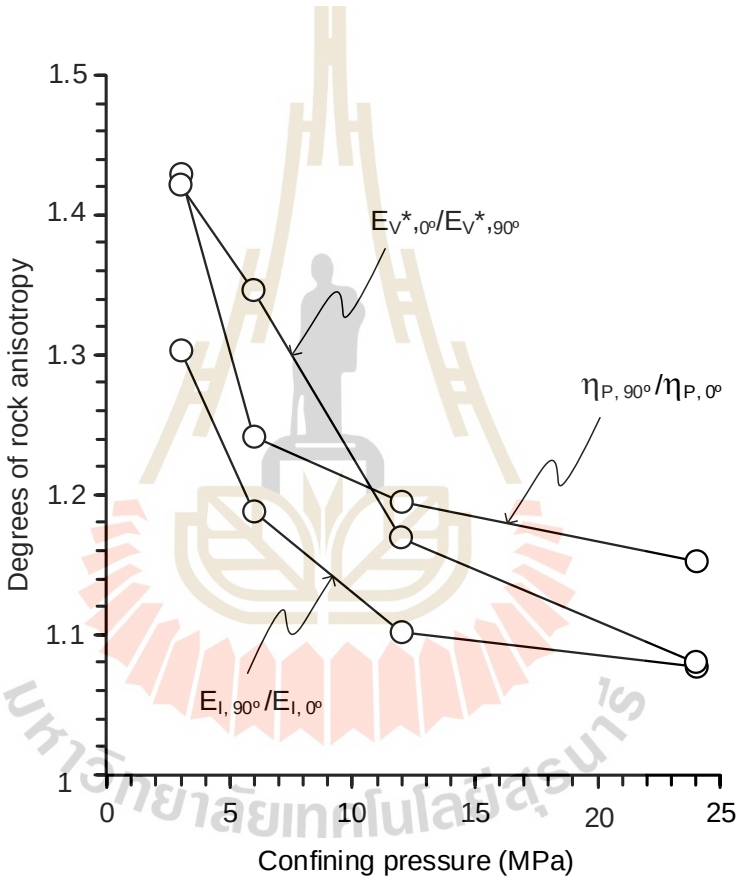

Figure 6.2 Degrees of anisotropy from creep parameters as a function of confining pressure.

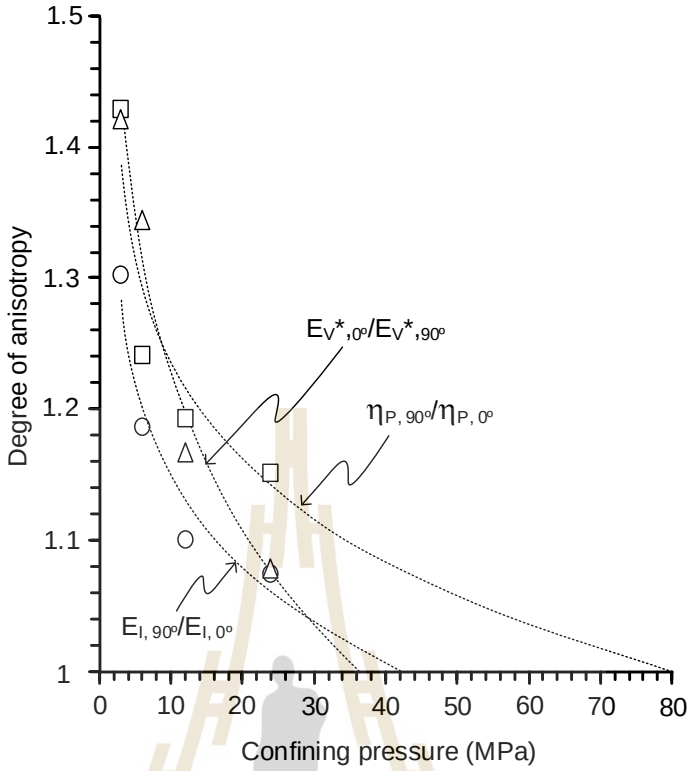

Figure 6.3 Prediction of confining at which salt becomes isotropic.

6.4 Octahedral shear strain (γ_{oct}) and volumetric strain (ε_v) relation under confinement

An attempt is made to determine the range of each phase of deformations from the triaxial creep test results. The transition strains from instantaneous to transient creep and subsequently to steady-state creep phases are difficult to determine precisely from the axial and lateral strain-time curves or from the strain deviation-time relations. As a result, the octahedral shear strains (γ_{oct}) are calculated as a function of volumetric strain (ε_v) for each salt specimen from start loading through the end of 10 days. They can be obtained by (Jaeger et al., 2007):

$$\gamma_{oct} = (1/3)[(\varepsilon_1 - \varepsilon_{3P})^2 + (\varepsilon_1 - \varepsilon_{3O})^2 + (\varepsilon_{3P} - \varepsilon_{3O})^2]^{1/2} \quad (6.9)$$

$$\varepsilon_v = \varepsilon_1 + \varepsilon_{3O} + \varepsilon_{3P} \quad (6.10)$$

Figure 6.4 shows the results of calculations. Immediately after the axial stress is applied and maintained constant, the octahedral shear strain increases linearly with the volumetric strain. This is due to the increase of axial strain which also induces the reduction of specimen volume. Note that the sign convention used throughout this study is that compression and contraction are positive and tension and expansion are negative. The linear relation between γ_{oct} and ε_v represents the range of instantaneous deformation of salt where time-dependent deformation has not yet been reached. The linear relation ends at a point where γ_{oct} continues to increase but the increasing rate of ε_v starts reducing. An example of this transition is denoted in Figure 6.4(a) as open points and the octahedral shear strain at this point are designated as $\gamma_{oct, V}$. As γ_{oct} continues to increase, ε_v tends to approach a constant value. This transition is denoted in Figure 6.4(a) as solid points and the octahedral shear strain at this point are designated as $\gamma_{oct, P}$. The shear strain induced between the two points represents transient creep phase where a combination of elastic and plastic creep occurs. The condition at which the octahedral shear strain increases while volumetric strain remains constant (beyond solid point in Figure 6.4(a)) represents the plastic deformation of the salt in steady-state creep phase. Here the specimen changes shape while its volume remains constant. The γ_{oct} -ε_v relation described above can be observed from all creep test specimens (Figure 6.4). Under the same confinement, the greatest γ_{oct} -ε_v slope in instantaneous phase is obtained from β = 90°. The slopes gradually reduce to the lowest at β = 0°. The specimens with higher transverse isotropic angles β tend to show narrower instantaneous and transient creep phases than those with lower angle β. This means that they can reach the two transition points quicker. This behaviour can be observed from all confining pressures, where the higher confining pressure also results in a narrower range of transient creep phase. The diagrams suggest also that the creep test period of 10 days is sufficient to allow all specimens to reach steady-state phase. The transition points of salt deformations through different creep phases allow determining the evolution of each phase with transverse isotropic angle and confining pressure. These strain values mentioned above are given in Table 6.2.

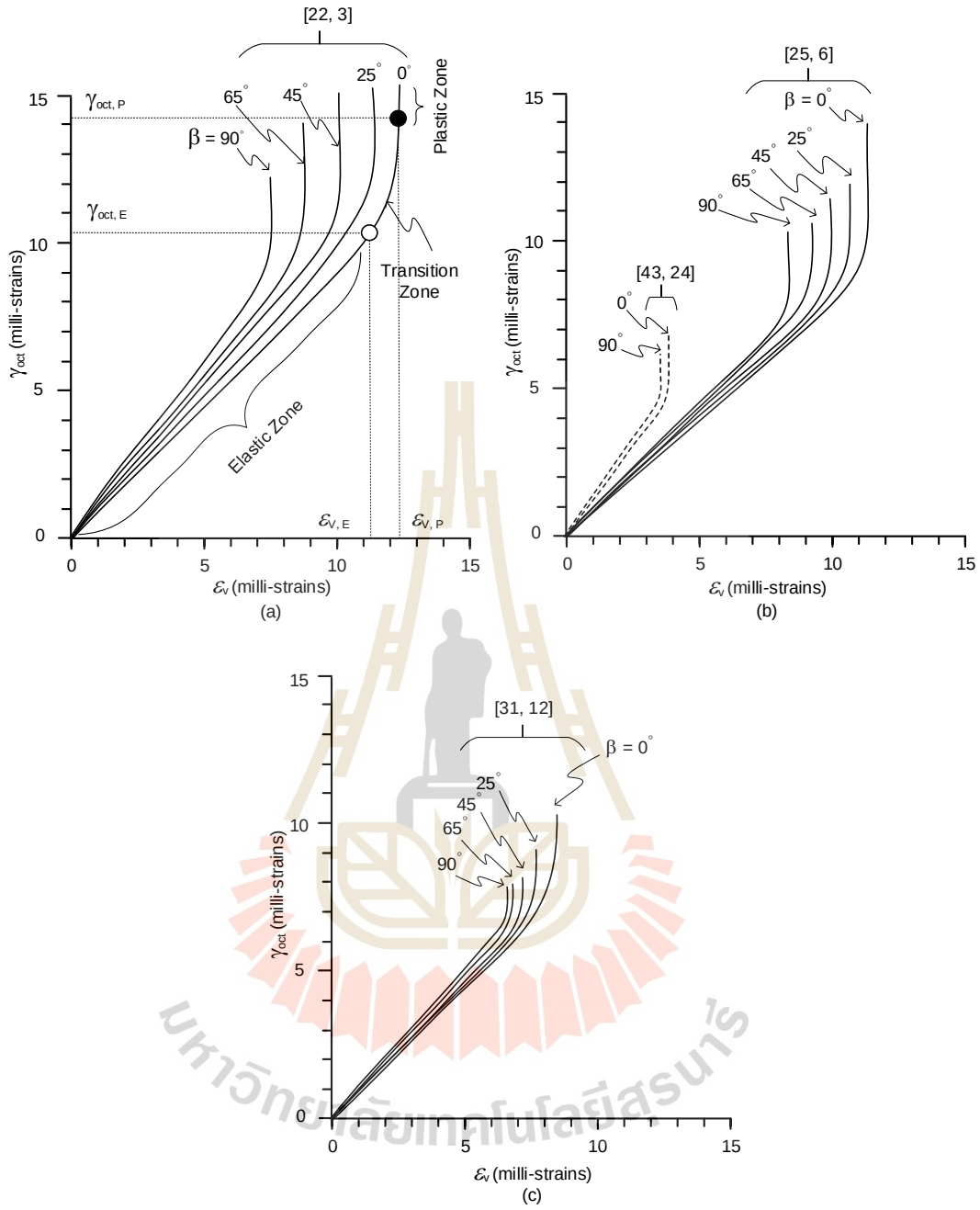

Figure 6.4 Octahedral shear strains as a function of volumetric strain for σ_3 = 3 MPa (a), σ_3 = 6 MPa and 24 MPa (b), and σ_3 = 12 MPa (c). Numbers in brackets indicate [σ_1, σ_3]. Open points indicate transition from instantaneous to transient phases, and solid points for transition from transient to steady-state creep phases.

Table 6.2 Octahedral shear strains and volumetric strains at transition points.

σ_3 (MPa)	β (Degrees)	Instantaneous phase into transient phase		transient phase into steady-state creep	
		$\varepsilon_{V,V}$ (milli-strains)	$\gamma_{oct,V}$ (milli-strains)	$\varepsilon_{V,P}$ (milli-strains)	$\gamma_{oct,P}$ (milli-strains)
3	0	11.58	10.32	11.67	14.29
	25	10.95	9.68	10.23	13.22
	45	9.45	9.14	9.36	12.25
	65	8.32	8.65	8.42	11.13
	90	6.83	8.15	7.61	10.02
6	0	9.09	7.12	11.32	11.02
	25	8.74	6.87	10.65	9.85
	45	8.02	6.61	9.25	9.13
	65	7.65	6.52	8.42	8.46
	90	7.05	6.22	7.89	7.59
12	0	7.23	5.26	8.66	7.12
	25	7.12	4.91	7.51	6.75
	45	7.03	4.75	7.02	6.31
	65	6.81	4.52	6.84	5.89
	90	6.22	4.31	6.43	5.21
24	0	3.02	3.86	3.58	4.87
	90	2.98	3.62	3.13	4.18

6.5 Evolution of creep phases with β and σ_3

Figure 6.5 shows a three-dimensional diagram of the transition points separating different phases of deformation under τ_{oct} = 9 MPa, where γ_{oct} at the transition points is presented as a function of angle β and σ_3. As the confining pressures increase the ranges of shear strains for the instantaneous and transient creep phases reduce. Under 24 MPa confinement, the creep strains become insensitive to the transverse isotropic (bedding plane) angle β. At this high confinement the instantaneous and transient phases become smaller, and hence the specimens reach the steady-state phase much quicker, as compared to those under lower confining pressures (e.g. σ_3 = 3 or 6 MPa). Wider ranges for instantaneous and transient creep

phases under low σ_3 are observed, as compared to those under high σ_3. They gradually reduce with increasing angle β.

The range of transient creep phase in terms of octahedral shear strain can be defined by the differences of shear strains between the two transition points as follows:

$$\overline{\gamma}_{oct} = \gamma_{oct,P} - \gamma_{oct,V} \tag{6.11}$$

where $\overline{\gamma}_{oct}$ represents the range of transient creep strain, and $\gamma_{oct,P}$ and $\gamma_{oct,V}$ are creep shear strains at plastic and elastic transition points obtained from the test results, shown as examples by solid and open points in Figure (6.4a). Figure 6.6 plots $\overline{\gamma}_{oct}$ as a function of σ_3 for β = 0° and 90°. Logarithmic equation can best describe their relation as evidenced by the coefficients of correlation are greater than 0.99. Numerical values of the empirical constants are given in the figure. The diagram suggests that the range of transient creep strains for β = 0° ($\overline{\gamma}_{oct,0^\circ}$) and β = 90° ($\overline{\gamma}_{oct,90^\circ}$) equals to zero when the confining pressure approaches 40 MPa. This means that under this high confinement the salt behaves as a Maxwell material where only instantaneous and steady-state creep deformations exist for all transverse isotropic angles.

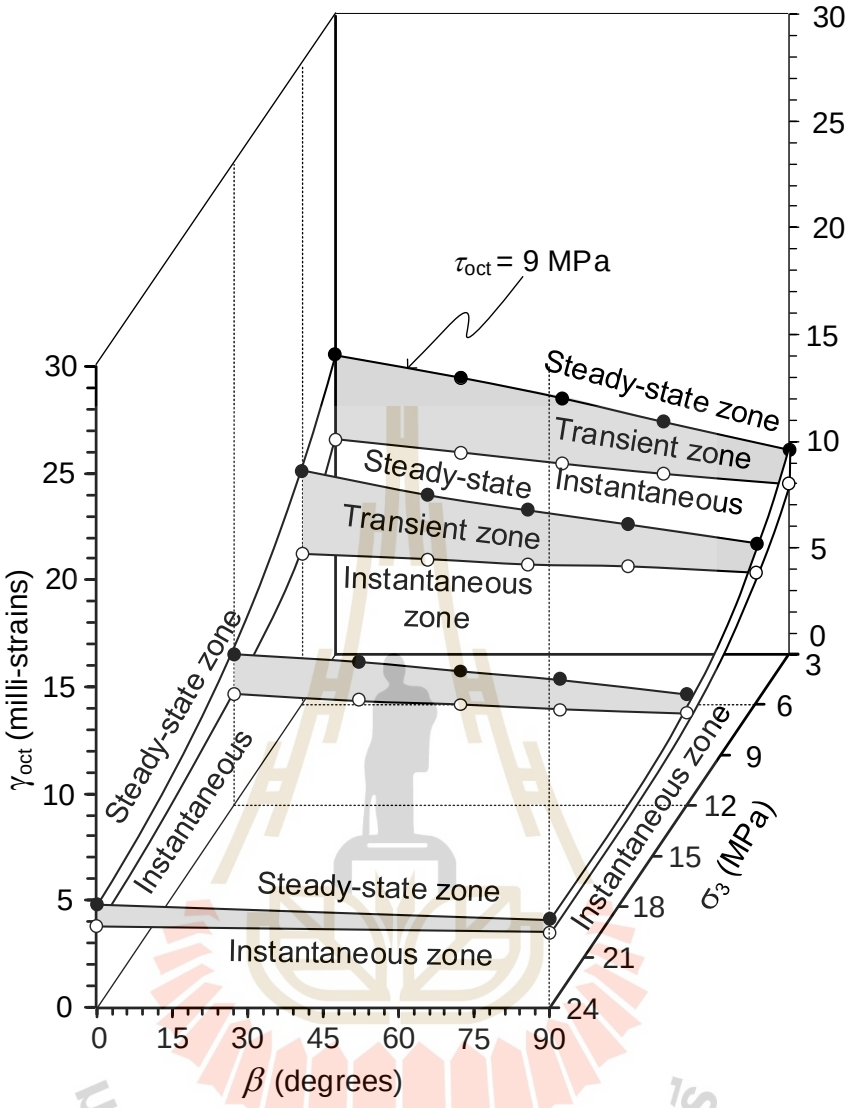

Figure 6.5 Evolution of creep phases as a function of confining pressure and angle β for τ_{oct} = 9 MPa from test results. Transient creep phases are represented by shade areas.

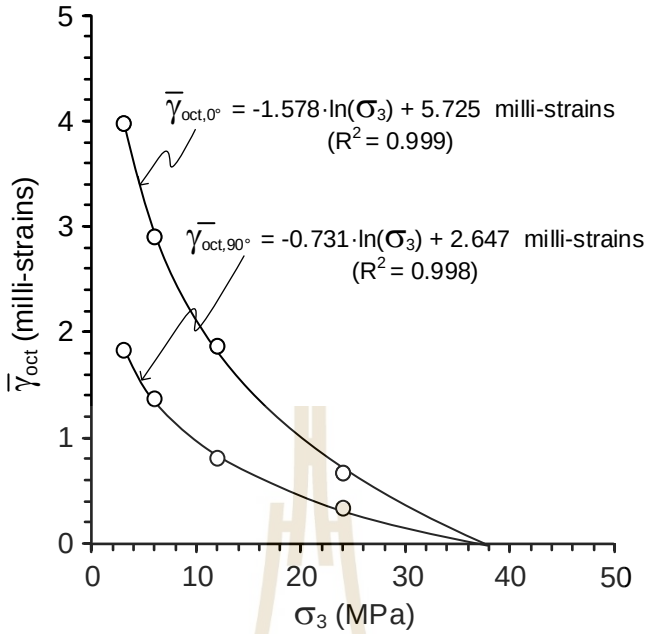

Figure 6.6 Range of transient creep phase ($\bar{\gamma}_{oct}$) as a function of σ_3 for intrinsic angles β = 0° and 90°, under τ_{oct} = 9 MPa.

CHAPTER VII
SALT CREEP UNDER VARIOUS OCTAHEDRAL SHEAR STRESSES

7.1 Introduction

As the postulation in previous chapter is true only if the salt is under 9 MPa octahedral shear stress. This chapter presents the calculation the time dependent deformation for various octahedral shear stresses based on linear visco-elastic theory. Included the Burgers parameter used to calculation under various transverse isotropic angle and confining pressure are determined. The governing equations are developed to predict the octahedral shear strains as a function of bedding plane orientation, confining pressure, loading duration and octahedral shear stress. The findings reveal octahedral shear stress responses on transverse isotropic salt creep phase, as detailed in the subsequent sections.

7.2 Prediction of apparent Burgers parameters

The intrinsic Burgers parameters (β = 0° and 90°) calibrated from triaxial creep test results (Table 5.1) are plotted as a function of confining pressures (σ_3), as shown by solid lines in Figure 7.1. The highest E_I, E_V and η_P are obtained when β = 90° ($E_{I,90°}$ and $\eta_{P,90°}$) and lowest when β = 0° ($E_{I,0°}$ and $\eta_{P,0°}$) as shown in Figures 7.1(a) through 7.1(c). The E_V shows highest values when β = 0° and lowest when β = 90° (Figure 7.1(b)). Additionally, the diagrams indicate that the intrinsic parameters E_I, E_V and η_P increase with σ_3, while η_V decreases as σ_3 increases. Their evolution with σ_3 can be best represented by logarithmic equations, as shown in Figure 7.1. The numerical values for their constants are given in the figure. Good correlations are obtained ($R^2 > 0.8$).

Burger parameters (E_I, E_V, η_V and η_P) for apparent angles ($0° < \beta < 90°$) under different confining pressures are calculated by elliptic equations. E_I (β) and η_P (β) can be obtained by recalling Equations (6.2) and (6.3). Similarly, E_V (β) and η_V (β) can be derived from the elliptic equation [Equation (6.1)] as:

$$E_V(\beta) = E_{V,90°} / \{1 + [((E_{V,90°} / E_{V,0°})^2 - 1) \cdot \cos^2 \beta]\}^{1/2} \quad (7.1)$$

$$\eta_V(\beta) = \eta_{V,90°} / \{1 + [((\eta_{V,90°} / \eta_{V,0°})^2 - 1) \cdot \cos^2 \beta]\}^{1/2} \quad (7.2)$$

The intrinsic creep parameters at any confining pressures used in elliptic equations are determined by logarithmic relation between confining pressures and Burgers parameters obtained from β = 0° and 90° in Figure 7.1.

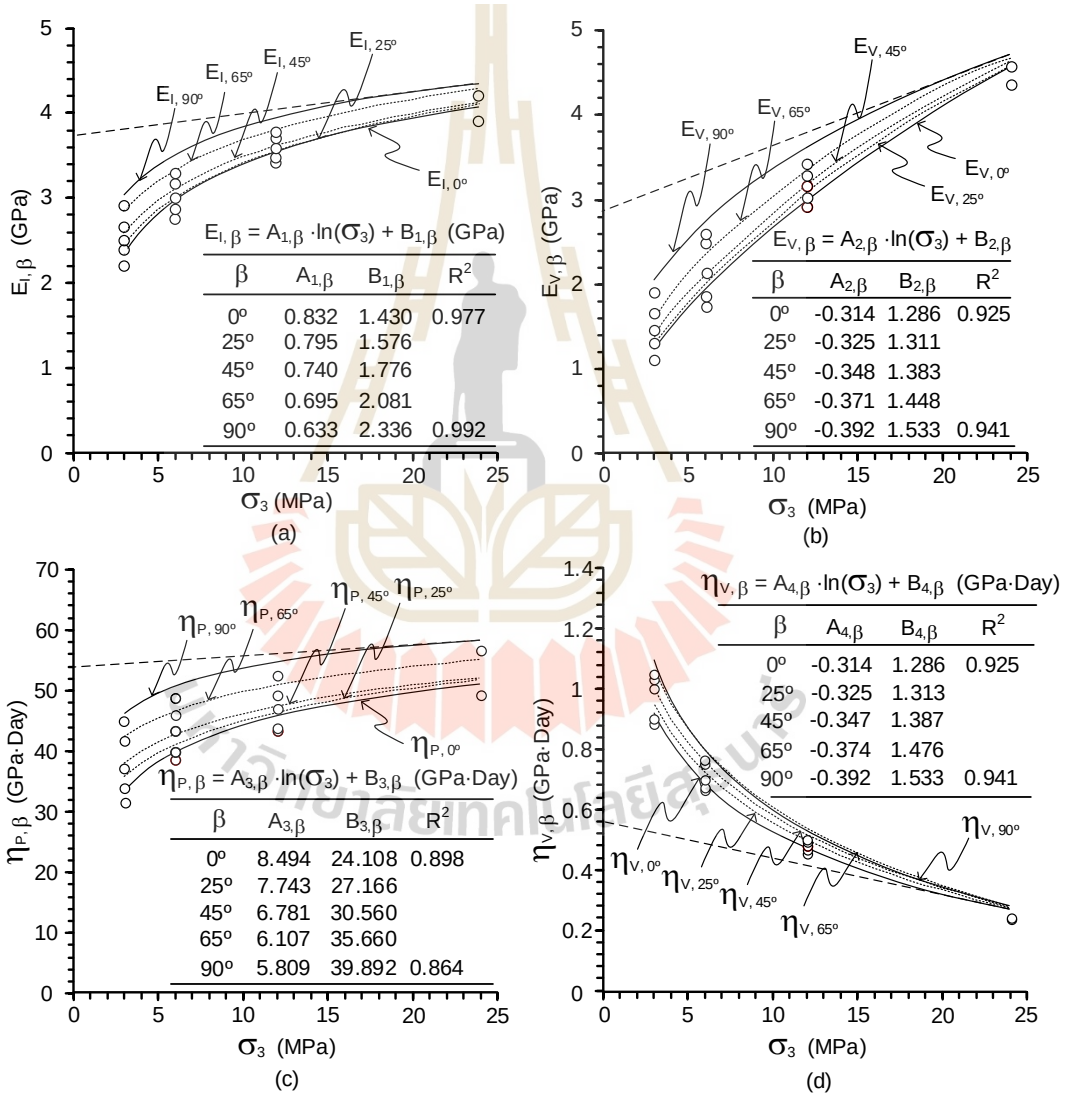

Figure 7.1 $E_{I,\beta}$ (a), $E_{V,\beta}$ (b), $\eta_{P,\beta}$ (c) and $\eta_{V,\beta}$ (d) for various angles β as a function of confining pressures (σ_3).

Figure 7.1 presents the comparisons of the logarithmic relation of calculated apparent creep parameters (dash lines) and test results (point). The $E_{I,\beta}$, $E_{V,\beta}$ and $\eta_{P,\beta}$ increase but the $\eta_{V,\beta}$ decreases, as the beds dip away from the major principal stress (β = 25°, 45° and 65°). These properties eventually reach $E_{I,90°}$, $E_{V,90°}$, $\eta_{P,90°}$ and $\eta_{V,0°}$ under high confinement.

Figures 7.2 and 7.3 show the evolutions of Burgers creep parameters under various bedding plane orientations and confining pressures in 3-D diagrams to clearly observe the effect of transverse isotropic angle on creep properties under confinement.

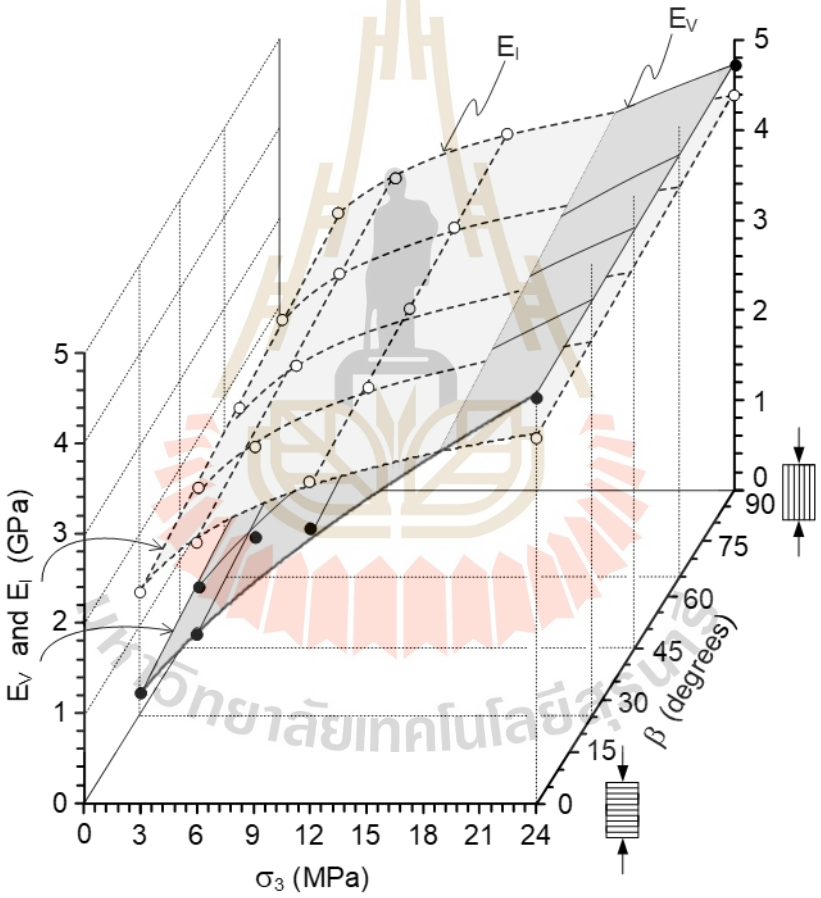

Figure 7.2 3-D diagram showing evolutions of E_1 and E_V as a function of transverse isotropic angle (β) and confining pressure (σ_3).

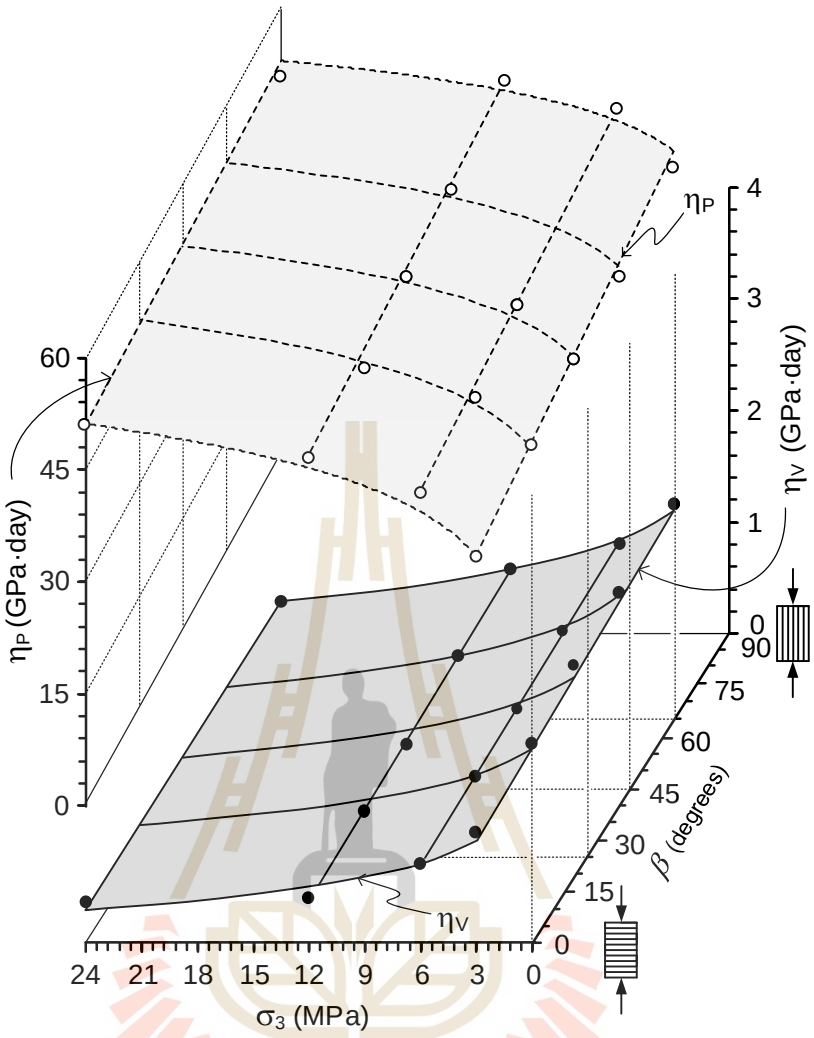

Figure 7.3 3-D diagram showing evolutions of η_P and η_V as a function of transverse isotropic angle (β) and confining pressure (σ_3).

7.3 Prediction octahedral shear strains – time curves under various octahedral shear stresses (τ_{oct})

The purpose of this section is to derive governing equations for transverse isotropic creep responses under various octahedral shear stresses. From the linear visco-elastic theory (Richards, 1993; Bland, 2016), the octahedral shear strain (γ_{oct}) can be presented as a function of octahedral shear stress (τ_{oct}) for the Burgers model as:

$$\gamma_{oct}(t) = \tau_{oct} \{1 / E_I(\beta) + t / \eta_P(\beta) + [(1 / E_V(\beta)) \cdot (1 - \exp(-E_V(\beta) \cdot t / \eta_V(\beta))]\} \quad (7.3)$$

where τ_{oct} is constant with time and the Burger parameters E_I, E_V, η_V and η_P are functions of transverse isotropic angle β.

By substituting Equations (6.2), (6.3), (7.1) and (7.2) into Equation (7.3), the octahedral shear strains at any constant octahedral shear stress can be predicted as a function of time and transverse isotropic angle. The comparisons of predictions under confining pressures of 3, 6, 12 and 24 MPa for constant octahedral shear stress of 9 MPa (dash lines) and test results (solid lines) are given in Figure 7.4. The agreement between predictions and the test results can be evaluated using the mean misfit (f) similarly from Equation (6.5) but p_c and p_m are predicted and tested values, n is number of data points used for each transverse isotropic angle, and m is number of transverse isotropic angles. The mean misfits (Riley et al., 1998) for the predictions under confining pressures of 3, 6, 12 and 24 MPa are determined as 0.531, 0.368, 0.316 and 0.367 milli-strain, respectively. These low values indicate good agreement between the prediction and the test result by low values of mean misfits.

The transverse isotropic creep deformations in the forms of γ_{oct} can be predicted for various τ_{oct} values. To demonstrate the predicted results, Figures 7.5 and 7.6 gives examples of the predicted γ_{oct} under τ_{oct} = 3 and 15 MPa. The predicted results coincide with those obtained from the test results under τ_{oct} = 9 MPa (Figure 7.4) that creep strains for β = 0° are always greater than those under β = 90°. Their differences become smaller under higher σ_3, and larger for higher τ_{oct}.

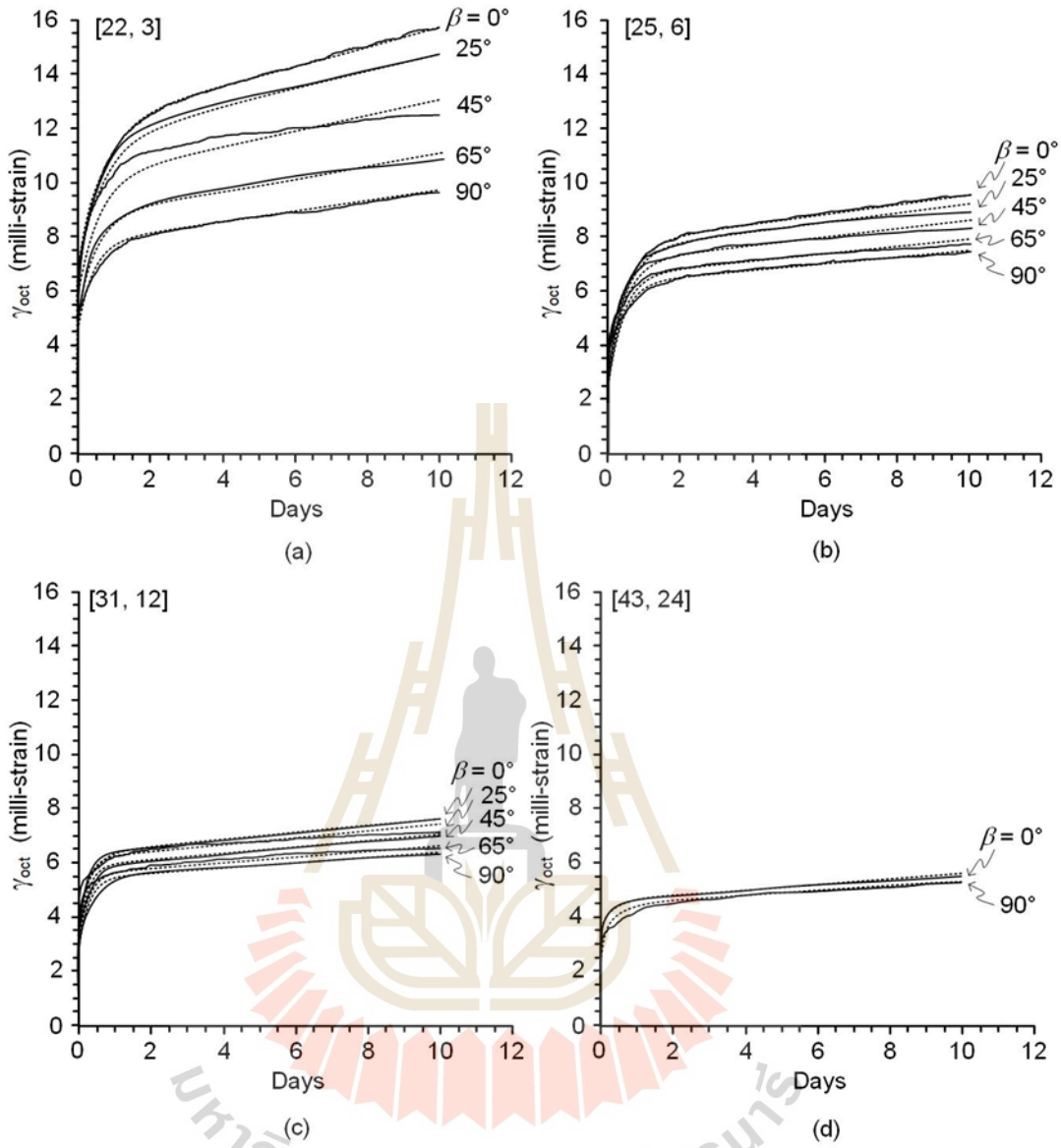

Figure 7.4 Predicted octahedral shear strains – time curves for confining pressures 3 MPa (a), 6 MPa (b), 12 MPa (c), and 24 MPa (d) under octahedral shear stress of 9 MPa.

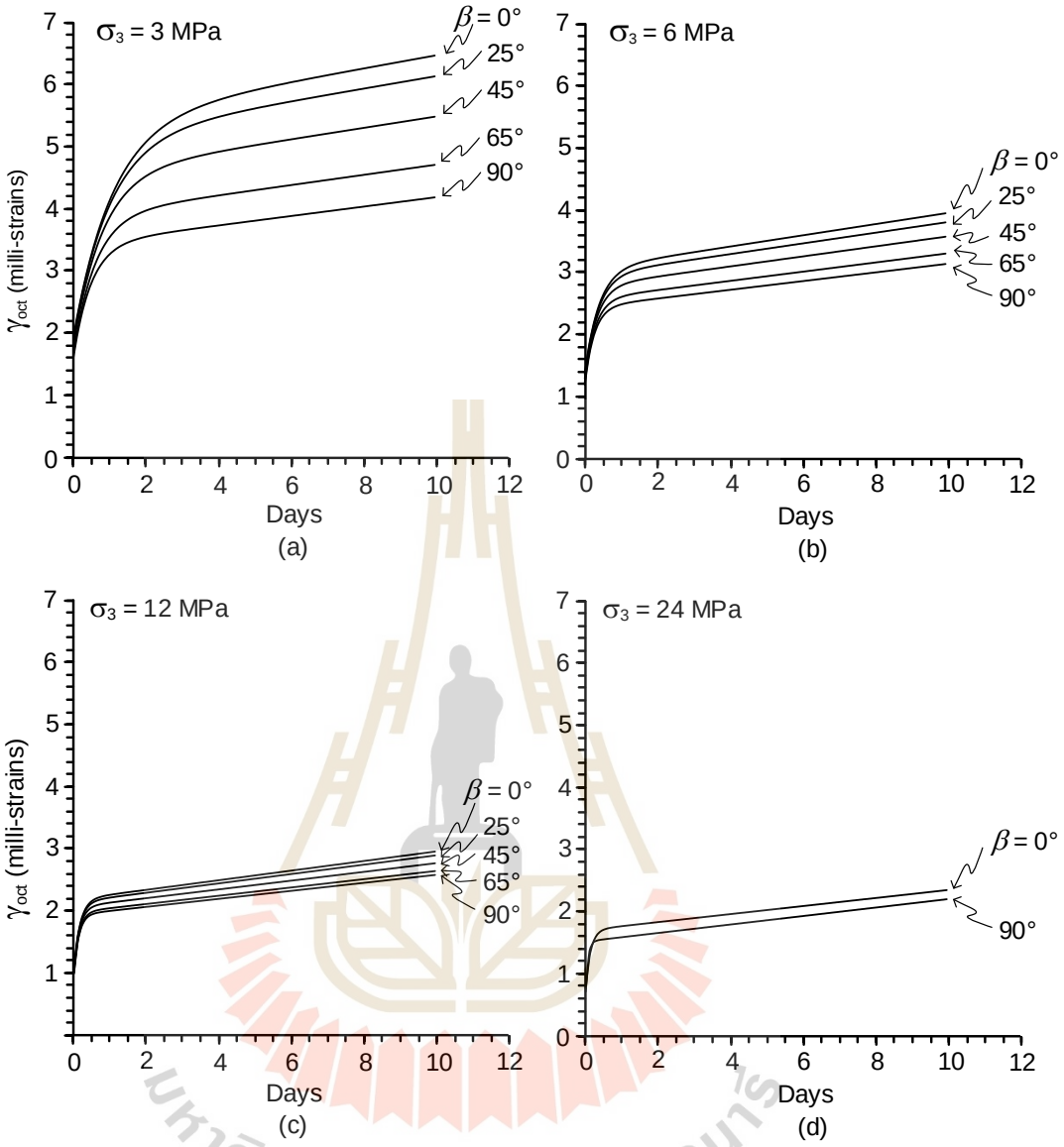

Figure 7.5 Predicted octahedral shear strains – time curves for confining pressures 3 MPa (a), 6 MPa (b), 12 MPa (c), and 24 MPa (d) under octahedral shear stress of 3 MPa.

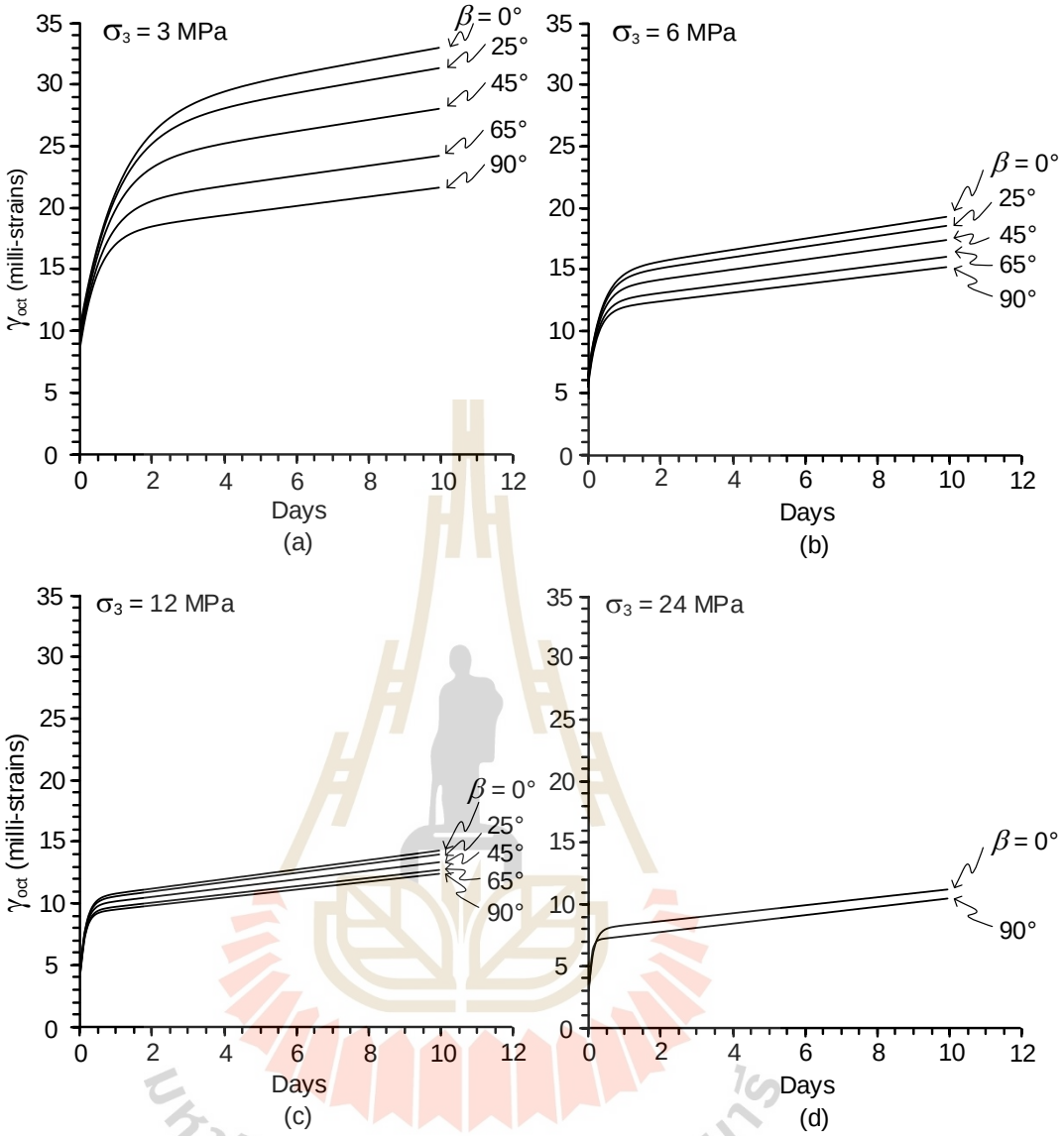

Figure 7.6 Predicted octahedral shear strains – time curves for confining pressures 3 MPa (a), 6 MPa (b), 12 MPa (c), and 24 MPa (d) under octahedral shear stress of 15 MPa.

7.4 Salt creep phases under various octahedral shear stresses (τ_{oct})

The evolution of creep phases in chapter 6 (section 6.4) only presented salt deformation under τ_{oct} = 9 MPa. The propose of this section is to described the salt creep phases under various τ_{oct}. Figure 7.7 shows the three-dimensional diagram of the predicted transition points separating different phases of deformation under τ_{oct} = 3 and 15 MPa. The γ_{oct} at transition points as a function of angle β and σ_3 is determined by using the predicted value in Figures 7.5 and 7.7 as shown in Table 7.1. They gradually reduce with increasing angle β. They suggest also that wider range of transient creep phase is obtained under low σ_3 and β, as compared to those under high σ_3 and β. These predicted results coincide with the creep phase under τ_{oct} = 9 MPa.

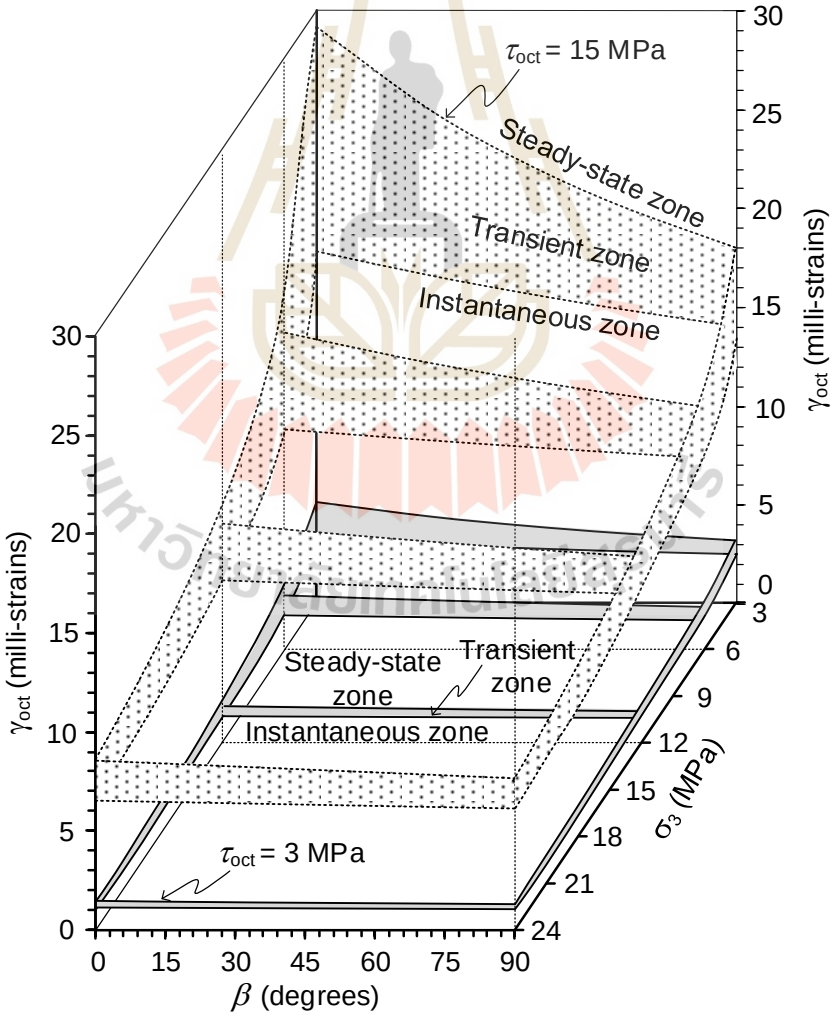

Figure 7.7 Predicted evolution of creep phases as a function of confining pressure and angle β for τ_{oct} = 3 and 15 MPa.

The ranges of shear strains for the instantaneous and transient creep phases increase and more sensitive to the transverse isotropic (bedding plane) angle β as the octahedral shear stresses increase. At this high octahedral shear stress, the instantaneous and transient phases become wider, and hence the specimens reach the steady-state phase slower than those under lower octahedral shear stress. Under the same confinement, the higher τ_{oct} is applied, the wider range of transient creep phase is obtained.

Table 7.1 Predicted octahedral shear strains under octahedral shear stresses of 3 and 15 MPa.

σ_3 (MPa)	β (Degrees)	τ_{oct} =3 MPa			τ_{oct} =15 MPa		
		$\gamma_{oct, E}$ (milli-strains)	$\gamma_{oct, V}$ (milli-strains)	$\bar{\gamma}_{oct}$ (milli-strains)	$\gamma_{oct, E}$ (milli-strains)	$\gamma_{oct, P}$ (milli-strains)	$\bar{\gamma}_{oct}$ (milli-strains)
3	0	3.62	5.90	2.29	18.09	29.52	9.30
	25	3.36	5.04		16.81	25.18	
	45	3.18	4.51		15.91	22.53	
	65	3.02	4.08		15.10	20.39	
	90	2.84	3.64	0.80	14.20	18.22	4.02
6	0	2.27	3.24	0.97	11.33	16.18	4.90
	25	2.17	2.99		10.87	14.96	
	45	2.10	2.82		10.52	14.11	
	65	2.04	2.67		10.20	13.35	
	90	1.96	2.50	0.54	9.82	12.50	2.68
12	0	1.65	2.23	0.58	8.25	11.15	3.76
	25	1.60	2.13		8.02	10.63	
	45	1.57	2.05		7.85	10.25	
	65	1.54	1.98		7.69	9.89	
	90	1.50	1.90	0.40	7.50	9.48	1.98
24	0	1.30	1.70	0.40	6.48	8.50	3.89
	90	1.21	1.52	0.31	6.06	7.62	1.56

The range of transient creep phase ($\bar{\gamma}_{oct}$) in terms of assumed octahedral shear strain of 3 and 15 MPa are determined. Figure 7.8 shows the comparison of test result (solid line) and prediction at τ_{oct} =3 and 15 MPa (dash line). The relations of transient creep phase range and confining pressure be best described by logarithmic equations. The empirical equations fit well to the test results ($R^2 > 0.9$). Extrapolation of these equations indicated that the range of transient creep strains obtained from β = 0° and β = 90° under τ_{oct} =3 and 15 MPa equals to zero when the confining pressure approaches 30 and 70 MPa, as shown in Table 7.2. These confining pressures the salt behave Maxwell material (no transient creep deformation) for all transverse isotropic angles. Suggesting that under low octahedral shear stress the salt behaves as a Maxwell material for all transverse isotropic angles and become isotropic condition much quicker. Under high octahedral shear stress, salt behaves as a Maxwell material but remains transverse isotropic condition that can be observed by the difference of confining pressure at $\bar{\gamma}_{oct}$ equal to zero for intrinsic angles under assumed τ_{oct} = 15 MPa.

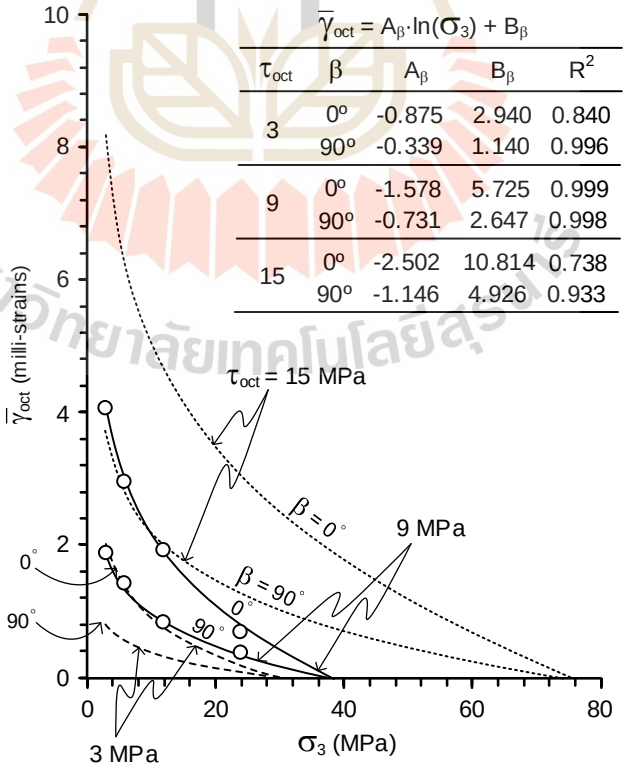

Figure 7.8 Ranges of transient creep phase ($\bar{\gamma}_{oct}$) as a function of σ_3 for intrinsic angles β = 0° and 90°, under assumed τ_{oct} = 3, 9, and 15 MPa.

Table 7.2 Confining pressures and octahedral shear strains at salt behaves Maxwell material.

τ_{oct} (MPa)	β =0°		β =90°	
	σ_3 (MPa)	γ_{oct} (milli-strains)	σ_3 (MPa)	γ_{oct} (milli-strains)
3	28.87	1.22	28.79	1.15
9	37.64	3.40	37.36	3.24
15	75.35	4.77	73.58	4.62

CHAPTER VIII
DISCUSSIONS AND CONCLUSIONS

8.1 Discussions

Results from this study reveal the effects of transverse isotropy caused by bedding planes on time-dependent deformations of rock salt based on experimental and analytical investigations. Such effort has never been attempted elsewhere, in particular, on the derivation of mathematical representations to predict the salt creep as affected by bedding plane orientations under different deviatoric and confining stresses. The same approach can be applied to salt from other source locations and other time-dependent materials posing transverse isotropic characteristics.

Larger instantaneous and creep deformations are obtained when the applied axial stress is normal to the bedding planes ($\beta = 0°$), as compared to those obtained parallel to the beds ($\beta = 90°$). Similar to the test result obtained by Liu et al. (2015) on clayey rock, Wu et al. (2018) on greenschist and Li et al (2020) on shale. This is probably caused by the alignment of inter-crystalline boundaries and the soft inclusions along bedding planes. The increases of confining pressures stiffen these soft layers and tighten the inter-crystalline boundaries, and subsequently reduce the transverse isotropic responses of the salt.

Anisotropy degrees for the instantaneous and creep deformations of Maha Sarakham salt are relatively low (less than 2 – Figure 6.4), which coincide with those of the elastic parameters and compressive strengths of the same salt experimentally obtained by Thongprapha et al. (2022). Bedded salt from other sources may however show different degrees of anisotropy depending upon their characteristics of transverse isotropic (bedding) planes.

It is recognized that the number of test specimens and test duration used here are relatively limited. The test results, nevertheless, provide sufficient and reliable trends of creep deformations under different applied stresses and bedding plane orientations (Figures 4.4 through 4.8). All deviation strain-time curves can be well described by the Burgers model with coefficients of correlation greater than 0.9

(section 5.2). The apparent elastic, visco-elastic and visco-plastic deformations ($0° < \beta < 90°$) conform to the elliptic equation (Figure 6.1), as indicated by their low mean misfit values. The γ_{oct}-ε_v curves in Fig. 6.6 show also that all specimens reach plastic deformation in steady-state creep phase where constant ε_v is obtained while γ_{oct} is increasing.

The γ_{oct}-ε_v curves show the transitional shear strains from instantaneous, visco-elastic to visco-plastic creep phases more clear than do the axial and lateral strain-time curves (Figures 4.4 through 4.8), and the strain deviation-time curves (Figures. 5.1 and 5.2). This is primarily because the linear relation between γ_{oct} and ε_v during elastic phase, and the independency of γ_{oct} on ε_v during visco-plastic phase can be easily distinguished from the non-linear curves of γ_{oct} - ε_v during transient creep phase. This allows defining the transitional shear strains between them more accurately, and hence showing the evolution of each deformation phase as affected by the confining pressure σ_3 and transverse isotropic angle β.

The evolutions of transient strains with σ_3 and β allow determining the range of transient strain ($\overline{\gamma}_{oct}$) for the two intrinsic angles ($\beta = 0°$ and $90°$). They decrease logarithmically with increase σ_3. Beyond σ_3 = 35 - 40 MPa, the transient strain no longer exists. This is however true only under τ_{oct} = 9 MPa.

Even though the effect of confining pressures on the variation of transient and steady-state creep phases has long been recognized, their mathematical representation has never been developed. The decrease of $\overline{\gamma}_{oct}$ under higher confining pressure is probably due to the predominance of dislocation glide mechanism (sliding along salt cleavages) over dislocation climb mechanism (sliding along salt crystal boundaries), as described by deformation-mechanism map developed by Senseny (1983). Differential stresses applied under high confinement induce plastic deformation. Supporting evidence from Figure 4.9 can be observed that salt has laterally elongated crystals under high confinement which coincide with the result obtained by Thongprapha et al. (2022). This enhances the visco-plastic deformation in the steady-state phase and minimizes the visco-elastic deformation in the transient phase, as shown in Figure. 6.6.

Under the same range of confining pressures used here, if the applied octahedral shear stress is higher than 9 MPa, this would result in a wider range of shear

strain in transient creep phase ($\overline{\gamma}_{oct}$) under both intrinsic angles, and give higher transition confining pressure at which the salt changes from a Burger to Maxwell materials. Opposite results would be obtained if τ_{oct} lower than 9 MPa is applied, as shown in Fig. 7.8. Note that these summaries are obtained from calculation using proposed equation in this study.

It is recognized that there are other factors that can affect the characteristics of transient creep strains of salt, e.g. temperature, intermediate principal stress and size of test specimens. These factors are excluded from this study. Elevated temperatures could minimize the range of transient creep strain and enhance the steady-state strain rate, as experimentally obtained by Senseny et al. (1986), Handin et al. (1984), Moslehy and Alshibli (2023), and Dong et al. (2023). Results from series of polyaxial creep tests ($\sigma_1 \neq \sigma_2 \neq \sigma_3$) by Archeeploha et al. (2017) suggest that increasing the intermediate principal stress from $\sigma_2 = \sigma_3$ toward $\sigma_2 = \sigma_1$ notably reduces the range of transient creep strains for the Maha Sarakham salt. The transient creep strain of small specimens tends to be more sensitive to the applied stress, temperature and test duration than that of larger specimens (Senseny, 1982, 1984; Linder and Brady, 1984).

The Burgers creep model is used in this study because it can implicitly incorporate the effect of transverse isotropic angle β into its parameters. The analysis performed here is based on the linear visco-elastic theory from which the Burgers model has been derived. Since the applied stress-strain rate relation of salt may not be strictly linear, care should be taken when applying the results beyond the range of confining pressures from which the model parameters have been calibrated.

8.2 Conclusions

Experimental and analytical investigations have been performed to determine the time-dependent responses of Maha Sarakham salt as affected by bedding plane orientations and confining pressures. Conclusions drawn from this study can be summarized as follows:

1) Bedding (transverse isotropic) planes do affect the time-dependent behavior of Maha Sarakham salt. Largest instantaneous and creep

deformations are obtained when the major principal stress is normal to the bedding planes (β = 0°), and gradually decrease to the smallest when β = 90°. Discrepancies of the deformations between the two intrinsic angles reduce as the confining pressures increase.

2) Via Laplace transformation the Burgers creep model fits well to the creep test results in terms of major principal strain deviation as a function of time. Elliptic equations can describe the evolutions of the instantaneous visco-elastic and visco-plastic deformations for all apparent transverse isotropic angles (0° < β < 90°) and confining pressures.

3) Anisotropy degrees for instantaneous, visco-elastic and visco-plastic deformations decrease with increasing confining pressure, where their relations can be described by power equations. Extrapolation of the equations toward higher confining pressures suggest that the instantaneous and visco-elastic responses of the salt would become isotropic at σ_3 about 35 - 40 MPa. Under σ_3 of 80 MPa and beyond the visco-plastic deformation also reaches isotropic condition.

4) Octahedral shear-volumetric strain (γ_{oct} - ε_v) curves can be used to define the transition shear strains from instantaneous, transient creep to steady-state creep phases, and hence allows determining the evolution of each deformation phase as affected by transverse isotropic angles and confining pressures.

5) The ranges of transient creep strains ($\overline{\gamma}_{oct}$) are wider under low confining pressures, as compared to those under higher confining pressures. They also become insensitive to the changes of transverse isotropic angles under high confinements.

6) For both intrinsic angles (β = 0° and 90°) the $\overline{\gamma}_{oct}$ logarithmically decrease with increasing σ_3. Under τ_{oct} = 9 MPa they reach zero under σ_3 about 35 - 40 MPa, where the salt transitional changes from Burgers to Maxwell materials, i.e. salt deforms only under instantaneous and steady-state creep phases.

7) Based on linear visco-elastic theory and the calibrated Burgers parameters under τ_{oct} = 9 MPa with σ_3 = 3 - 24 MPa, the transverse isotropic creep of the salt under different magnitudes of τ_{oct} and σ_3 can be calculated. This is useful for the prediction of time-dependent deformations of supported pillars and sidewalls in salt mines and around solution caverns.

8) Under low octahedral shear stress, rock salt changes behavior to Maxwell material and becomes isotropic material quicker than under high octahedral shear stresses.

8.3 Recommendations for future studies

The uncertainties of the investigation and results discussed above lead to the recommendations for further studies. To confirm the results concluded in this study and enhance comprehension of effect of transverse isotropy on time-dependent properties of rock salt, more issues are required as follows:

1) Testing of various bedding plane orientations (interval bedding plane orientation) than those used here would confirm the postulated creep behavior under transverse isotropic effect.

2) Increasing the number of salt specimens and test duration would statistically enhance the reliability of the test results and the predictability of the proposed equation.

3) Performing triaxial creep test under various octahedral shear stresses is desirable to confirm the calculated creep behavior in this study.

4) Studying the transverse isotropy on time-dependent behavior of rock under cyclic and multi-state loading may also be desirable.

REFERENCES

Aditya, S., Chandan, K., Gopi, K. L., Seshagiri, R. K., & Ayothiraman, R. (2018). Engineering properties of rock salt and simplified closed-form deformation solution for circular opening in rock salt under the true triaxial stress state. *Engineering Geology, 243*, 218–230.

Al-Harthi, A. A. (1998). Effect of planar structures on the anisotropy of Ranyah sandstone, Saudi Arabia. *Engineering geology, 50*(1-2), 49-57.

Amadei, B. (1996, April). Importance of anisotropy when estimating and measuring in situ stresses in rock. *International journal of rock mechanics and mining sciences & geomechanics abstracts, 33*(3), 293-325.

Amadei, B., Savage, W. Z., & Swolfs, H. S. (1987, February). Gravitational stresses in anisotropic rock masses. *International Journal of Rock Mechanics and Mining Sciences & Geomechanics Abstracts, 24*(1), 5-14.

Archeeploha, S., Khamrat, S., & Fuenkajorn, K. (2017). Effects of intermediate principal stress on creep closure of storage caverns in Maha Sarakham salt. *Songklanakarin Journal of Science and Technology, 39*(2), 143-151.

ASTM D7070-08. (2016). Standard test methods for creep of rock core under constant stress and temperature. In *Annual Book of ASTM Standards* (Vol. 04.08). Philadelphia: American Society for Testing and Materials.

Aydan, Ö., Ito, T., Özbay, U., Kwasniewski, M., Shariar, K., Okuno, T., ... & Okada, T. (2015). ISRM suggested methods for determining the creep characteristics of rock. *The ISRM Suggested Methods for Rock Characterization, Testing and Monitoring: 2007-2014,* 115-130.

Aydan, O., Tokashiki, N., & Genis, M. (2012, June). Some considerations on yield (failure) criteria in rock mechanics. *In ARMA US Rock Mechanics/Geomechanics Symposium,* Chicago.

Barla, G. (1974). Rock anisotropy: Theory and laboratory testing. In *Rock mechanics* (pp. 131-169). Udine,Italy: Springer.

Bland, D. R. (2016*). The Theory of Linear Viscoelasticity.* Mineola, New York: Courier Dover Publications.

Cheng, C., Li, X., & Qian, H. (2017). Anisotropic failure strength of shale with increasing confinement: behaviors, factors and mechanism. *Materials, 10*(11), 1310.

Colak, K., & Unlu, T. (2004). Effect of transverse anisotropy on the Hoek–Brown strength parameter 'mi'for intact rocks. *International journal of rock mechanics and mining sciences, 41*(6), 1045-1052.

Cristescu, N., & Hunsche, U. (1996). A comprehensive constitutive equation for rocksalt determination and application. In Proceedings of the Third Conferenceon the Mechanical Behavior of Salt (pp. 191-205). Clausthal- Zellerfeld, Germany: Trans Tech Publications.

Daemen, J.J.K., & Fuenkajorn, K. (1996). *Design of borehole seals: process, criteria and considerations*. Berlin: Springer.

Dawson, P. R., & Munson, D. E. (1983). Numerical simulation of creep deformations around a room in a deep potash mine. *International Journal of Rock Mechanics and Mining Sciences & Geomechanics Abstracts, 20*(1), 33-42. doi:10.1016/0148-9062(83)91612-1

Dong, Z., Li, Y., Li, H., Wang, Z., Shi, X., Chen, X., & Lu, Q. (2023). Experimental study on the influence of temperature on rock salt creep. *Rock Mechanics and Rock Engineering, 56*(5), 3499-3518. Doi:10.1007/s00603-023-03219-0

Dong, Z., Li, Y., Li, H., Wang, Z., Shi, X., Chen, X., & Lu, Q. (2023). Experimental study on the influence of temperature on rock salt creep. *Rock Mechanics and Rock Engineering, 56*(5), 3499-3518. doi:10.1007/s00603-023-03219-0

Dubey, R. K. (2018). Bearing of structural anisotropy on deformation and mechanical response of rocks: an experimental example of rocksalt deformation under variable compression rates. *Journal of the Geological Society of India, 91*, 109-114.

Dubey, R. K., & Gairola, V. K. (2008). Influence of structural anisotropy on creep of rocksalt from Simla Himalaya, India: an experimental approach. *Journal of structural geology, 30*(6), 710-718.

Dubey, R.K., & Gairola, V.K. (2000). Influence of structural anisotropy on uniaxial compressive strength of pre-fatigued rocksalt from Himachal Pradesh, India. *International Journal of Rock Mechanics and Mining Sciences & Geomechanics Abstracts, 37*(6), 293-299.

Dubey, R.K., Nath, R., & Gairola, V.K. (1999). Textural control on strength and deformation of rocksalt of Shali Formation, Simla Himalayadan experimental approach. *Rocksite,* 571-576.

Ehgartner, B. L., & Sobolik, S. R. (2006). Analysis of cavern shapes for the strategic petroleum reserve. United States: Sandia National Laboratories.

Fereidooni, D., Khanlari, G. R., Heidari, M., Sepahigero, A. A., & Kolahi-Azar, A. P. (2016). Assessment of inherent anisotropy and confining pressure influences on mechanical behavior of anisotropic foliated rocks under triaxial compression. *Rock Mechanics and Rock Engineering, 49*, 2155-2163.

Franklin, B., & Dusseault, M. B. (1989). *Rock Engineering.* New York: McGraw—Hill.

Franssen, R.C.M.W., & Spiers, C.J. (1990). Deformation of polycrystalline salt in compression and in shear at 250-350°C. *Deformation Mechanisms, Rheology and Tectonics, Geological Society Special Publication, 45,* 201-213.

Fuenkajorn, K., & Daemen, J.J.K. (1988). Boreholes closure in salt. *Technical Report Prepared for the U.S. Nuclear Regulatory Commission.* Report No. NUREG/CR-5243 RW. University of Arizona.

Fuenkajorn, K., & Phueakphum, D. (2010). Effects of cyclic loading on mechanical properties of Maha Sarakham salt. *Engineering Geology, 112*(1-4), 43-52.

Fuenkajorn, K., Sriapai, T., & Samsri, P. (2012). Effects of loading rate on strength and deformability of Maha Sarakham salt. *Engineering Geology, 135*, 10-23.

Fuenkajorn, K., Walsri, C., & Phueakphum, D. (2011, November). Intrinsic variability of the mechanical properties of Maha Sarakham salt. *Journal of Engineering Geology and Hydrogeology, 44*(4), 445-456.

Gholami, R., & Rasouli, V. (2014). Mechanical and elastic properties of transversely isotropic slate. *Rock Mechanics and Rock Engineering, 47*, 1763-1773.

Gnirk, P.F., & Johnson, R.E. (1964). The deformational behavior of a circular mineshaft situated in a viscoelastic medium under hydrostatic stress. In *Proceedings of the 6th U.S. Symposium on Rock Mechanics (pp. 233-259).* University of Missouri, Rolla.

Goodman, R. E. (1989). Introduction to rock mechanics (2nd ed). New York: Wiley.

Günther, R. M., Salzer, K., Popp, T., & Lüdeling, C. (2015). Steady-state creep of rock salt: improved approaches for lab determination and modelling. *Rock mechanics and rock engineering, 48*, 2603-2613.

Hakala, M., Kuula, H., & Hudson, J. A. (2007). Estimating the transversely isotropic elastic intact rock properties for in situ stress measurement data reduction: a case study of the Olkiluoto mica gneiss, Finland. *International Journal of Rock Mechanics and Mining Sciences, 44*(1), 14-46.

Hamami, M. (1999). Simultaneous effect of loading rate and confining pressure on the deviator evolution in rock salt. *International Journal of Rock Mechanics and Mining Sciences, 36*(6), 827-831.

Hampel, A., Hunsche, U., Weidinger, P., & Blum, W. (1998). Description of the creep of rock salt with the composite model-II. Steady-State creep. *Series on rock and soil mechanics,* 287-299.

Handin, J., Russell, J.E., & Carter, N.L. (1984). Transient Creep of Repository Rocks. Final Report: *Mechanistic Creep Laws for Rock Salts*, Texas A & M research Foundation, Office of Nuclear Waste Isolation, Battelled Memorial Institute, Report, BMI/ONWI-550.

Hansen, F. D. (1997). Reconsolidating salt: compaction, constitutive modelling, and physical processes. *International Journal of Rock Mechanics and Mining Sciences, 34*(3-4), 119.e1-119.e12. doi:10.1016/S1365-1609(97)00072-5

Hardy, H. R., & Sun, X. (1986). A nonlinear rheological model for time-dependent behavior of geologic materials. *Proceeding of 27th US Symposium on Rock Mechanics* (pp. 205–212), Tuscaloosa: University of Albama.

Harrison, J.P., & Hudson, J.A. (2002). *Engineering Rock Mechanics: Part 2. Illustrative Worked Examples*. Netherlands: Elsevier.

Hatzor, Y. H., & Heyman, E. P. (1997). Dilation of anisotropic rock salt: Evidence from Mount Sedom diapir. *Journal of Geophysical Research: Solid Earth, 102*(B7), 14853-14868.

Heng, S., Guo, Y., Yang, C., Daemen, J. J., & Li, Z. (2015). Experimental and theoretical study of the anisotropic properties of shale. *International Journal of Rock Mechanics and Mining Sciences,* 74, 58-68.

Holcomb, D. J., & Hannum, D. W. (1982). Consolidation of crushed-salt backfill under conditions appropriate to the WIPP facility (Report No. SAND82-0630). Albuquerque, USA: Sandia National Laboratories.

Hu, S. C., Tan, Y. L., Zhou, H., Guo, W. Y., Hu, D. W., Meng, F. Z., & Liu, Z. G. (2017). Impact of bedding planes on mechanical properties of sandstone. *Rock Mechanics and Rock Engineering, 50*, 2243-2251.

Hunsche, U., & Hampel, A. (1999). Rock salt-the mechanical properties of the host rock material for a radioactive waste repository. *Engineering Geology, 52*(3-4), 271-291. doi:10.1016/S0013-7952(99)00011-3

Hunter, T.O. (1979). Technical issues of nuclear waste isolation in the Waste Isolation Pilot Plant (WIPP). *Proceedings of the 87th National Meeting American Institute of Chemical Engineers.* SAND79-1U7C, Sandia National Laboratories, United States.

Hwu, C., & Ting, T. C. T. (1989). Two-dimensional problems of the anisotropic elastic solid with an elliptic inclusion. *The Quarterly Journal of Mechanics and Applied Mathematics, 42*(4), 553-572.

Jaeger, J.C., Cook, N.G.W., & Zimmerman, R.W. (2007). *Fundamentals of Rock Mechanics.* Oxford: Blackweel.

Jandakaew, M. (2007). Stress-path dependency of rock salt. In Proc. of the First Thailand *Symposium on Rock Mechanics* (pp. 171-188). September 13-14, Greenery Resort, Khao Yai, Nakhon Ratchasima, Suranaree University of Technology.

Jeremic, M.K. (1994). Rock Mechanics in Salt Mining. Netherlands: A.A. Balkema.

Jiang, D. (2016). Viscous inclusions in anisotropic materials: Theoretical development and perspective applications. *Tectonophysics, 693*, 116-142.

Kensakoo, T. (2006). Relationship between mineralogy and engineering properties of rock salt (Doctoral dissertation). Suranaree University of Technology: School of Engineering in Civil, Transportation and Geo-resources Engineering.

Khaledi, K., Mahmoudi, E., Datcheva, M., & Schanz, T. (2016). Stability and serviceability of underground energy storage caverns in rock salt subjected to mechanical cyclic loading. *International Journal of Rock Mechanics and Mining Sciences, 86,* 115-131. doi:10.1016/j.ijrmms.2016.04.010

Khamrat, S., & Fuenkajorn, K. (2016). Time-dependent behavior of Maha Sarakham salt. under true triaxial stress state. *Songklanakarin Journal of Science and Technology, 27*(1), 23-30.

Khamrat, S., Tepnarong, P., Artkhonghan, K., & Fuenkajorn, K. (2018). Crushed salt consolidation for borehole sealing in potash mines. *Geotechnical and Geological Engineering, 36*, 49-62. doi:10.1007/s10706-017-0301-1

Kim, H., Cho, J. W., Song, I., & Min, K. B. (2012). Anisotropy of elastic moduli, P-wave velocities, and thermal conductivities of Asan Gneiss, Boryeong Shale, and Yeoncheon Schist in Korea. *Engineering Geology, 147*, 68-77.

Korn, G. A., & Korn, T. M. (1961). *Mathematical Handbook for Scientists and Engineers.* New York: McGraw-Hill.

Kou, H., He, C., Yang, W., Wu, F., Zhou, Z., Fu, J., & Xiao, L. (2023). A Fractional Nonlinear Creep Damage Model for Transversely Isotropic Rock. *Rock Mechanics and Rock Engineering, 56*(2), 831-846.

Langer, M. (1984). The rheological behavior of rock salt. Proceedings of the second conference on the mechanical behavior of salt (pp. 201–240). Clausthal, Germany: Trans Tech Publications.

Langer, M. (1993). Use of solution-mined caverns in salt for oil and gas storage and toxic waste disposal in Germany. *Engineering Geology, 35*(3-4), 183-190. doi:10.1016/0013-7952(93)90005-W

Langer, M. (1999). Principles of geomechanical safety assessment for radioactive waste disposal in salt structures. *Engineering Geology, 52*(3-4), 257-269. doi:10.1016/S0013-7952(99)00010-1

Li, C., Wang, J., & Xie, H. (2020). Anisotropic creep characteristics and mechanism of shale under elevated deviatoric stress. *Journal of Petroleum Science and Engineering, 185,* 106670.

Liang, W. G., Zhao, Y. S., Xu, S. G., & Dusseault, M. B. (2011). Effect of strain rate on the mechanical properties of salt rock. *International Journal of Rock Mechanics and Mining Sciences, 48*(1), 161-167.

Lindner, E. N., & Brady, B. H. G. (1984). Memory aspects of salt creep. *Proceedings of the first conference on the mechanics behavior of salt* (pp. 241-273). Clausthal-Zellerfeld: Trans Tech Publications

Ling, W. G., Xu, S. G., & Liu, J. (2007). Research on creep property and practical constitutive equation of rock salt in Jintan gas storage of China. *Journal of Liaoning Technical University, 26*(3), 354-356.

Liu, J., Yang, C. H., Wu, W., & Gao, X. P. (2006). Study on creep characteristics and constitutive relation ofrock salt. *Yantu Lixue(Rock and Soil Mechanics), 27*(8), 1267-1271.

Liu, Z. B., Xie, S. Y., Shao, J. F., and Conil, N. (2015). Effects of deviatoric stress and structural anisotropy on compressive creep behavior of a clayey rock. *Applied Clay Science, 114,* 491-496.

Luangthip, A., Wilalak, N., Thongprapha, T., & Fuenkajorn, K. (2017). Effects of carnallite content on mechanical properties of Maha Sarakham rock salt. *Arabian Journal of Geosciences, 10*(6), 149.

Luo, G., Yang, W., Bo, C., Zhang, L., Duan, K., Jing, W., & Zhao, Y. (2021). Viscoelastic analysis of the creep characteristics of interlayered rock specimens under uniaxial compression. *Mechanics of Time-Dependent Materials, 25,* 37-60.

Mansouri, H., & Ajalloeian, R. (2018). Mechanical behavior of salt rock under uniaxial compression and creep tests. *International Journal of Rock Mechanics and Mining Sciences, 110*, 19-27.

McLamore, R., & Gray, K. E. (1967). The mechanical behavior of anisotropic sedimentary rocks. *Journal of Engineering for Industry, 89*(1), 62-73.

Meng, L., Li, T., Liao, A., and Zeng, P. (2018). Anisotropic mechanical properties of sandstone under unloading confining pressure at high temperatures. *Arabian Journal for Science and Engineering, 43*(10), 5283-5294.

Miller D, Plumb R, & Boitnott G. (2013). Compressive strength and elastic properties of a transversely isotropic calcareous mudstone. *Geophysical Prospecting, 61*, 315–328.

Moslehy, A., & Alshibli, K. A. (2023). Influence of temperature and deviatoric stress on creep behavior of rock salt. *IOP Conference Series: Earth and Environmental Science* (pp. 012018). Finland: IOP Publishing. doi:10.1088/1755-1315/1124/1/012018

Moslehy, A., & Alshibli, K. A. (2023). Influence of temperature and deviatoric stress on creep behavior of rock salt. *IOP Conference Series: Earth and Environmental Science* (Vol. 1124, No. 1, pp. 012018). Finland: IOP Publishing. doi:10.1088/1755-1315/1124/1/012018

Motta, G. E., & Pinto, C. L. L. (2014). New constitutive equation for salt rock creep. *Rem: Revista Escola de Minas, 67,* 397-403. doi:10.1590/0370-44672014670165

Munson, D. E. (1997). Constitutive model of creep in rock salt applied to underground room closure. *International Journal of Rock Mechanics and Mining Sciences, 34*(2), 233-247.

Munson, D.E. (1997). Constitutive model of creep in rock salt applied to underground. *International Journal of Rock Mechanics and Mining Sciences, 34*(2), 233-247. doi:10.1016/S0148-9062(96)00047-2

Nair, K., Chang, C. Y., Singh, R. D., & Abdullah, A. M. (1974). Time-dependent analysis to predict closure in salt cavities. *Proceedings of the 4th Symposium on Salt* (pp. 129-139). Ohio: Cleveland.

Nasseri, M. H. B., Rao, K. S., & Ramamurthy, T. (2003). Anisotropic strength and deformational behavior of Himalayan schists. *International Journal of Rock Mechanics and Mining Sciences, 40*(1), 3-23.

Naumann, M., Hunsche, U., & Schulze, O. (2007). Experimental investigations on anisotropy in dilatancy, failure and creep of Opalinus Clay. *Physics and Chemistry of the Earth, Parts A/B/C, 32*(8-14), 889-895.

Nejati, M., Dambly, M.L.T., & Saar, M.O. (2019). A methodology to determine the elastic properties of anisotropic rocks from a single uniaxial compression test. Journal of Rock Mechanics and Geotechnical Engineering, 11(6), 1166–1183. doi:10.1016/j.jrmge.2019.04.004

Oksenkrug, E. S., & Shafarenko, E. M. (1974). Creep and creep strength of rock salt. *Soil Mechanics and Foundation Engineering, **11***(6), 387-389. doi:10.1007/BF01703810

Phatthaisong, K., Sartkaew, S., & Fuenkajorn, K. (2018). Effects of loading rate and temperature on strength and deformability of Maha Sarakham salt. *Songklanakarin J. Sci. Technol, 40*(2), 359-366.

Polyanin, A. D., & Manzhirov, A. V. (2006). Handbook of Mathematics for Engineers and Scientists. New York: Taylor & Francis Group.

Raj, S.V., & Pharr, G.M. (1992). Effect of temperature on the formation of creep substructure in sodium chloride single crystal. *American Ceramic Society, 75*(2), 347-352.

Ramamurthy, T. (1993). Strength and Modulus Responses of anisotropic rocks. *Comprehensive rock engineering, 1,* 313-329.

Richard, J. (1993). *Plasticity and creep.* Theory, Example, and Problems, English Edition Editor, Rochester Institute of Technology, Rochester, New York: Springer Science & Business Media.

Riley, K.F., Hobson, M.P., & Bence, S.J. (1998). Mathematical Methods for Physics and Engineering. Cambridge, Cambridge University Press.

Rouabhi, A., Labaune, P., Tijani, M., Gatelier, N., & Hévin, G. (2019). Phenomenological behavior of rock salt: On the influence of laboratory conditions on the

dilatancy onset. *Journal of Rock Mechanics and Geotechnical Engineering, 11*(4), 723-738.

Saeidi, O., Rasouli, V., Vaneghi, R. G., Gholami, R., & Torabi, S. R. (2014). A modified failure criterion for transversely isotropic rocks. *Geoscience Frontiers, 5*(2), 215-225.

Samsri, P., Sriapai, T., Walsri ,C., & Fuenkajorn, K. (2010). Polyaxial creep testing of rock salt. In *Proceedings of the 3th Thailand Symposium on Rock Mechanics* (pp. 125-132). Thailand.

Sartkaew, S., & Fuenkajorn, K. (2013). Effects of stress rate on uniaxial compressive strength of rock salt under 0-100 C. In *The 11th International Conference on Mining, Materials and Petroleum Engineering* (pp. 13-20). Chiang Mai, Thailand.

Senseny, P. E. (1982). Influence of specimen size on the creep of rock salt. Virginia: National Technical Information Service U. S. Department of Commerce Springfield.

Senseny, P. E. (1984). Specimen size and history effects on creep of salt. *Proceedings of the 1st Conference on the Mechanics Behavior of Salt* (pp. 369-379). Clausthal-Zellerfeld, Germany, Trans Tech Publications.

Senseny, P.E. (1983). *Review of Constitutive Laws used to Describe the Creep of Salt.* United States: Office of Nuclear Waste Isolation, Batelle Memorial Institute.

Senseny, P.E., Hansen, F.D., & Russell, J.E. (1992). Mechanical behaviour of rock salt: phenomenology and micromechanisms. *International Journal of Rock Mechanics and Mining Sciences & Geomechanics Abstracts, 29*, 363–378. doi:10.1016/0148- 9062(92)90513-Y

Senseny, P.E., Hansen, F.D., Russell, J.E., Carter, N.L., & Handin, J.W. (1992). Mechanical behaviour of rock salt: phenomenology and micromechanisms. *International Journal of Rock Mechanics and Mining Sciences, 29*(4), 363-378.

Senseny, P.E., Pfeifle, T.W., Mellegard, & K.D. (1986). *Exponential-time Constitutive Law for Palo Duro Unit 4 Salt from the J. Friemel No. 1 Well:* Technical Report (Vol. 595). Batttelle Memorial Institute, Columbus, Ohio: Office of Nuclear Waste Isolation.

Shen, L. J., & Siritongkham, N. (2020). The characteristics, formation and exploration progress of the potash deposits on the Khorat Plateau, Thailand and Laos, Southeast Asia. *China Geology, 3*(1), 67-82.

Sriapai T, Walsri C, & Fuenkajorn K. (2013). True-triaxial compressive strength of Maha Sarakham salt. *International Journal of Rock Mechanics and Mining Sciences, 61,* 256–265.

Sriapai, T., Samsri, P., & Fuenkajorn, K. (2011). Polyaxial strengths of Maha Sarakham salt. In *Proceedings of the 3th Thailand Symposium on Rock Mechanics* (pp. 79-87). Nakhon Ratchasima, Thailand.

Staudtmeister, K., & Rokahr, R. B. (1997). Rock mechanical design of storage caverns for natural gas in rock salt mass. *International Journal of Rock Mechanics and Mining Sciences, 34*(3-4), 300.e1-300.e13. doi:10.1016/S1365-1609(97)00199-8

Sukjaroen, N., Thongprapha, T., Artkhonghan, K., & Fuenkajorn, K. (2021). Effects of transverse isotropy on compressive strength and elastic properties of rock salt. *Engineering Journal of Research and Development, 32*(1), 47-54.

Thongprapha, T., Tengpakwaen, K., Daemen, J. J. K., & Fuenkajorn, K. (2022). Effect of confining pressures on transverse isotropy of Maha Sarakham salt. *International Journal of Rock Mechanics and Mining Sciences, 152*, 105077.

Tsidzi, K. (1990). The influence of foliation on point load strength anisotropy of foliated rocks. Bull. *Int. Association of Eng. Geology, 29*, 49-58.

Wang, G., Zhang, L., Zhang, Y., & Ding, G. (2014). Experimental investigations of the creep–damage–rupture behaviour of rock salt. *International Journal of Rock Mechanics and Mining Sciences, 66*, 181-187.

Wang, J. B., Liu, X. R., Guo, J. J., & Huang, M. (2014). Creep properties of salt rock and its nonlinear constitutive model. *Journal of China Coal Society, 39*(3), 445-451. (in Chinese)

Wang, J. B., Liu, X. R., Song, Z. P., Zhao, B. Y., Jiang, B., & Huang, T. Z. (2018). A whole process creeping model of salt rock under uniaxial compression based on inverse S function. *Chinese Journal of Rock Mechanics and Engineering, 37*(11), 27-40.

Wang, J., Xie, L., Xie, H., Ren, L., He, B., Li, C., ..., & Gao, C. (2016). Effect of layer orientation on acoustic emission characteristics of anisotropic shale in Brazilian tests. *Journal of Natural Gas Science and Engineering, 36*, 1120-1129.

Wang, T. T., Ma, H. L., Shi, X. L., Yang, C. H., Zhang, N., Li, J. L., Ding, S. L., & Daemen, J. J. K. (2018). Salt cavern gas storage in an ultra-deep formation in Hubei, China. *International Journal of Rock Mechanics and Mining Sciences, **102***, 57-70. doi:10.1016/j.ijrmms.2017.12.001

Wang, T., Yang, C., Ma, H., Li, Y., & Shi, X. (2016). Safety evaluation of salt cavern gas storage close to an old cavern. *International Journal of Rock Mechanics and Mining Sciences, 83*(3), 95–106. doi: 10.1016/j.ijrmms.2016.01.005

Wang, W., Yajun, C., Zhu, Q., Xu, W., & Shao, J. (2015). Experimental investigation and constitutive modelling of creep-damage behaviours in monzogranite. *European Journal of Environmental and Civil Engineering, 19*, 54-69.

Wang, Z., Zong, Z., Qiao, L., & Li, W. (2018). Transversely Isotropic Creep Model for Rocks. *International Journal of Geomechanics, 18*(6).

Warren, J.K. (1999). *Evaporites: Their Evolution and Economics.* Oxford: Blackwell Science.

Wawersik, W.R. (1988). Alternatives to a power law creep model for rock salt at temperatures below 160 °C. In *Proceedings of the Second Conference on the Mechanical Behavior of Salt,* Germany.

Wendai, L. (2000). *Regression Analysis, Linear Regression and Probit Regression In 13 Chapters.* Beijing: Publishing House of Electronic Industry.

Worotnicki, G. (1993). CSIRO triaxial stress measurement cell. In *Comprehensive Rock engineering* (Edited by Hudson J. A.), Chap. 13*, 3*, 329-394.

Wu, C., Chen, Q., Basack, S., & Karekal, S. (2018). Laboratory investigation on rheological properties of greenschist considering anisotropy under multi-stage compressive creep condition. *Journal of Structural Geology, 114*, 111-120.

Wu, C., Chen, Q., Basack, S., Xu, R., & Shi, Z. (2016). Biaxial creep test study on the influence of structural anisotropy on rheological behavior of hard rock. *Journal of Materials in Civil Engineering,* 28(10).

Wu, F., Chen, J., & Zou, Q. (2019). A nonlinear creep damage model for salt rock. *International Journal of Damage Mechanics, 28*(5), 758-771.

Wu, F., Liu, J. F., & Wang, J. (2015). An improved Maxwell creep model for rock based on variable-order fractional derivatives. *Environmental earth sciences, 73*, 6965-6971.

Xiong, L., Li, T., & Yang, L. (2014). Biaxial compression creep test on green-schist considering the effects of water content and anisotropy. *KSCE Journal of Civil Engineering, 18,* 103-112.

Xu, G., He, C., Su, A., & Chen, Z. (2018). Experimental investigation of the anisotropic mechanical behavior of phyllite under triaxial compression. International *Journal of Rock Mechanics and Mining Sciences, 104*, 100-112.

Xu, G., He, C., Yan, J., & Ma, G. (2019). A new transversely isotropic nonlinear creep model for layered phyllite and its application. *Bulletin of Engineering Geology and the Environment, 78,* 5387-5408.

Yang, C., Daemen, J. J. K., & Yin, J.-H. (1999). Experimental investigation of creep behavior of salt rock. *International Journal of Rock Mechanics and Mining Sciences, 36*(2), 233-242.

Yun-si, L, Xiao, Z, & Quan, Y. (2012). The five elastic parameters for the anisotropy of slate under the influence of different bedding orientations. *Electronic Journal of Geotechnical Engineering, 17*, 3695-3707.

Zhang, L. (2006). *Engineering Properties of Rocks* (2nd ed). Cambridge: Butterworth-Heinemann.

Zhang, H., Wang, Z., Zheng, Y., Duan, P., & Ding, S. (2012). Study on tri-axial creep experiment and constitutive relation of different rock salt. *Safety Science, 50*(4), 801-805.

Zhang, J., Zhang, X., Huang, Z., & Fu, H. (2022). Transversely isotropic creep characteristics and damage mechanism of layered phyllite under uniaxial compression creep test and its application. *Environmental Earth Sciences, 81*(20), 499.

Zhou, H. W., Wang, C. P., Mishnaevsky, L., Duan, Z. Q., & Ding, J. Y. (2013). A fractional derivative approach to full creep regions in salt rock. *Mechanics of Time-Dependent Materials, 17*, 413-425.

APPENDIX A

RESULTS OF CALIBRATION BY USING BURGERS MODEL

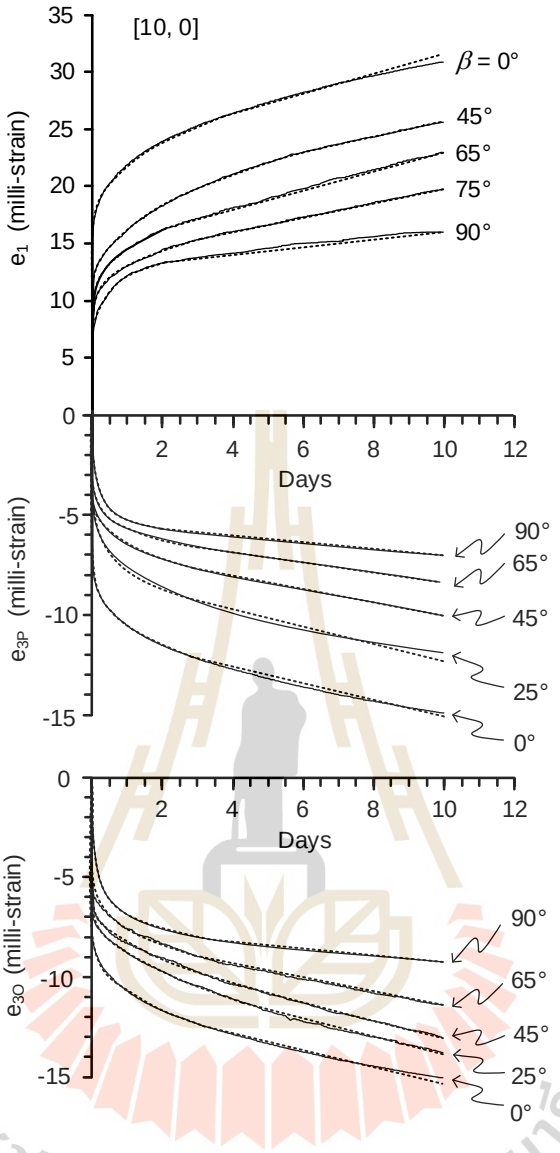

Figure A.1 Strain deviation-time curves of salt specimens with angles β for uniaxial creep test (solid lines) and curves fitting with Burgers model (dash lines). Numbers in bracket represent [σ_1, σ_3].

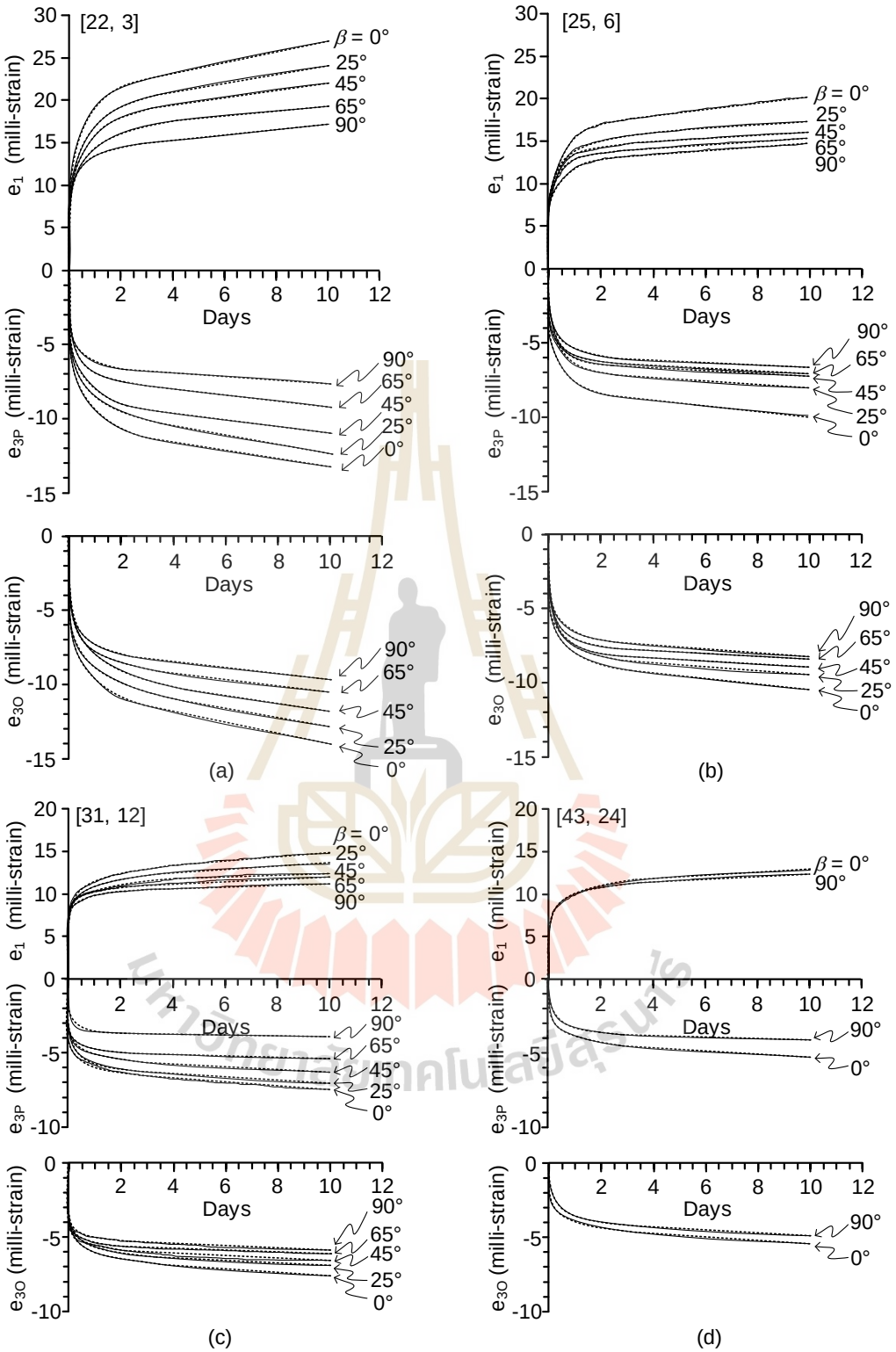

Figure A.2 Strain deviation-time curves of salt specimens with angles β for triaxial creep test (solid lines) under the confining pressure of 3 MPa (a), 6 MPa (b), 12 MPa (c), and 24 MPa (d) and curves fitting with Burgers model (dash lines). Numbers in bracket represent [σ_1, σ_3].

APPENDIX B
LIST OF PUBLICATION

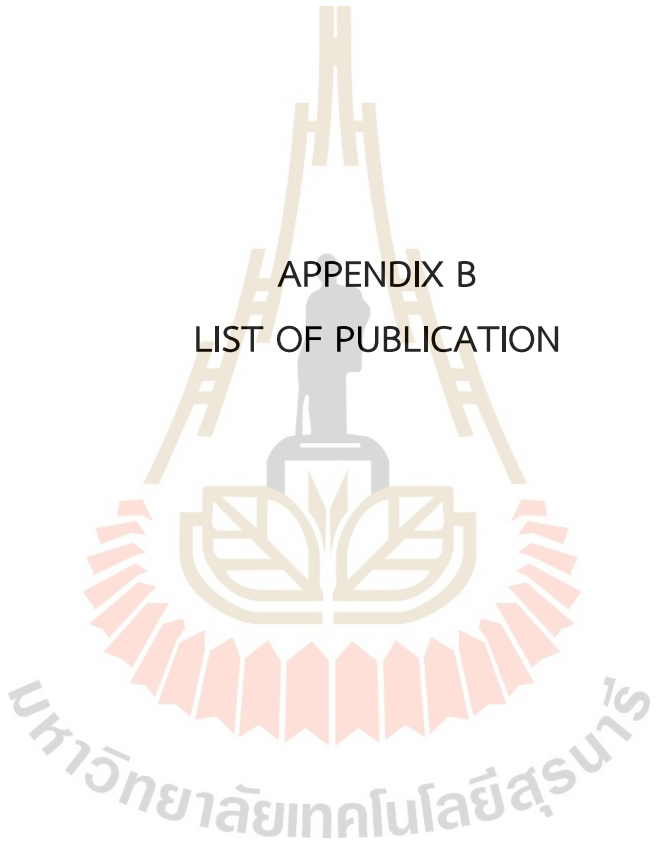

วารสารวิชาการพระจอมเกล้าพระนครเหนือ ปีที่ 34 ฉบับที่ 2 เม.ย.–มิ.ย. 2567
The Journal of KMUTNB., Vol. 34, No. 2, Apr.–Jun. 2024

บทความวิจัย

การพัฒนาสมการแสดงคุณสมบัติที่ขึ้นกับเวลาของเกลือหินแบบทรานซ์เวอร์สไอโซทรอปี

กัญญา ไกรปรุ และ ธนิษฐา ทองประภา*
หน่วยวิจัยกลศาสตร์ธรณี สำนักวิชาวิศวกรรมศาสตร์ มหาวิทยาลัยเทคโนโลยีสุรนารี

* ผู้นิพนธ์ประสานงาน โทรศัพท์ 0 4422 3363 อีเมล: thanittha@sut.ac.th
DOI: 10.14416/j.kmutnb.2023.xx.xxx
รับเมื่อ 20 พฤษภาคม 2565 แก้ไขเมื่อ 18 กรกฎาคม 2565 ตอบรับเมื่อ 9 สิงหาคม 2565 เผยแพร่ออนไลน์ x 2566

บทคัดย่อ

งานวิจัยนี้มีวัตถุประสงค์เพื่อหาคุณสมบัติที่ขึ้นกับเวลาของเกลือหินชุดมหาสารคามที่มีลักษณะแบบทรานซ์เวอร์สไอโซทรอปี แบบจำลองการคืบของหินแบบทรานซ์เวอร์สไอโซทรอปีถูกพัฒนาจากสมการของ Amadei ให้อยู่ในรูปค่าคงที่ของเบอเกอร์และมุมการวางตัวของชั้นหิน งานวิจัยนี้ได้ทดสอบการคืบในแกนเดียวกับตัวอย่างเกลือหินที่มีระนาบการวางตัวของชั้นหิน (β) ผันแปรตั้งแต่ 0 45 60 75 ถึง 90 องศา ตามลำดับ เพื่อเปรียบเทียบกับแบบจำลองที่ถูกพัฒนาขึ้น ผลการทดสอบระบุว่า ความเครียดในแนวแกนและแนวด้านข้างมีค่าสูงสุดเมื่อแนวแรงกดตั้งฉากกับระนาบของชั้นหิน (β = 0°) และมีค่าต่ำสุดเมื่อแนวแรงกดขนานกับระนาบของชั้นหิน (β = 90°) การวิเคราะห์เชิงถดถอยระบุว่าสัมประสิทธิ์ความยืดหยุ่น ความหนืดเชิงยืดหยุ่น และความหนืดเชิงพลาสติกมีค่าสูงขึ้นเมื่อมุม β มากขึ้น แบบจำลองการคืบของหินแบบ ทรานซ์เวอร์สไอโซทรอปีสามารถคาดคะเนการเปลี่ยนแปลงรูปร่างและหาค่าสัมประสิทธิ์ความยืดหยุ่นปรากฏและอัตราส่วนปัวส์ซองปรากฏเชิงเวลาของเกลือหินภายใต้สภาวะที่ชั้นหินมีระนาบการวางตัวแตกต่างกันได้ และสามารถใช้ในการคาดคะเนการเปลี่ยนแปลงรูปร่างเชิงเวลาของโครงสร้างใต้ดิน เช่น เสาค้ำยันและผนังด้านข้างของเหมืองเกลือหินได้

คำสำคัญ: การคืบของหิน ระนาบชั้นหิน แบบจำลองแบบเบอเกอร์ เกลือหินมหาสารคาม

การอ้างอิงบทความ: กัญญา ไกรปรุ และ ธนิษฐา ทองประภา, "การพัฒนาสมการแสดงคุณสมบัติที่ขึ้นกับเวลาของเกลือหินแบบทรานซ์เวอร์สไอโซทรอปี," *วารสารวิชาการพระจอมเกล้าพระนครเหนือ*, ปีที่ 34, ฉบับที่ 2, หน้า 1–11, เลขที่บทความ 242-066081, เม.ย.–มิ.ย. 2567.

2 วารสารวิชาการพระจอมเกล้าพระนครเหนือ ปีที่ 34 ฉบับที่ 2 เม.ย.–มิ.ย. 2567
The Journal of KMUTNB., Vol. 34, No. 2, Apr.–Jun. 2024

Research Article

Development of Constitutive Equations for Time-Dependent Behavior of Transverse Isotropic Rock Salt

Kanya Kraipru and Thanittha Thongprapha*
Geomechanics Research Unit, Suranaree University of Technology, Nakhon Ratchasima, Thailand

* Corresponding Author, Tel. 0 4422 3363, E–mail: thanittha@sut.ac.th
DOI: 10.14416/j.kmutnb.2023.xx.xxx
Received 20 May 2022; Revised 18 July 2022; Accepted 9 August 2022; Published online: x 2023

Abstract

The objective of this study is to determine the time- dependent properties of transverse isotropic Maha Sarakham rock salt. The transverse isotropic creep models have been derived in the form of Burgers parameters and bedding plane orientations based on Amadei' s solutions. Uniaxial creep tests have been performed on the rock salt specimens with bedding plane orientations (β) varying from 0, 45, 65, 75, to 90° to compare with the proposed creep models. The axial and lateral strains of rock salt specimens are the largest when the loading direction is normal to the bedding plane (β = 0°) and smallest when parallel to the bedding plane (β = 90°). Regression analyses of the results indicate that the elastic, viscoelastic, and visco- plastic parameters increase with increasing angle. The transverse isotropic creep models are capable of predicting the measured creep strains and determining the apparent time-dependent Young's modulus and Poisson' ratios of rock salt under various bedding orientations. The transverse isotropic creep models can be used to predict the time-dependence deformation of underground structures such as salt pillars and mine sidewalls.

Keywords: Creep, Bedding Plane, Burgers Model, Maha Sarakham Salt

Please cite this article as: K. Kraipru and T. Thongprapha, "Development of Constitutive Equations for Time-Dependent Behavior of Transverse Isotropic Rock Salt," *The Journal of KMUTNB*, vol. 34, no. 2, pp. 1–11, ID. 242-066081, Apr.–Jun. 2024 (in Thai).

วารสารวิชาการพระจอมเกล้าพระนครเหนือ ปีที่ 34 ฉบับที่ 2 เม.ย.–มิ.ย. 2567
The Journal of KMUTNB., Vol. 34, No. 2, Apr.–Jun. 2024

1. บทนำ

เกลือหินชุดมหาสารคามในพื้นที่ภาคตะวันออกเฉียงเหนือของประเทศไทย มีการวางตัวเป็นระนาบและมักพบลักษณะแบบทรานซ์เวอร์สไอโซทรอปิเนื่องจากชั้นของการตกผลึกและแร่เจือปน ได้แก่ แอนไฮไดรต์ โพแทช ยิปซัม และแร่ดินเหนียว ซึ่งแร่เจือปนเหล่านี้อาจแทรกอยู่ระหว่างชั้นหรือกระจายตัวอยู่ระหว่างผลึกของเกลือหิน ลักษณะทรานซ์เวอร์สไอโซทรอปินี้ส่งผลกระทบต่อสมบัติเชิงกลศาสตร์ของหิน Jeremic [1] พบว่า ค่ากำลังรับแรงกดในแกนเดียวของเกลือหินจากประเทศโปแลนด์มีค่าต่ำสุดเมื่อมุมระหว่างแนวแกนที่ตั้งฉากกับระนาบชั้นหินและแนวแรงในแกนหลัก (β) เท่ากับ 45 องศา Sukjaroen และคณะ [2] พบว่า ค่ากำลังรับแรงกดในแกนเดียวของเกลือหินมีค่าต่ำสุดเมื่อมุม β เท่ากับ 60 องศา ซึ่งสอดคล้องกับผลการทดสอบในหินชนวน หินดินดาน [3] หินทราย หินทรายแป้ง หินโคลน [4], [5] หินปูน หินแกรนิต และหินชีสต์ [6] และค่าสัมประสิทธิ์ความยืดหยุ่นแปรผันตามมุม β [7]–[9] Thongprapha และคณะ [10] พบว่า ค่าสัมประสิทธิ์ความยืดหยุ่นในการทดสอบกำลังรับแรงกดในแกนเดียวและในสามแกนของเกลือหินมีค่าต่ำสุดเมื่อมุม β เท่ากับ 0 องศา และสูงสุดเมื่อมุม β เท่ากับ 90 องศา เกลือหินจะมีการเปลี่ยนแปลงพฤติกรรมจากแบบทรานซ์เวอร์สไอโซทรอปิเป็นแบบไอโซทรอปิภายใต้ความเค้นล้อมรอบสูงกว่า 30 เมกกะปาสคาล โดยค่ากำลังรับแรงกดในทุกมุม β จะมีค่าเท่ากัน Dubey [11] พบว่า ภายใต้อัตราการกดต่ำจะมีการแตกแบบแรงดึงเนื่องจากผลกระทบของทรานซ์เวอร์สไอโซทรอปิ ลักษณะทรานซ์เวอร์สไอโซทรอปิมีผลกระทบต่อพฤติกรรมการคืบ โดยผลกระทบจะลดลงเมื่ออัตราการกดสูงขึ้น [12] ผลสรุปข้างต้นบ่งชี้ว่าหินที่มีลักษณะแบบทรานซ์เวอร์สไอโซทรอปิส่งผลต่อคุณสมบัติเชิงกลศาสตร์และเชิงเวลาของเกลือหิน ดังนั้นในการวิเคราะห์และออกแบบทางด้านวิศวกรรมธรณีของเกลือหิน จึงควรพิจารณามุมของระนาบชั้นหินร่วมด้วยเพื่อลดผลกระทบดังกล่าว

นักวิจัยหลายท่านได้พัฒนาสมการสำหรับใช้ในการวิเคราะห์ผลกระทบของทรานซ์เวอร์สไอโซทรอปิต่อคุณสมบัติของหิน โดย Amadei [13] ได้พัฒนาสมการที่ใช้ในการหาค่าสัมประสิทธิ์ความยืดหยุ่นของหินแบบทรานซ์เวอร์สไอโซทรอปิภายใต้การทดสอบกำลังรับแรงกดในแกนเดียวบนตัวอย่างหินที่มีระนาบชั้นหินตั้งฉากและขนานกับทิศทางการเจาะ Hatzor และคณะ [14] ได้พัฒนาสมการสำหรับวิเคราะห์การยุบตัวและขยายตัวของเกลือหินแบบทรานซ์เวอร์สไอโซทรอปิ Zhang และคณะ [15] ใช้สมการแบบจำลองการคืบแบบ ubhm ซึ่งประกอบด้วย แบบจำลองแม็กซ์เวล แบบจำลองเคลวิน และแบบจำลองไม่เป็นเชิงเส้นแบบวิสโคพลาสติก ในการวิเคราะห์พฤติกรรมการคืบของหินที่มีการวางตัวแบบชั้นในสองมิติ และต่อมาได้มีการวิเคราะห์แบบสามมิติพบว่า แบบจำลอง ubhm [16] สามารถอธิบายพฤติกรรมการคืบทุกช่วงของหินได้ และประยุกต์ใช้แบบจำลองนี้ในการประเมินความปลอดภัยของอุโมงค์ที่หินโดยรอบมีลักษณะแบบทรานซ์เวอร์สไอโซทรอปิ Luo และคณะ [17] พัฒนาสมการจำลองการคืบแบบวิสโคอิลาสติกสำหรับหินเนื้ออ่อนและหินเนื้อแข็งวางตัวสลับชั้นกันโดยระนาบระหว่างชั้นตั้งฉากและขนานกับแนวแรง อย่างไรก็ตามพบว่า ยังไม่มีการพัฒนาแบบจำลองที่สามารถคาดคะเนการเปลี่ยนแปลงรูปร่างและคุณสมบัติเชิงเวลาของเกลือหินภายใต้การผันแปรมุมของระนาบชั้นหิน งานวิจัยนี้มีวัตถุประสงค์เพื่อพัฒนาสมการจำลองการคืบของเกลือหินแบบทรานซ์เวอร์สไอโซทรอปิเพื่อนำมาใช้ในการคาดคะเนการเปลี่ยนแปลงรูปร่างและคุณสมบัติที่ขึ้นกับเวลาของเกลือหิน

2. วัสดุ อุปกรณ์และวิธีการวิจัย

2.1 ทฤษฎีและสมการที่เกี่ยวข้อง

การศึกษานี้ได้มุ่งเน้นในหินที่มีลักษณะแบบทรานซ์-เวอร์สไอโซทรอปิ ซึ่งจะมีสมบัติเหมือนกันในทิศทางของระนาบหนึ่งและคุณสมบัติจะเปลี่ยนแปลงไปในทิศทางที่ตั้งฉากกับระนาบนั้น เมื่อพิจารณาภายใต้ระบบแกน x, y และ z จะกำหนดให้แกน x และแกน y ทำมุมตั้งฉากกันในระนาบที่ตั้งฉากกับแกนหมุนสมมาตรรอบแกน z ในกรณีที่ชั้นหินวางตัวขนานกับทิศทางของแนวแกน y ($\beta = 90^{o}$) ระนาบ y-z จะเป็นระนาบที่มีคุณสมบัติเหมือนกันในทิศทางแกน y และแกน z เรียกว่า ระนาบทรานซ์เวอร์สไอโซทรอปิ (ระนาบการ

วางตัวของชั้นหิน) ซึ่งสามารถกำหนดคุณสมบัติด้วยค่าคงที่ของความยืดหยุ่นจำนวน 5 ค่า ได้แก่ ค่าสัมประสิทธิ์ความยืดหยุ่นและค่าอัตราส่วนปัวส์ซองในระนาบสมมาตร y-z ($E_y = E_z$ และ ν_{yz}) ค่าสัมประสิทธิ์ความยืดหยุ่นและค่าอัตราส่วนปัวส์ซองในแกน x (E_x และ $\nu_{yx} = \nu_{zx}$) และค่าสัมประสิทธิ์ความเฉือนในแกน x (G_{xy}) แต่ในกรณีที่ชั้นหินวางตัวตั้งฉากกับทิศทางของแนวแกน y (β = 0°) ระนาบทรานซ์เวอร์สไอโซทรอปี คือ ระนาบสมมาตรของแกน z-x

Amadei [13] พัฒนาสมการวิเคราะห์คุณสมบัติของวัสดุแบบทรานซ์เวอร์สไอโซทรอปีภายใต้การรับแรงอย่างสม่ำเสมอ (Uniform Stress) ตามกฎของฮุค โดยกำหนดให้สมการประกอบด้วยค่าคงที่ 5 ค่า ได้แก่ E (E_y ที่ β = 90°), E' (E_y ที่ β = 0°), ν (ν_{yz} ที่ β = 90°), ν' (ν_{yx} ที่ β = 90°) และ G' (G_{xy} ที่ β = 90°) ความสัมพันธ์ระหว่างความเครียดในแนวแกน x, y และ z (ε_x ε_y และ ε_z) กับความเค้น (σ) อธิบายได้ดังสมการที่ (1)

$$\varepsilon_x = a_{12}\sigma; \quad \varepsilon_y = a_{22}\sigma; \quad \varepsilon_z = a_{23}\sigma \tag{1}$$

โดย a_{12} a_{22} และ a_{23} คือ องค์ประกอบของเมทริกซ์ Compliance ที่อยู่ในฟังก์ชันของค่าคงที่และมุมของระนาบทรานซ์เวอร์สไอโซทรอปี (β) แสดงดังสมการที่ (2)–(4)

$$a_{12} = -\frac{\nu'}{E'}\sin^4\beta - \frac{\nu'}{E'}\cos^4\beta + \frac{\sin^2 2\beta}{4}\left(\frac{1}{E} + \frac{1}{E'} - \frac{1}{G'}\right) \tag{2}$$

$$a_{22} = \frac{\cos^4\beta}{E'} + \frac{\sin^4\beta}{E} + \frac{\sin^2 2\beta}{4}\left(\frac{1}{G'} - \frac{2\nu'}{E'}\right) \tag{3}$$

$$a_{23} = -\frac{\nu'}{E'}\cos^2\beta - \frac{\nu}{E}\sin^2\beta \tag{4}$$

โดยที่ E และ E' คือ สัมประสิทธิ์ความยืดหยุ่นที่ขนานและตั้งฉากกับทิศทางแนวระดับของระนาบชั้นหิน ตามลำดับ ν คือ อัตราส่วนปัวส์ซองบนระนาบชั้นหิน ν' คือ อัตราส่วนปัวส์ซองบนระนาบระหว่างแกนที่ตั้งฉากและขนานของระนาบชั้นหิน G' คือ มอดูลัสต้านแรงเฉือนบนระนาบที่

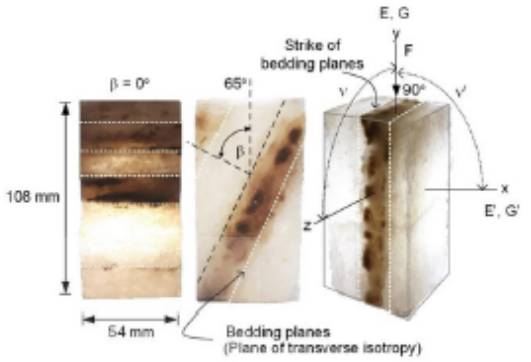

รูปที่ 1 ตัวอย่างเกลือหินที่ถูกเตรียมเพื่อทดสอบการคืบในแกนเดียว

ตั้งฉากกับระนาบชั้นหิน และ β คือ มุมระหว่างแกนที่ตั้งฉากกับระนาบชั้นหินและทิศทางของแนวแรง (รูปที่ 1) โดย G' คำนวณได้ดังสมการที่ (5)

$$\frac{1}{G'} = \left(\frac{1}{E} + \frac{1}{E'} + \frac{2\nu'}{E'}\right) \tag{5}$$

เนื่องจากหินที่มีลักษณะแบบทรานซ์เวอร์สไอโซทรอปีจะมีคุณสมบัติที่ขึ้นกับทิศทางของระนาบชั้นหิน จึงมีการพัฒนาสมการที่ใช้หาค่าคงที่เพื่อเป็นตัวแทนของคุณสมบัติในทิศทางของระนาบชั้นหินใดๆ จากความสัมพันธ์ของสมการที่ (1)–(5) ค่าดังกล่าว คือ ค่าสัมประสิทธิ์ความยืดหยุ่นปรากฏ ($E_{y(\beta)}$) อัตราส่วนปัวส์ซองปรากฏบนระนาบระหว่างแกน y และแกน x ($\nu_{yx(\beta)}$) และอัตราส่วนปัวส์ซองปรากฏบนระนาบระหว่างแกน y และแกน z ($\nu_{yz(\beta)}$) ดังแสดงในสมการที่ (6)

$$E_{y(\beta)} = \frac{1}{a_{22}}; \quad \nu_{yx(\beta)} = -\frac{a_{12}}{a_{22}}; \quad \nu_{yz(\beta)} = -\frac{a_{23}}{a_{22}} \tag{6}$$

โดยข้อดีของสมการวิเคราะห์คุณสมบัติทรานซ์เวอร์สไอโซทรอปีของ Amadei [13] คือ สามารถหาค่าคงที่ในการคำนวณได้จากการทดสอบกำลังรับแรงกดในแกนเดียว และสามารถจำลองพฤติกรรมของหินที่มีลักษณะแบบทรานซ์เวอร์สไอโซทรอปีได้ครอบคลุม แต่ยังไม่สามารถอธิบายพฤติกรรมที่ขึ้นกับเวลาของหินได้

2.2 การพัฒนาสมการสำหรับจำลองการคืบของหินแบบทรานซ์เวอร์สไอโซทรอปี

แบบจำลองการคืบในหินที่มีลักษณะแบบทรานซ์เวอร์ส-ไอโซทรอปีถูกพัฒนาขึ้นจากสมการการวิเคราะห์คุณสมบัติทรานซ์เวอร์สไอโซทรอปีของ Amadei [13] ด้วยวิธีการทางคณิตศาสตร์ขั้นสูงในรูปแบบการแปลงลาปลาซ กำหนดให้เกลือหินมีพฤติกรรมการคืบแบบเบอเกอร์ เนื่องจากสามารถจำลองพฤติกรรมการคืบของเกลือหินได้เหมาะสมที่สุด [18] โดยได้ถูกพัฒนาขึ้นเพื่อใช้สำหรับจำลองพฤติกรรมที่ขึ้นกับเวลาของหินที่มีมุมของระนาบชั้นหินแตกต่างกัน สมมุติฐานของการพัฒนาแบบจำลองการคืบของหินสำหรับงานวิจัยนี้ คือ กำหนดให้เกลือหินมีพฤติกรรมการคืบตามแบบจำลองกลุ่มวิสโคอิลาสติกเชิงเส้น (Linear Viscoelastic Material) ที่มีพฤติกรรมแบบยืดหยุ่นและแบบหนืดร่วมกัน มีความสัมพันธ์กับหินแบบทรานซ์เวอร์สไอโซทรอปีที่มีพฤติกรรมแบบยืดหยุ่นเชิงเส้น (Linear Elastic Material) ภายใต้การใช้ทฤษฎีบทการซ้อนทับ (Superposition Principle)

จากสมการที่ (1)–(5) สามารถเขียนในรูปของการแปลงลาปลาซด้วยตัวแปร “s” ดังสมการที่ (7)–(9)

$$\hat{\varepsilon}_x(s) = \hat{a}_{12}(s)\hat{\sigma}(s) = -\hat{\sigma}(s)\left(\frac{\hat{\nu}'(s)}{\hat{E}'(s)}\right)A \tag{7}$$

$$\hat{\varepsilon}_y(s) = \hat{a}_{22}(s)\hat{\sigma}(s) = \hat{\sigma}(s)\left[\left(\frac{1}{\hat{E}'(s)}\right)(B)+\left(\frac{1}{\hat{E}(s)}\right)(C)\right] \tag{8}$$

$$\hat{\varepsilon}_z(s) = \hat{a}_{23}(s)\hat{\sigma}(s) = -\hat{\sigma}(s)\left[\left(\frac{\hat{\nu}'(s)}{\hat{E}'(s)}\right)(D)+\left(\frac{\hat{\nu}(s)}{\hat{E}(s)}\right)(F)\right] \tag{9}$$

และ

$$A = \left(\sin^4\beta + \cos^4\beta + \frac{\sin^2 2\beta}{2}\right)$$

$$B = \left(\cos^4\beta + \frac{\sin^2 2\beta}{4}\right),\ C = \left(\sin^4\beta + \frac{\sin^2 2\beta}{4}\right)$$

$$D = \cos^2\beta;\ F = \sin^2\beta$$

ความเค้น σ เป็นตัวแปรที่ไม่ขึ้นกับเวลา ดังนั้น ตัวแปร $\hat{\sigma}(s)$ แทนด้วย $\frac{\sigma}{s}$

กำหนดให้เกลือหินอยู่ภายใต้สภาวะความเค้นอุทกสถิต (Hydrostatic Stress) และใช้สัมประสิทธิ์ความหนืดยืดหยุ่น (Viscoelastic Coefficients) และตัวดำเนินการเวลา (Time Operators) ดังสมการที่ (10) และ (11)

$$\hat{E}_v(s) = \frac{9K\hat{Q}_1}{\hat{Q}_1 + 6K\hat{P}_1},\ \hat{\nu}_v(s) = \frac{3K\hat{Q}_1 - \hat{Q}_1}{\hat{Q}_1 + 6K\hat{P}_1} \tag{10}$$

$$\hat{E}'_v(s) = \frac{9K\hat{Q}'_1}{\hat{Q}'_1 + 6K\hat{P}'_1},\ \hat{\nu}'_v(s) = \frac{3K\hat{Q}'_1 - \hat{Q}'_1}{\hat{Q}'_1 + 6K\hat{P}'_1} \tag{11}$$

โดย $\hat{E}_v(s)$ และ $\hat{E}'_v(s)$ คือสัมประสิทธิ์ความยืดหยุ่นแบบวิสโคอิลาสติกที่ขนานและตั้งฉากกับทิศทางแนวระดับของระนาบชั้นหิน $\hat{\nu}_v(s)$ คือ อัตราส่วนปัวส์ซองแบบวิสโคอิลาสติกบนระนาบชั้นหิน $\hat{\nu}'_v(s)$ คือ อัตราส่วนปัวส์ซองแบบวิสโคอิลาสติกบนระนาบระหว่างแกนที่ตั้งฉากและขนานของระนาบชั้นหิน และ $\hat{P}'_1$, $\hat{P}_1$, $\hat{Q}'_1$ และ $\hat{Q}_1$ คือ ตัวดำเนินการเชิงเวลาที่อยู่ในรูปของค่าคงที่ของแบบจำลองเบอเกอร์ E_1, E_2, η_1 และ η_2 โดยตัวดำเนินการแปลงลาปลาซของแบบจำลองเบอเกอร์ (Transformed Operators) [19] แสดงดังสมการ

$$\hat{P}_1 = 1 + \left(\frac{\eta_1}{E_1} + \frac{\eta_1}{E_2} + \frac{\eta_2}{E_2}\right)s + \frac{\eta_1\eta_2}{E_1E_2}s^2,$$

$$\hat{Q}_1 = \eta_1 s + \frac{\eta_1\eta_2}{E_2}s^2$$

$$\hat{P}'_1 = 1 + \left(\frac{\eta'_1}{E'_1} + \frac{\eta'_1}{E'_2} + \frac{\eta'_2}{E'_2}\right)s + \frac{\eta'_1\eta'_2}{E'_1E'_2}s^2,$$

$$\hat{Q}'_1 = \eta'_1 s + \frac{\eta'_1\eta'_2}{E'_2}s^2$$

E_1 และ E'_1 คือ ค่าสัมประสิทธิ์ความยืดหยุ่นตัวที่ 1 ที่ขนานและตั้งฉากกับแนวระดับของระนาบชั้นหิน η_1 และ η'_1

คือ ความหนืดเชิงพลาสติกที่ขนานและตั้งฉากกับแนวระดับของระนาบชั้นหิน E_2 และ E_2' คือ สัมประสิทธิ์ความยืดหยุ่นตัวที่ 2 ที่ขนานและตั้งฉากกับแนวระดับของระนาบชั้นหิน η_2 และ η_2' คือ ค่าความหนืดเชิงยืดหยุ่นที่ขนานและตั้งฉากกับแนวระดับของระนาบชั้นหิน

นำสมการที่ (10) และ (11) และตัวดำเนินการเชิงเวลาแบบเบอเกอร์แทนในสมการที่ (7)–(9) และแก้สมการโดยการดำเนินการลาปลาซผกผัน ทำให้สามารถเขียนความสัมพันธ์ระหว่างความเครียดที่ขึ้นกับเวลาและความเค้นของเกลือหินแบบทรานซ์เวอร์สไอโซทรอปี ได้ดังสมการที่ (12)

$$\varepsilon_x(t) = a_{12}(t)\sigma;\ \varepsilon_y(t) = a_{22}(t)\sigma;\ \varepsilon_z(t) = a_{23}(t)\sigma \tag{12}$$

และองค์ประกอบของ Compliance Matrix a_{12}, a_{22} และ a_{23} ที่ขึ้นกับเวลาสามารถแสดงได้ดังสมการที่ (13)–(15)

$$a_{12}(t) = -\left[\left(\frac{1}{3}G - \frac{1}{9K}\right)A\right] \tag{13}$$

$$a_{22}(t) = \left[\left(\frac{2}{3}G + \frac{1}{9K}\right)B + \left(\frac{2}{3}H + \frac{1}{9K}\right)C\right] \tag{14}$$

$$a_{23}(t) = -\left[\left(\frac{1}{3}G - \frac{1}{9K}\right)D + \left(\frac{1}{3}H - \frac{1}{9K}\right)F\right] \tag{15}$$

โดยที่

$$G = \left(\frac{1}{E_1'} + \frac{t}{\eta_1'} + \frac{1}{E_2'}\left(1 - \exp^{-\frac{E_2'}{\eta_2'}t}\right)\right) \tag{16}$$

$$H = \left(\frac{1}{E_1} + \frac{t}{\eta_1} + \frac{1}{E_2}\left(1 - \exp^{-\frac{E_2}{\eta_2}t}\right)\right) \tag{17}$$

โดย K คือ มอดูลัสต้านการบีบอัด โดยมอดูลัสต้านการบีบอัด สามารถคำนวณจาก

$$K = \frac{p}{\Delta} \tag{18}$$

โดย p คือ แรงกด และ Δ คือ ความเครียดเชิงปริมาตร

นอกจากนี้ได้พัฒนาสมการสำหรับหาค่าสัมประสิทธิ์ความยืดหยุ่นปรากฏเชิงเวลา ($E_{y(\beta)}(t)$) อัตราส่วนปัวส์ซองปรากฏเชิงเวลาบนระนาบระหว่างแกน y และแกน x ($\nu_{yx(\beta)}(t)$) และอัตราส่วนปัวส์ซองปรากฏเชิงเวลาบนระนาบระหว่างแกน y และแกน z ($\nu_{yz(\beta)}(t)$) ณ เวลา t เพื่อหาค่าคงที่สำหรับใช้เป็นตัวแทนของคุณสมบัติที่ขึ้นกับเวลาของระนาบชั้นหินที่มีมุมเอียงแตกต่างกัน แสดงดังสมการที่ (19)

$$E_{y(\beta)}(t) = \frac{1}{a_{22}(t)};\ \nu_{yx(\beta)}(t) = -\frac{a_{12}(t)}{a_{22}(t)};$$
$$\nu_{yz(\beta)}(t) = -\frac{a_{23}(t)}{a_{22}(t)}; \tag{19}$$

2.3 การเปรียบเทียบผลการทดสอบในห้องปฏิบัติการกับแบบจำลองการคืบ

แบบจำลองการคืบได้ถูกนำมาวิเคราะห์พฤติกรรมการคืบในแกนเดียวของเกลือหินในห้องปฏิบัติการ เพื่อตรวจสอบความถูกต้องและแม่นยำของแบบจำลอง โดยตัวอย่างเกลือหินชุดมหาสารคามถูกรวบรวมจากเหมืองแร่โพแทชของบริษัท ไทยคาลี จำกัด จังหวัดนครราชสีมา นำมาจัดเตรียมเป็นรูปทรงสี่เหลี่ยมผืนผ้า ขนาด 54 × 54 × 108 ลูกบาศก์มิลลิเมตร โดยมีมุมระหว่างแนวแกนที่ตั้งฉากกับระนาบชั้นหินและแนวแรงในแกนหลัก (β) ผันแปรตั้งแต่ 0, 45, 65, 75 ถึง 90 องศา และทิศทางแนวระดับของระนาบชั้นหินจะต้องขนานกับด้านใดด้านหนึ่งของตัวอย่างหินเสมอ ดังแสดงในรูปที่ 1 การทดสอบการคืบในแกนเดียวจะใช้เครื่อง Consolidation Load Frame [20] ดำเนินการตามมาตรฐาน ASTM D7070-08 [21] ในงานวิจัยนี้ให้แรงกดในแนวแกนมีค่าคงที่เท่ากับ 10 เมกกะปาสคาล และทำการติดตั้งเกจเพื่อวัดระยะการเคลื่อนตัว 3 ด้าน (รูปที่ 1) คือ 1) การเคลื่อนตัวในแนวแกน (แกน y) 2) การเคลื่อนตัวในแนวด้านข้างที่ขนานกับทิศทางแนวระดับของระนาบชั้นหิน (แกน z) และ 3) การเคลื่อนตัวในแนวด้านข้างที่ตั้งฉากกับทิศทางแนวระดับของระนาบชั้นหิน (แกน x) ระหว่างการทดสอบได้มีการจดบันทึกระยะการเคลื่อนตัวและเวลา โดยงานวิจัยนี้ใช้เวลาในการทดสอบตัวอย่างละ 10 วัน เกลือหินมีความหนาแน่นเฉลี่ย 2.16±0.09 กรัมต่อลูกบาศก์เซนติเมตร

วารสารวิชาการพระจอมเกล้าพระนครเหนือ ปีที่ 34 ฉบับที่ 2 เม.ย.–มิ.ย. 2567
The Journal of KMUTNB., Vol. 34, No. 2, Apr.–Jun. 2024

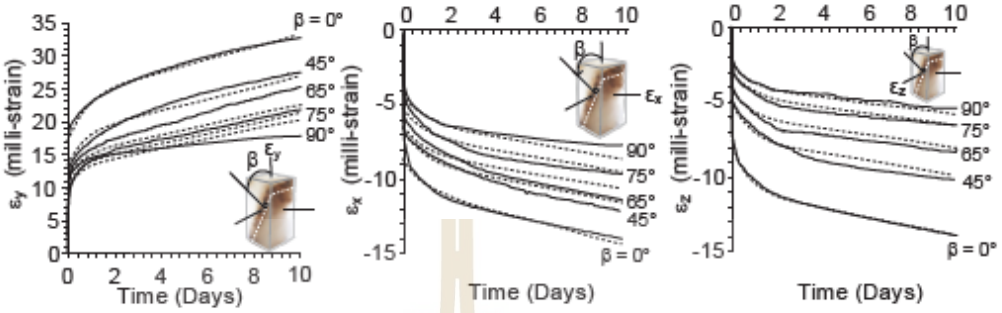

รูปที่ 2 ความสัมพันธ์ระหว่างความเครียดในแนวแกน y (ก) ความเครียดในแนวแกน x (ข) และความเครียดในแนวแกน z (ค) กับเวลาภายใต้มุมของระนาบชั้นหินที่ได้จากผลการทดสอบ (เส้นทึบ) และที่ได้จากการคำนวณโดยใช้แบบจำลองการคืบ (เส้นประ)

3. ผลการทดลอง

3.1 ผลการทดสอบการคืบในห้องปฏิบัติการ

ความสัมพันธ์ระหว่างความเครียดในแนวแกน (ε_y) ความเครียดในแนวด้านข้างที่ขนาน (ε_x) และตั้งฉาก (ε_z) กับทิศทางแนวระดับของระนาบชั้นหินกับเวลา แสดงในรูปที่ 2 (เส้นทึบ) จากแผนภูมิแสดงการเปลี่ยนรูปของเกลือหินปรากฏ 3 ช่วง คือ ช่วงที่อัตราความเครียดเปลี่ยนแปลงอย่างทันทีทันใด ช่วงที่อัตราความเครียดเปลี่ยนแปลงตามเวลา และช่วงที่อัตราการเปลี่ยนแปลงความเครียดต่อช่วงเวลาคงที่ ผลกระทบของทรานซ์เวอร์สไอโซทรอปิส่งผลต่อความเครียดของระนาบชั้นหินอย่างเห็นได้ชัด ความเครียดทั้ง 3 แกน จะมีค่าลดลงเมื่อมุม β เพิ่มขึ้น และ ε_x มีค่าสูงกว่า ε_z ในทุกมุม β การวิเคราะห์ความเครียดในแนวแกนและแนวด้านข้าง ถูกนำมาพิจารณาร่วมกันในรูปของความเครียดเฉือนแบบสามมิติ (γ_{oct}) ตลอดระยะเวลาในการทดสอบ ดังแสดงในรูปที่ 3 (เส้นทึบ) โดยใช้สมการเชิงคณิตศาสตร์ของ Jaeger และ Cook [22]

$$\gamma_{oct} = \frac{1}{3}\sqrt{\{(\varepsilon_1-\varepsilon_2)^2+(\varepsilon_2-\varepsilon_3)^2+(\varepsilon_3-\varepsilon_1)^2\}} \quad (20)$$

โดยที่ ε_1 คือ ความเครียดในแนวแกนหลักสูงสุด ε_2 คือ ความเครียดในแนวแกนหลักกลาง และ ε_3 คือ ความเครียดในแนวแกนหลักต่ำสุด

ผลการทดสอบการคืบในห้องปฏิบัติการถูกนำมาวิเคราะห์เพื่อศึกษาพฤติกรรมที่ขึ้นกับเวลาของตัวอย่างเกลือหินภายใต้ผลกระทบของทรานซ์เวอร์สไอโซทรอปิ ผลลัพธ์ที่ได้ถูกนำไปสอบเทียบเพื่อให้ได้มาซึ่งคุณสมบัติที่ขึ้นกับเวลาในรูปของความหนืดเชิงยืดหยุ่นและเชิงพลาสติกของเกลือหินโดยใช้สมการความเครียดเฉือนเชิงเวลาในสามมิติ ($\gamma_{oct(t)}$) ที่อยู่บนพื้นฐานของแบบจำลองเบอเกอร์ [22] สามารถแสดงได้ดังสมการที่ (21) และ (22)

$$\gamma_{oct}(t) = \tau_{oct}\left[\frac{1}{E_{1,i}}+\frac{t}{\eta_{1,i}}+\frac{1}{E_{2,i}}\left(1-e^{-\frac{E_{2,i}}{\eta_{2,i}}}\right)\right] \quad (21)$$

$$\tau_{oct} = \frac{1}{3}\sqrt{\left((\sigma_1-\sigma_2)^2+(\sigma_2-\sigma_3)^2+(\sigma_3-\sigma_1)^2\right)} \quad (22)$$

โดยที่ τ_{oct} คือ ความเค้นในแนวเฉือน $E_{1,i}$ คือ ค่าสัมประสิทธิ์ความยืดหยุ่นตัวที่ 1 แท้จริง $E_{2,i}$ คือ ค่าสัมประสิทธิ์ความยืดหยุ่นตัวที่ 2 แท้จริง $\eta_{1,i}$ คือ ค่าความหนืดเชิงพลาสติกแท้จริง $\eta_{2,i}$ คือ ค่าความหนืดเชิงยืดหยุ่นแท้จริง และ t คือ เวลา การสอบเทียบค่าคงที่ใช้โปรแกรมการวิเคราะห์ข้อมูลเชิงสถิติ [23] รูปที่ 3 แสดงผลการสอบเทียบค่า (เส้นประ) ซึ่งมีความสอดคล้องเป็นอย่างดีกับผลการทดสอบในห้องปฏิบัติการ (เส้นทึบ)

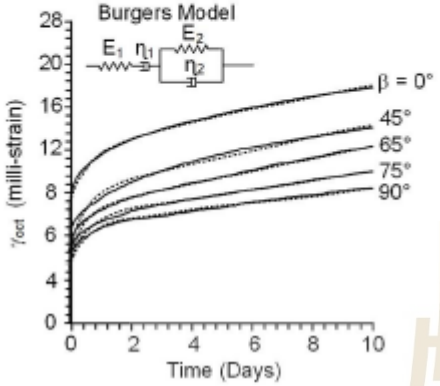

รูปที่ 3 ความสัมพันธ์ระหว่างความเครียดในแนวเฉือนกับเวลาที่ได้จากผลการทดสอบ (เส้นทึบ) และจากการสอบเทียบค่า (เส้นประ)

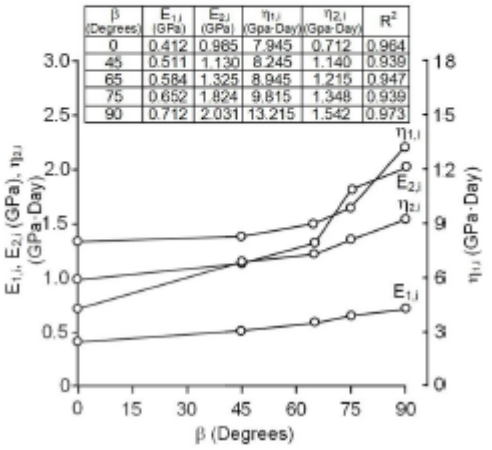

รูปที่ 4 ความสัมพันธ์ระหว่างค่าคงที่ $E_{1,i}, E_{2,i}, \eta_{1,i}$ และ $\eta_{2,i}$ กับมุมของระนาบชั้นหิน

โดยมีค่าสัมประสิทธิ์สหสัมพันธ์มากกว่า 0.9 **รูปที่** 4 แสดงความสัมพันธ์ระหว่างค่าคงที่ $E_{1,i}$, $E_{2,i}$, $\eta_{1,i}$ และ $\eta_{2,i}$ ของแบบจำลองเบอเกอร์กับมุม β พบว่าค่าคงที่เหล่านี้มีค่าสูงขึ้นเมื่อมุม β สูงขึ้น

3.2 ผลการเปรียบเทียบผลการทดสอบกับแบบจำลองการคืบในหินที่มีลักษณะทรานซ์เวอร์สไอโซทรอปี

แบบจำลองการคืบของหินแบบทรานซ์เวอร์ส-ไอโซทรอปีสามารถคำนวณค่าความเครียดที่ขึ้นกับเวลา ณ มุม β ใด ๆ โดยใช้สมการที่ (12)–(18) และตัวแปรที่ใช้ในการคำนวณแสดงดังตารางที่ 1 โดย E_1', E_2', η' และ η_1' คือ ค่าคงที่เทียบเท่าแท้จริงจากการทดสอบที่มุม β เท่ากับ 0 องศา และ E_1, E_2, η_1 และ η_2 คือ ค่าคงที่เทียบเท่าแท้จริงจากการทดสอบที่มุม β เท่ากับ 90 องศา

ผลของการเปรียบเทียบค่าความเครียดที่ขึ้นกับเวลาในแนวแกน ε_y ความเครียดที่ขึ้นกับเวลาในแนวด้านข้างที่ขนาน ε_z และตั้งฉาก ε_x กับทิศทางแนวระดับของระนาบชั้นหินจากแบบจำลองกับผลการทดสอบในห้องปฏิบัติการ แสดงดังรูปที่ 2 (เส้นประ) ความถูกต้องและแม่นยำของแบบจำลองประเมินได้จากค่าเฉลี่ยความไม่สอดคล้องกับแบบจำลอง (Mean Misfit; $\bar{s}$) [24] โดยหาได้จากสมการที่ (23)

$$\bar{s} = \frac{1}{m}\sum_{i}^{m} s_i \quad \text{เมื่อ} \quad s_i = \sqrt{\frac{1}{n}\sum_{j=1}^{n}(d_{calc} - d_{test})^2} \qquad (23)$$

พบว่าค่าเฉลี่ยความไม่สอดคล้องกับแบบจำลองความเครียดที่ขึ้นกับเวลา $\varepsilon_y(t)$ $\varepsilon_z(t)$ และ $\varepsilon x(_i)$ มีค่าเท่ากับ 1.949, 2.453 และ 0.927 Milli-strain ตามลำดับ ซึ่งถือว่ามีค่าต่ำ จึงระบุได้ว่าแบบจำลองการคืบของหินแบบทรานซ์เวอร์สไอโซทรอปีสามารถจำลองผลกระทบของทรานซ์เวอร์สไอโซทรอปีต่อความเครียดที่ขึ้นกับเวลาได้ดี

สมการที่ (19) สามารถคำนวณหา $E_{y(\beta)}(t)$ $\nu_{yx(\beta)}(t)$ และ $\nu_{yz(\beta)}(t)$ โดยงานวิจัยนี้พิจารณาที่เวลา t เท่ากับ 0 (ยังไม่มีพฤติกรรมเชิงเวลา) 10 วัน 100 วัน และ 1000 วัน ตามลำดับ ดังแสดงในรูปที่ 5 พบว่า ลักษณะทรานซ์เวอร์สไอโซทรอปีส่งผลให้ค่าสัมประสิทธิ์ความยืดหยุ่นปรากฏเชิงเวลาและอัตราส่วนปัวส์ซองปรากฏเชิงเวลาจากแบบจำลองมีลักษณะเป็นวงรี และผลการคำนวณจากแบบจำลองการคืบ (เส้นทึบ) สามารถคำนวณค่าดังกล่าวได้ใกล้เคียงกับผลการทดสอบ (จุดข้อมูล) โดยค่าเฉลี่ยความไม่สอดคล้องกับการจำลอง $E_y(t)$ $\nu_{yx}(t)$ และ $\nu_{yz}(t)$ มีค่าเท่ากับ 0.02, 0.01 และ 0.01 เมกกะปาสคาล ตามลำดับ

วารสารวิชาการพระจอมเกล้าพระนครเหนือ ปีที่ 34 ฉบับที่ 2 เม.ย.–มิ.ย. 2567
The Journal of KMUTNB., Vol. 34, No. 2, Apr.–Jun. 2024

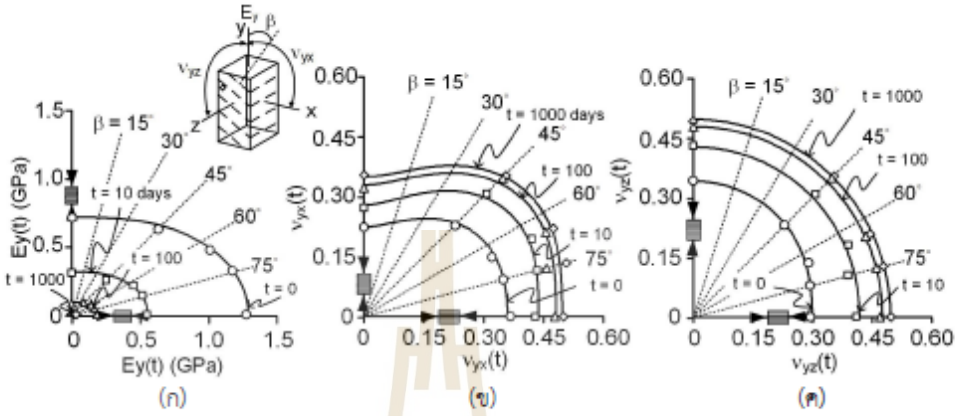

รูปที่ 5 ความสัมพันธ์ระหว่างค่าสัมประสิทธิ์ความยืดหยุ่นปรากฏเชิงเวลา ($E_y(t)$) (ก) อัตราส่วนปัวส์ซองปรากฏเชิงเวลาบนระนาบระหว่างแกน y กับแกน x ($\nu_{yx}(t)$) (ข) และอัตราส่วนปัวส์ซองปรากฏเชิงเวลาบนระนาบระหว่างแกน y กับแกน z ($\nu_{yz}(t)$) (ค) กับมุมของระนาบชั้นหิน

ตารางที่ 1 ค่าคงที่แท้จริงในการคำนวณแบบจำลองการคืบของหินแบบทรานซ์เวอร์สไอโซทรอปี

E_1' (GPa)	E_2' (GPa)	η_1' (GPa-Day)	η_2' (GPa-Day)	E_1 (GPa)	E_2 (GPa)	η_1 (GPa-Day)	η_2 (GPa-Day)	K (GPa)
0.412	0.985	7.945	0.712	0.712	2.031	13.215	1.542	2.110

4. อภิปรายผลและสรุป

จากการทดสอบการคืบภายใต้แรงกดในแกนเดียวเพื่อศึกษาผลกระทบของทรานซ์เวอร์สไอโซทรอปีต่อคุณสมบัติที่ขึ้นกับเวลาของเกลือหินพบว่า เมื่อเกลือหินมี β เท่ากับ 0 องศา จะมีความเครียดทั้งในแนวแกนและแนวด้านข้างสูงที่สุด เนื่องจากแรงที่มากระทำจะทำให้เกิดช่องว่างและรอยแตกตามแนวระนาบการวางตัวของชั้นหินได้ง่าย ตัวอย่างหินที่มีมุม $0 < \beta < 90°$ จะมีความเครียดอยู่ในช่วงระหว่างตัวอย่างหินที่มีมุม β เท่ากับ 0 และ 90 องศา ซึ่งเป็นลักษณะการวางตัวของระนาบชั้นหินที่มีความใกล้เคียงกับระนาบการเกิดแรงเฉือนตามธรรมชาติ และตัวอย่างหินที่มี β เท่ากับ 90 องศา จะมีความเครียดทั้งในแนวแกนและแนวด้านข้างต่ำที่สุด เนื่องจากมีค่าสัมประสิทธิ์ความยืดหยุ่นสูงที่สุด ซึ่งสอดคล้องกับผลการทดสอบของ Xu และคณะ [16] และ Wu และคณะ [25] หรืออาจกล่าวอีกนัยหนึ่งได้ว่าเมื่อมุม β สูงขึ้น ความเครียดจะมีค่าลดลง เป็นผลมาจากค่าสัมประสิทธิ์ความยืดหยุ่นที่จะมีค่าสูงขึ้นตามมุม β ([2], [7]–[9]

สัมประสิทธิ์ความยืดหยุ่นตัวที่ 1 แท้จริง ($E_{1,i}$) สัมประสิทธิ์ความยืดหยุ่นตัวที่ 2 ($E_{2,i}$) ความหนืดเชิงพลาสติก ($\eta_{1,i}$) และความหนืดเชิงยืดหยุ่น ($\eta_{2,i}$) มีค่าสูงขึ้นเมื่อมุม β สูงขึ้น

จากผลการวิเคราะห์และเปรียบเทียบผลการทดสอบในห้องปฏิบัติการกับแบบจำลองการคืบ แสดงให้เห็นว่าแบบจำลองที่พัฒนาขึ้นมาใหม่นี้สามารถจำลอง $E_{y(\beta)}(t)$ $\nu_{yx(\beta)}(t)$ และ $\nu_{yz(\beta)}(t)$ ที่มีมุมการวางตัวของระนาบชั้นหินใด ๆ ได้ค่อนข้างใกล้เคียงกับผลการทดสอบ

แบบจำลองสามารถจำลองความเครียดที่ขึ้นกับเวลาได้ดี เมื่อมุม β เท่ากับ 0 องศา และ 90 องศา แต่สำหรับมุมอื่น ๆ ยังค่อนข้างมีความคลาดเคลื่อน เนื่องจากในสมการแบบจำลองทาง คณิตศาสตร์ใช้ตัวแปรในการคำนวณจากการทดสอบเพียง 2 ทิศทาง คือทิศทางที่ขนานและตั้งฉากกับแนวระดับของระนาบชั้นหิน ในอนาคตควรมีการศึกษา

เพิ่มเติมเพื่อลดความคลาดเคลื่อนดังกล่าว

แบบจำลองสามารถสะท้อนผลกระทบของทรานซ์เวอร์สไอโซทรอปีต่อคุณสมบัติที่ขึ้นกับเวลาของเกลือหินได้ และนำไปประยุกต์ใช้ในการประเมินการเปลี่ยนแปลงรูปร่างเชิงเวลาของเสาค้ำยันและผนังด้านข้างของเหมืองเกลือหินเพื่อให้ได้ข้อมูลที่ใกล้เคียงกับสภาวะจริงในภาคสนามมากยิ่งขึ้น

5. กิตติกรรมประกาศ

งานวิจัยนี้ได้รับทุนสนับสนุนจากสำนักงานกองทุนสนับสนุนการวิจัย (สกว.) สำนักงานคณะกรรมการส่งเสริมวิทยาศาสตร์ วิจัย และนวัตกรรม (สกสว.) และสำนักงานวิจัยแห่งชาติ (วช.)ภายใต้โครงการปริญญาเอกกาญจนาภิเษกร่วมกับมหาวิทยาลัยเทคโนโลยีสุรนารี (ดปก.) ภายใต้สัญญาเลขที่ PHD/0215/2561 จึงขอขอบพระคุณที่อนุญาตให้เผยแพร่บทความนี้

เอกสารอ้างอิง

[1] M. K. Jeremic, *Rock Mechanics in Salt Mining*, A.A. Balkema: Netherlands, 1994.

[2] N. Sukjaroen, T. Thongprapha, K. Artkhonghan, and K. Fuenkajorn, "Effects of transverse isotropy on compressive strength and elastic properties of rock salt," *Engineering Journal of Research and Development*, vol. 32, no. 1, pp. 47–54, 2021 (in Thai).

[3] R. McLamore and K.E. Gray, "The mechanical behavior of anisotropic sedimentary rocks," *Journal of Engineering for Industry*, vol. 89, no. 1, pp. 62–73, 1967.

[4] A. A. Al-Harthi, "Effect of planar structures on the anisotropy of Ranyah sandstone," *Saudi Arabia. Engineering Geology*, vol. 50, no. 1–2, pp. 49–57, 1998.

[5] K. Colak, and T. Unlu, "Effect of transverse anisotropy on the Hoek-Brown strength parameter 'mi' for intact rocks," *International Journal of Rock Mechanics and Mining Sciences*, vol. 41, no. 6, pp. 1045–1052, 2004.

[6] O. Saeidi, V. Rasouli, R. G. Vaneghi, R. Gholami, and S. R. Torabi, "A modified failure criterion for transversely isotropic rocks," *Geoscience Frontiers*, vol. 5, no. 2, pp. 215–225, 2014.

[7] L. Yun-si, Z. Xiao, and Y. Quan, "The five elastic parameters for the anisotropy of slate under the influence of different bedding orientations," *Electronic Journal of Geotechnical Engineering*, vol. 17, pp. 3695–3707, 2012.

[8] H. Kim, J. W. Cho, I. Song, and K. B. Min, "Anisotropy of elastic moduli, P-wave velocities, and thermal conductivities of Asan Gneiss, Boryeong Shale, and Yeoncheon Schist in Korea," *Engineering Geology*, vol. 147, pp. 68–77, 2012.

[9] C. Cheng, X. Li, and H. Qian, "Anisotropic failure strength of shale with increasing confinement: behaviors, factors and mechanism," *Materials*, vol. 10, no. 11, pp. 1310, 2017.

[10] T. Thongprapha, K. Tengpakwaen, J. J. K. Daemen, and K. Fuenkajorn, "Effect of confining pressures on transverse isotropy of Maha Sarakham salt," *International Journal of Rock Mechanics and Mining Sciences*, vol. 152, 2022.

[11] R. K. Dubey, "Bearing of structural anisotropy on deformation and mechanical response of rocks: An experimental example of rocksalt deformation under variable compression rates," *Journal of the Geological Society of India*, vol. 91, pp. 109–114, 2018.

[12] R. K. Dubey and V. K. Gairola, "Influence of structural anisotropy on creep of rocksalt from Simla Himalaya, India: An experimental

approach," *Journal of Structural Geology*, vol. 30, no. 6, pp. 710–718, 2008.

[13] B. Amadei, "Importance of anisotropy when estimating and measuring in situ stresses in rock," *International Journal of Rock Mechanics and Mining Sciences and Geomechanics Abstracts*, vol. 33, no. 3, pp. 293–325,1996.

[14] Y. H. Hatzor and E. P. Heyman, "Dilation of anisotropic rock salt: Evidence from mount sedom diapir," *Journal of Geophysical Research: Solid Earth*, vol. 102, no. B7, pp. 14853–14868, 1997.

[15] J. Zhang, X. Zhang, Z. Huang, and H. Fu, "Transversely isotropic creep characteristics and damage mechanism of layered phyllite under uniaxial compression creep test," *Environmental Earth Sciences*, to be published, 2021.

[16] G. Xu, C. He, J. Yan, and G. Ma, "A new transversely isotropic nonlinear creep model for layered phyllite and its application," *Bulletin of Engineering Geology and the Environment*, vol. 78, no. 7, pp. 5387–5408, 2019.

[17] G. Luo, W. Yang, C Bo, L. Zhang, K. Duan, W. Jing, and Y. Zhao, "Viscoelastic analysis of the creep characteristics of interlayered rock specimens under uniaxial compression," *Mechanics of Time-Dependent Materials*, vol. 25, no. 1, pp. 37–60, 2021.

[18] N. A. Ghavidel, A. Nazem, M. Heidarizadeh, M. Moosavi, and H. Memarian, "Identification of rheological behavior of salt rock at elevated temperature, case study: Gachsaran evaporative formation, Iran," presented at ISRM Regional Symposium-EUROCK, Vigo, Spain, May. 26–28, 2014.

[19] W.N. Findley, J.S.Lai, and K. Onaran, *Creep and relaxation of nonlinear viscoelastic materials*, Dover, NewYork, 1976.

[20] M. Jandakaew, "Stress-path dependency of rock salt," presented at the First Thailand Symposium on Rock Mechanics, Greenery Resort, Khao Yai, Nakhon Ratchasima, Thailand, sep. 13–14, 2007.

[21] *Standard test methods for creep of rock core under constant stress and temperature*, ASTM D7070-08, 2021.

[22] J. C. Jaeger and N. G. W. Cook, *Fundamentals of Rock Mechanics*, London: Chapman and Hall, 1979.

[23] L. Wendai, "In 13 chapters. SPSS for windows: Statistical analysis," in *Regression analysis, linear regression and probit regression*, Beijing, China: House of Electronics Industry, 2000.

[24] K. F. Riley, M. P. Hobson, and S. J. Bence, *Mathematical Methods for Physics and Engineering*, Cambridge: Cambridge University Press, 1998.

[25] C. Wu, Q. Chen, S. Basack, and S. Karekal, "Laboratory investigation on rheological properties of greenschist considering anisotropy under multi-stage compressive creep condition," *Journal of Structural Geology*, vol. 114, pp. 111–120, 2018

Original Article

The effect of Transverse Isotropy on the Creep Behavior of Bedded Salt under Confining Pressures

Kanya Kraipru[1], Kittitep Fuenkajorn[1], and Thanittha Thongprapha[1]*

[1] **Geomechanics Research Unit, Institute of Engineering, Suranaree University of Technology, 111 University Avenue Muang, Nakhon Ratchasima, 30000, Thailand**

* **Corresponding author, Email address: thanittha@sut.ac.th**

Abstract

In this paper, we investigate the role of transverse isotropy on the creep behavior of bedded salt. We conducted a series of triaxial creep tests on prismatic specimens subjected to confining pressures ($\sigma 3$) of up to 24 MPa and a constant octahedral shear stress (τo) of 9 MPa. The specimens were oriented with their bedding planes at various angles (β) to the major principal axis to simulate transverse isotropic conditions. Our findings reveal that both instantaneous and creep deformations are most significant when $\beta = 0°$, decreasing progressively to a minimum at $\beta = 90°$ across all confining pressures. The discrepancy in deformations between these intrinsic angles narrows with increasing $\sigma 3$. Creep deformations for intermediate angles ($0° < \beta < 90°$) follow the elliptical equations. Utilizing the Burgers creep model, we observed that the instantaneous, visco-elastic moduli, and visco-plastic coefficients escalate with β. The degree of anisotropy declines sharply as confining pressures increase, reaching an isotropic state under $\tau o = 9$ MPa and $\sigma 3$ around 40 MPa, beyond which transient creep ceases, indicating a transition to Maxwell material behavior. Employing linear viscoelastic theory, we derived an equation for time-dependent deformation under varying octahedral shear stresses. This enables the formulation of governing equations for Burgers

model parameters, considering bedding plane orientations, loading durations, and the interactions between shear and confining stresses.

Keywords: Burgers model, Transverse isotropy, Anisotropy degree, Visco-elasticity, Visco-plasticity

1. Introduction

Time-dependent deformation of rock salt has long been recognized and investigated. Major research efforts, particularly, in the US and in several European countries, are aimed at developing safe storage facilities in rock salt for nuclear waste disposal (e.g., Hunter 1979; Senseny et al. 1992; Munson 1997; Hunsche and Hampel 1999; Langer 1999), for utilizing rock salt caverns for energy storage (e.g., Langer 1993; Staudtmeister and Rokahr 1997; Ehgartner and Sobolik 2006; Wang et al. 2016; Khaledi et al. 2016; Wang et al. 2018), and for salt and potash mining (e.g., Holcomb and Hannum 1982; Dawson and Munson 1983; Jeramic 1994; Daemen and Fuenkajorn 1996; Hansen 1997; Khamrat et al. 2018). Several constitutive creep models have been derived to describe the time-dependent behavior of rock salt under various environmental conditions (e.g. confining pressures, loading rates, temperatures and moisture contents). These include rheological models (Lindner and Brady 1984; Hardy and Sun 1986; Wang et al. 2014), empirical models (Nair et al. 1974; Langer 1984; Motta and Pinto 2014), and physical theory models (Oksenkrug and Shafarenko 1974; Senseny 1983). Recently a variety of creep damage models has been incorporated into the constitutive equations (Dawson 1979; Chan et al. 1992, 1994; Wang 2004). Zhou et al. (2013) propose a new fractional-derivative creep model for rock salt from central China under uniaxial and triaxial creep tests. The results show that the model is capable of describing the entire creep phases. Fei et al. (2021) propose 3-D model under multi-stage loading on rock salt from China which

shows an accurate description of the accelerated creep stage. Liu et al. (2017) improve the Nishihara model (Nishihara 1957) to be more proficient to reflect creep properties of mica-quartz schist in each stage.

Bedded rock salt can exhibit transverse isotropic behavior in terms of its mechanical and rheological properties. This is caused by the layers of crystallization and the inclusions (e.g. anhydrite, potash, gypsum and clay minerals). Jeremic (1994) reports that rock salt from Poland shows the transverse isotropic effect on uniaxial compressive strength where the minimum strength is obtained when normal to bedding plane makes an angle (β) of 45° with the loading direction. Thongprapha et al. (2022) find that the minimum compressive strength of salt from Thailand is obtained when β is 60° under confining pressures from 2 to 40 MPa. Intrinsic elastic moduli are highest when loading is parallel to the bedding plane ($\beta = 90°$), and lowest when it is normal to the bedding ($\beta = 0°$). The apparent elastic moduli and Poisson's ratios for $0° < \beta < 90°$ can be described by Amadei's solution (Amadei 1996). The solution has been widely applied to describe the evolution of the apparent elastic moduli and Poisson's ratios for other strong and brittle rocks (e.g. Nasseri et al. 2003; Miller et al. 2013; Gholami and Rasouli 2014; Nejati et al. 2019).

The effect of transverse isotropy on salt creep has however rarely been investigated. Dubey and Gairola (2008) perform uniaxial creep tests on transverse isotropic salt from India under three bedding orientations (0°, 45°, and 90°), and find that steady-state creep rate is highest when $\beta = 45°$ and lowest for $\beta = 0°$. Most salt researchers have studied the effect of transverse isotropy on salt only under unconfined condition. In addition, governing equations for describing the salt creep as affected by transverse isotropic characteristics have never been derived for practical use.

The objective of this study is to determine the effect of transverse isotropy on time-dependent behaviour of Maha Sarakham salt under confinements. The main tasks involve

performing triaxial creep tests on prismatic salt specimens containing various bedding plane orientations with respect to the major principal axis and identifying the evolution of each creep phase with the transverse isotropic angles and applied stresses. The specimens are subjected to confining pressures from 3 to 24 MPa under constant octahedral shear stress of 9 MPa for 10 days. The anisotropy degrees are determined in terms of elastic, visco-elastic and visco-plastic deformations of salt specimens. This involves instantaneous, transient and steady-state creep phases. The tertiary creep phase is excluded from this study. The Burgers creep parameters are used to represent instantaneous, visco-elastic and visco-plastic deformations of the salt samples. Empirical equations are derived to describe the evolutions of the Burgers parameters as a function of transverse isotropic angle, loading duration, confining pressure and deviatoric stress.

2. Salt specimens and test methods

Salt blocks with approximate sizes of $50\times50\times50$ cm^3 have been collected from an underground mine opening at a depth of 250 m. They belong to the lower salt member of Maha Sarakham formation located in the northeast of Thailand. Warren (1999) and Shen and Siritongkham (2020) describe the origin and geological structures of the Maha Sarakham salt. Rock salt beds can be observed by alternation of light and dark bands of halite (sometimes called banded halite).

Prismatic salt specimens with nominal dimensions of $54\times54\times108$ mm^3 are cut from the salt blocks using organic oil as lubricant. The specimens have nominal angles (β) between the specimen main axis and the normal to bedding planes varying from 0, 25, 45, 65 to 90°. The bedding plane strike is parallel to one of the specimen side surfaces. Seventeen specimens have been prepared. Results from X-ray diffraction analyses (XRD) indicate that the salt consists mainly of halite (95.48%) and minor amounts of trace minerals (4.52%) by weight.

These minerals include carnallite, tachyhydrite, gypsum and clay minerals. The average density of salt specimens is 2.13 ± 0.04 g/cc.

Test procedure and calculation of triaxial creep test follow the ASTM D7070-08 standard, except for specimen shape. The constant axial stress (σ_1) and lateral stresses (σ_3) are applied by polyaxial load frame, as shown in Fig. 1 (Fuenkajorn et al. 2012; Sriapai et al. 2013). The lateral deformations of the specimen parallel and normal to the strike of bedding planes are measure from the upward movement of two lower steel bars hanging from the outer ends of cantilever beam using high-precision development dial gage (±0.001 mm), as shown in Fig. 1. This upward movement is induced by the lateral expansion of salt specimen during loading. The axial (vertical) displacement is also measured using displacement dial gage mounting between the top and bottom ends of the specimen.

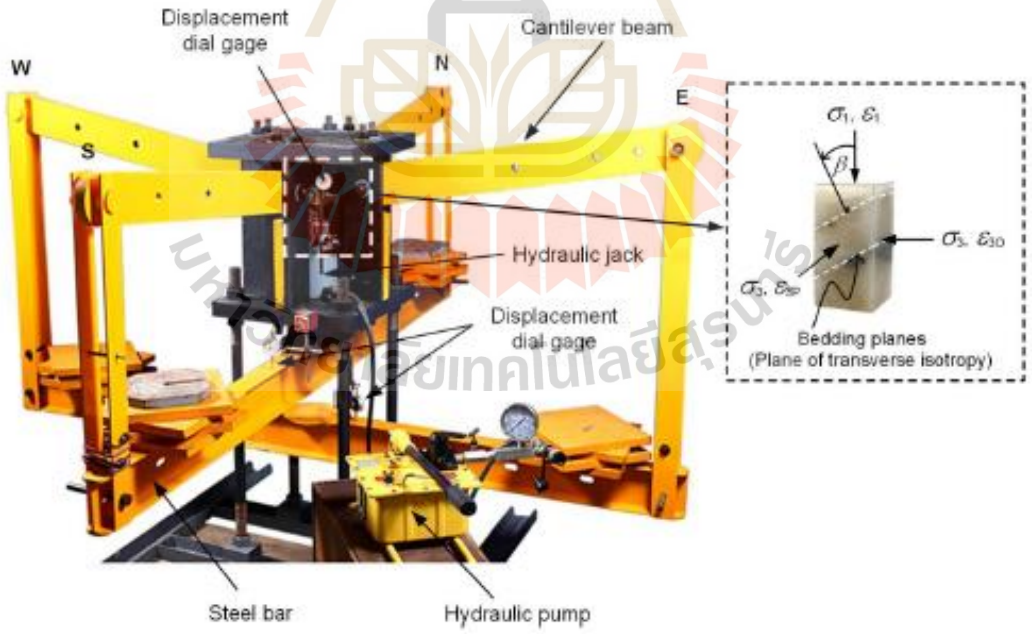

Fig. 1 Polyaxial load frame and notations defining directions of major principal stress and strain (σ_1 and ε_1), minor principal stress (σ_3) and strains normal and parallel to bedding plane (ε_{3O} and ε_{3P}).

The specimens are subjected to confining pressures (lateral stresses) ranging from 3, 6, 12 to 24 MPa, while they are under constant axial stresses of 22, 25, 31, and 43 MPa, respectively. This results in a constant octahedral shear stress (τ_0) of 9 MPa for all specimens, and hence isolating the test results from differences in stress deviations. The shear stress magnitude is selected based on previous experimental studies on the same salt obtained by Fuenkajorn et al. (2012) who perform triaxial compression tests for σ_3 = 3 to 28 MPa and Archeeploha et al. (2017) who perform triaxial creep tests under σ_3 = 5 to 11.5 MPa with τ_0 = 5 to 14 MPa. The selected τ_0 is sufficiently high to induce plastic creep to the salt specimen, but not too high to cause failure within the test period of 10 days.

The polyaxial load frame allows applying constant lateral (confining) stresses normal and parallel to the bedding planes using cantilever beams and a dead weight system. Neoprene sheets are placed at all interfaces between the platens and specimen surfaces to minimize the friction. Prior to performing creep test, the axial and lateral stresses are simultaneously applied to a pre-defined confining pressure and are maintained constant for 24 hours (lithostatic condition). The test is started by increasing the axial stress to obtain octahedral shear stress of 9 MPa. Salt deformations along the axial and lateral directions are monitored to the nearest 0.001 mm. The specimens are tested under ambient temperature (30 ± 2°C). Fig. 1 also shows the notations defining the principal directions of stresses and strains, where ε_1 represents axial strain, and ε_{3P} and ε_{3O} are lateral strains parallel and normal to the strike of bedding planes.

3. Test results

Fig. 2 shows example results of strains induced along the principal directions as a function of time for 10 days. Instantaneous, transient and steady-state creep phases can be observed for all angles β. Axial strains obtained from β = 0° (normal to bedding plane) are always greater than those from β = 90°. This holds true for all confining pressures.

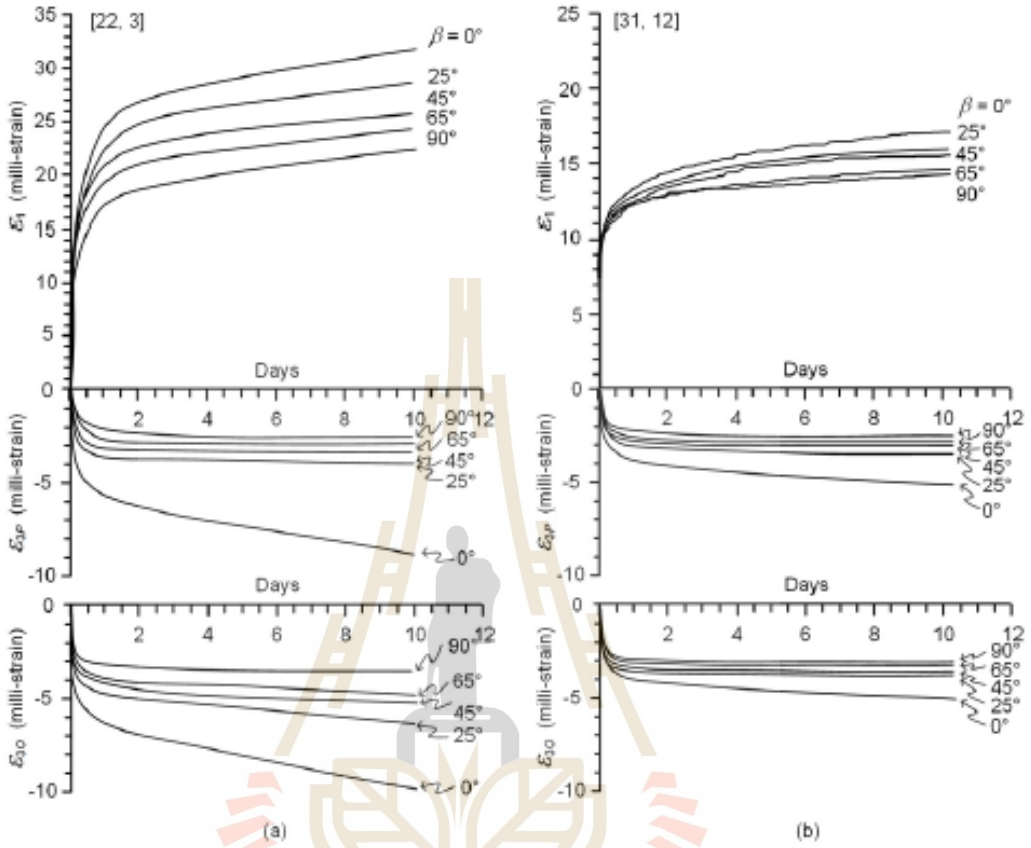

Fig. 2 Examples of strain-time curves under confining pressures of 3 MPa (a) and 12 MPa (b). Numbers in bracket indicate applied stresses in MPa [σ_1, σ_3]. All specimens are under τ_o = 9 MPa.

The differences between ε_{3P} and ε_{3O} magnitudes decrease when angles β decrease toward 0°. The instantaneous and creep strains measured from the intrinsic angles β = 0° and 90° also become closer as the confining pressures increase.

Test results can also be represented by strain deviations (e_1, e_{3P}, e_{3O}) as a function of time under different confining pressures. They can be calculated as:

$$e_1 = \varepsilon_1 - e_m \quad (1)$$

8

$$e_{3P} = \varepsilon_{3P} - e_m \quad (2)$$

$$e_{3O} = \varepsilon_{3O} - e_m \quad (3)$$

where e_1 is axial strain deviation, e_{3P} and e_{3O} are lateral strain deviations parallel and normal to the strike of bedding planes, and e_m is mean strain which equals to $(\varepsilon_1 + \varepsilon_{3P} + \varepsilon_{3O})/3$.

Fig. 3 shows the three strain deviations as a function of time. For all specimens and confining pressures, the largest strain deviations (e_1, e_{3P}, e_{3O}) are obtained at $\beta = 0°$, and the lowest at $\beta = 90°$. The diagrams can later be used to derive governing equations for salt creep under different bedding plane orientations (β) and confining pressures (σ_3).

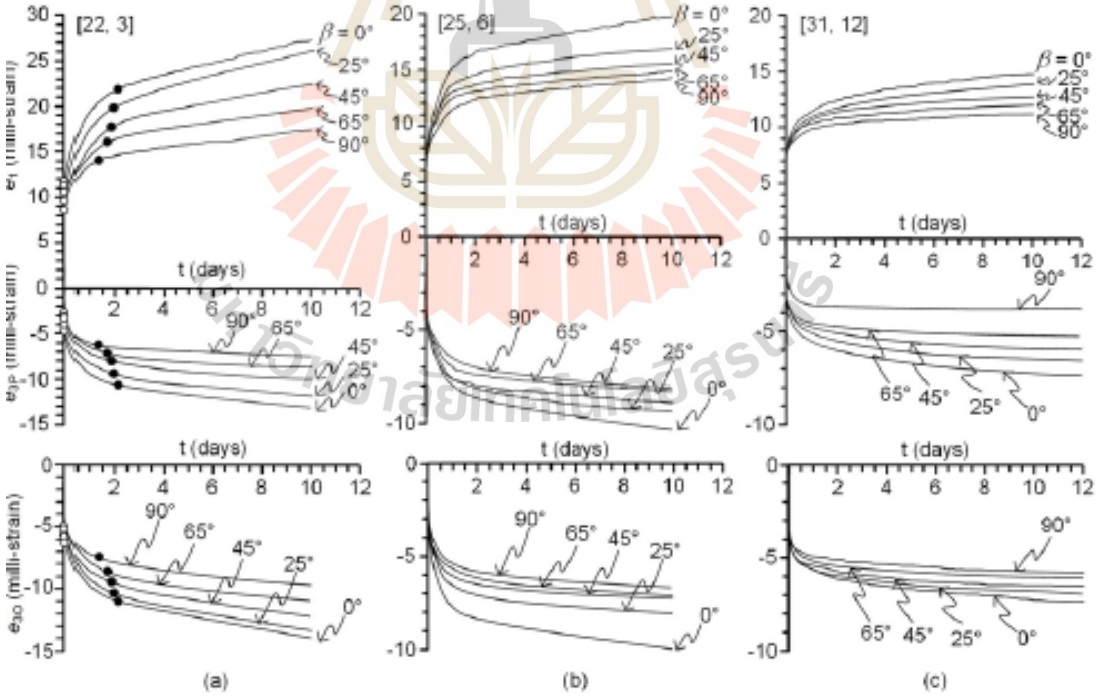

Fig. 3 Examples of strain deviation-time curves under confining pressures of 3 MPa (a), 6 MPa (b) and 12 MPa (c). Numbers in brackets indicate $[\sigma_1, \sigma_3]$.

4. Burgers creep model

The Burgers model (Richard 1993) is proposed to describe the time-dependent deformation of the transverse isotropic salt. It is recognized that numerous creep models or constitutive equations have been developed to represent time-dependent behaviour of rock salt (e.g., Gnirk and Johnson 1964; Senseny 1983; Handin et al. 1984; Langer 1984; Hardy and Sun 1986; Archeeploha et al. 2017; Luo et al. 2021). The Burgers model is used here because of its simplicity and its capability of describing the elastic, visco-elastic, and visco-plastic phases of deformation. Fig. 4 shows modular components of the model, where E_I and E_V are spring constants in instantaneous and visco-elastic phases, and η_V and η_P are viscosity coefficients in visco-elastic and visco-plastic phases.

To determine the numerical values of these parameters, a relationship between strain and stress deviations is developed first. For linear elastic material, the strain and stress deviations can be related as (Jaeger et al. 2007):

$$e_1 = s_1 / 2G \tag{4}$$

where G is shear modulus. The applied stress deviations along major principal axis can be expressed as:

$$s_1 = \sigma_1 - s_m \tag{5}$$

where s_1 is axial stress deviation and s_m is mean stress which equals to $(\sigma_1 + 2\sigma_3)/3$. Eq. (4) can be further developed to form a linear visco-elastic relation by taking Laplace transformation (Schiff 1999; McLachlan 2014) and using the transform operations of the Burger model (Findley et al. 1976) and using the transformed operators of the Burgers model (Findley et al. 1976).

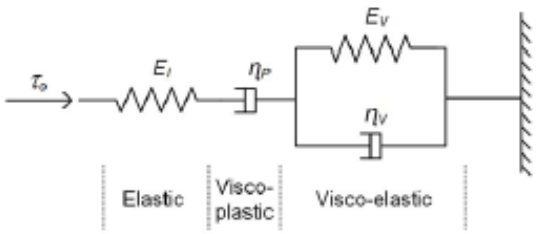

Fig. 4 Modular components of Burgers model.

After performing inverse Laplace transformation, the governing equation for the axial strain deviation for each transverse isotropic angle β can be expressed as:

$$e_1(t)=\left\{\frac{1}{E_I}+\frac{t}{\eta_P}+\frac{1}{E_V}\left[1-exp\left(\frac{-E_V t}{\eta_V}\right)\right]\right\}s_1 \qquad (6)$$

where t is elapsed time. The Burgers parameters can be determined for each transverse isotropic angle (β) and confining pressure (σ_3) by performing regression analysis on the test results shown in Fig. 3 using Statistical Package for the Social Sciences (SPSS) code (Wendai 2000). This is a non-linear regression software for determining the independent variables (E_1, E_2, η_1, η_2) using bivariate statistics based on analysis of variance (ANOVA) technique. Table 1 gives the results. Good correlations are obtained for all test conditions ($R^2 > 0.9$).

5. Calculation of apparent Burgers parameters

Deformations described by the Burgers model can be separated into three phases: instantaneous deformation, visco-elastic, and visco-plastic creep phases, which can be represented here by $1/E_I$, $(1/E_V)$ $[1- exp(-E_V/\eta_V)]$ and $1/\eta_P$, respectively. The visco-elastic term is, hereafter, represented in short by E_V^*. Elliptic equation is applied to represent the evolution of the three Burgers terms with the transverse isotropic angle β. Similar approach has been

Table 1 Burgers parameters calibrated from principal strain deviation-time curves for each specimen under $\tau_0 = 9$ MPa.

β	σ_1 (MPa)	σ_3 (MPa)	s_1 (MPa)	Burgers Parameters				
				E_I (GPa)	E_V (GPa)	η_P (GPa·Day)	η_V (GPa·Day)	R^2
0°	22	3	12.73	2.343	1.222	31.07	0.987	0.984
	25	6		2.889	1.856	42.08	0.707	0.986
	31	12		3.559	3.031	46.81	0.401	0.913
	43	24		4.041	4.466	49.12	0.364	0.923
25°	22	3	12.73	2.525	1.416	33.33	1.006	0.953
	25	6		2.987	1.961	43.27	0.713	0.947
	31	12		3.642	3.124	47.27	0.411	0.968
45°	22	3	12.73	2.642	1.575	36.55	1.108	0.971
	25	6		3.122	2.253	46.68	0.741	0.938
	31	12		3.742	3.282	50.51	0.426	0.913
65°	22	3	12.73	2.795	1.768	41.26	1.134	0.941
	25	6		3.298	2.591	49.50	0.789	0.922
	31	12		3.806	3.395	52.79	0.438	0.931
90°	22	3	12.73	3.053	2.020	44.43	1.156	0.964
	25	6		3.431	2.711	52.27	0.806	0.968
	31	12		3.922	3.544	55.93	0.445	0.928
	43	24		4.352	4.685	56.63	0.370	0.946

used by Hwu and Ting (1989) and Jiang (2016) who apply elliptic equation to describing apparent elastic moduli of anisotropic materials. The classical elliptic equation in the form of polar coordinate can be written as (Korn and Korn 1961; Polyanin and Manzhirov 2006):

$$r(\beta) = a \Big/ \left\{1 + \left[\left(\left(a^2 / b^2\right) - 1\right) \cdot cos^2\, \beta\right]\right\}^{1/2} \tag{7}$$

where r is radius of ellipse, a and b are constants along x and y axes, and β is transverse isotropic angle measured clockwise from y-axis. Here, the parameters a and b represent the intrinsic deformation terms used in the Burgers model obtained from $\beta = 90°$ and $0°$.

From Eq. (7) the Burgers parameters (E_I, η_P, E_V^*) can then be written as a function for transverse isotropic angle β in the forms of elliptic equations as:

$$E_1(\beta) = E_{1,90^\circ} / \left\{1 + \left[\left(\left(E_{1,90^\circ} / E_{1,0^\circ}\right)^2 - 1\right) \cdot \cos^2\beta\right]\right\}^{1/2} \quad (8)$$

$$\eta_P(\beta) = \eta_{P,90^\circ} / \left\{1 + \left[\left(\left(\eta_{P,90^\circ} / \eta_{P,0^\circ}\right)^2 - 1\right) \cdot \cos^2\beta\right]\right\}^{1/2} \quad (9)$$

$$E_V^*(\beta) = E_{V,90^\circ}^* / \left\{1 + \left[\left(\left(E_{V,90^\circ}^* / E_{V,0^\circ}^*\right)^2 - 1\right) \cdot \cos^2\beta\right]\right\}^{1/2} \quad (10)$$

For $\beta = 0°$ and $90°$, $E_{1,0^\circ}$ and $E_{1,90^\circ}$ are intrinsic spring constants, $\eta_{P,0^\circ}$ and $\eta_{P,90^\circ}$ are intrinsic viscosity coefficients in steady-state creep phase, and $E_V^*{}_{,0^\circ}$ and $E_V^*{}_{,90^\circ}$ are intrinsic visco-elastic terms. From elliptic equations [Eqs. (8) through (10)], E_1, η_P, E_V^* can be calculated for $0° < \beta < 90°$. The results are compared with the measurements in the forms of polar plots in Fig. 5. The diagrams show that E_1 and η_P (Figs. 5a and 5c) are greatest at $\beta = 90°$ (axial stress parallel to bedding plane) and lowest at $\beta = 0°$ (axial stress normal to bedding plane). Both parameters increase with confining pressure for all transverse isotropic angles β. The parameter E_V^* are lowest at $\beta = 90°$ and greatest at $\beta = 0°$ (Fig. 5b). They become smaller as the confining pressure increases.

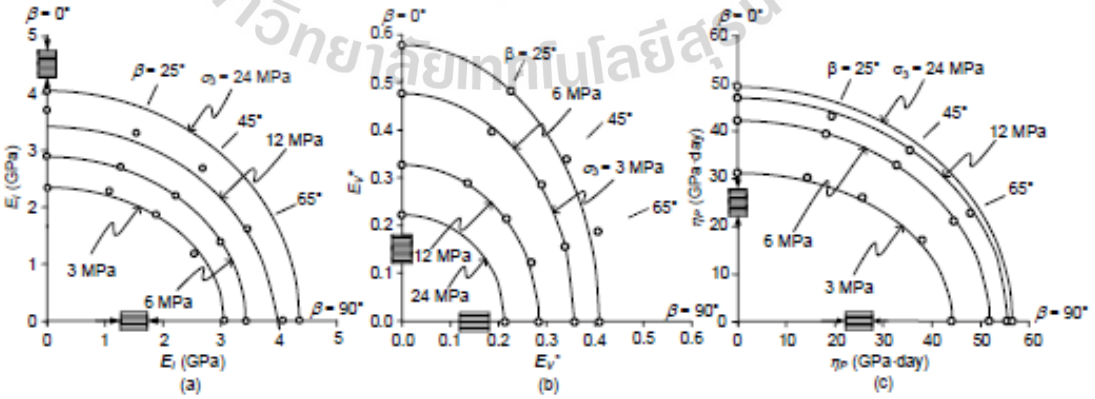

Fig. 5 Polar plots of E_1 (a), E_V^* (b) and η_P (c) and for various angles β and confining pressures (σ_3). Points are test results and lines are elliptical equation.

The discrepancies of the Burgers parameters from all angles β also getting smaller with increasing the confining pressure, suggesting that salt specimens become more isotropic under high confinements.

The agreement between the measurements and calculations by elliptic equations can be evaluated using the mean misfit (f) as an indicator. It is calculated by (Riley et al. 1998):

$$f = 1/m \sum_{i}^{m} \left[(1/n) \left(\sum_{j=1}^{n} (p_c - p_m)^2 \right) \right]^{1/2} \quad (11)$$

where p_c and p_m are calculated and measured values, n is number of bedding plane angles (β) used for each confining pressure, and m is the number of confining pressures. The mean misfits for the apparent E_I, η_P and E_V^* values are determined as 0.05 GPa, 0.84 GPa·Day and 0.02 GPa. These low values indicate good agreements between the measurements and the elliptic calculations.

6. Degree of anisotropy

The degree of anisotropy for transverse isotropic materials is commonly expressed as the maximum-to-minimum Young's modulus ratios or the strength ratios as a function of confining pressures (Fereidooni et al. 2016; Hu et al. 2017; Xu et al. 2018). An attempt is made here to reveal the anisotropy degree of the creep behaviour of bedded salt under octahedral shear stress at 9 MPa. The ratios of the maximum-to-minimum values of E_I, η_P and E_V^* obtained at $\beta = 0°$ and 90° are plotted as a function of confining pressure in Fig. 6. The diagrams suggest that the anisotropy degrees for the three creep phases rapidly decrease with increasing confining pressure. They can be best described by following power equations:

$$E_{I,90^\circ} / E_{I,0^\circ} = 1.421 \cdot \sigma_3^{-0.093} \quad (12)$$

$$\eta_{P,90^\circ} / \eta_{P,0^\circ} = 1.544 \cdot \sigma_3^{-0.099} \quad (13)$$

$$E^*_{V,0^\circ} / E^*_{V,90^\circ} = 1.678 \cdot \sigma_3^{-0.139} \quad (14)$$

The proposed equations fit well with test results ($R^2 > 0.9$). Extrapolation of these empirical equations beyond the confining pressures used here (24 MPa) suggests that at σ_3 about 35-40 MPa instantaneous and visco-elastic creep phase would become isotropic ($E_{I,90^\circ}/E_{I,0^\circ}$ and $Ev^*_{,0^\circ}/Ev^*_{,90^\circ}$ equal to 1). Beyond 80 MPa the visco-plastic creep of salt also reaches an isotropic condition ($\eta_{P,90^\circ}/\eta_{P,0^\circ} = 1$, Fig. 6). Note that the above postulation is true only if the salt is under 9 MPa octahedral shear stress. More discussions on this issue are given in section 9.

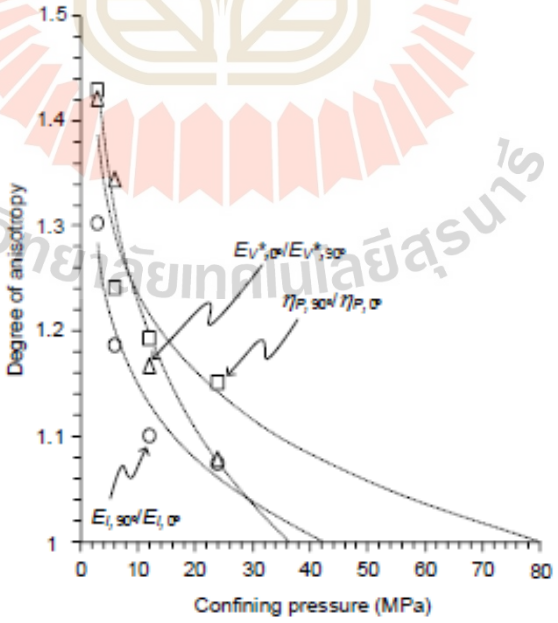

Fig. 6 Degree of anisotropy of Burgers parameters for instantaneous ($E_{I,90^\circ}/E_{I,0^\circ}$), visco-elastic ($Ev^*_{,0^\circ}/Ev^*_{,90^\circ}$), and visco-plastic ($\eta_{P,90^\circ}/\eta_{P,0^\circ}$) phases as a function of confining pressure.

7. Octahedral shear and volumetric strains relation

An attempt is made to determine the range of each phase of deformations from the triaxial creep test results. The transition strains from instantaneous to transient creep and subsequently to steady-state creep phases are difficult to determine precisely from the axial and lateral strain-time curves (Fig. 2) or from the strain deviation-time relations (Fig. 3). As a result, the octahedral shear strains (γ_o) are calculated as a function of volumetric strain (ε_v) for each salt specimen from start loading through the end of 10 days. They can be obtained as following (Jaeger et al. 2007):

$$\gamma_o = (1/3)\left[(\varepsilon_1 - \varepsilon_{3P})^2 + (\varepsilon_1 - \varepsilon_{3O})^2 + (\varepsilon_{3P} - \varepsilon_{3O})^2\right]^{1/2} \quad (15)$$

$$\varepsilon_v = \varepsilon_1 + \varepsilon_{3O} + \varepsilon_{3P} \quad (16)$$

Fig. 7 shows the results of calculations. Immediately after the axial stress is applied and maintained constant, the octahedral shear strain increases linearly with volumetric strain. This is due to the increase of axial strain which also induces a reduction of the specimen's volume. Note that the sign convention used throughout this study is that compression and contraction are positive and tension and expansion are negative. The linear relation between γ_o and ε_v represents the range of instantaneous deformation of salt where time-dependent deformation has not yet been reached. The linear relation ends at a point where γ_o continues to increase but the increasing rate of ε_v starts to decrease. An example of this transition is denoted in Fig. 7(a) as open points. As γ_o continues to increase, ε_v tends to approach a constant value. This transition is denoted in Fig. 7a as solid points. The shear strain induced between the two points represents transient creep phase where a combination of elastic and plastic creep occurs. The condition at which the octahedral shear strain increases while volumetric strain remains constant (beyond solid point in Fig. 7(a)) represents the plastic deformation of the salt in steady-state creep phase.

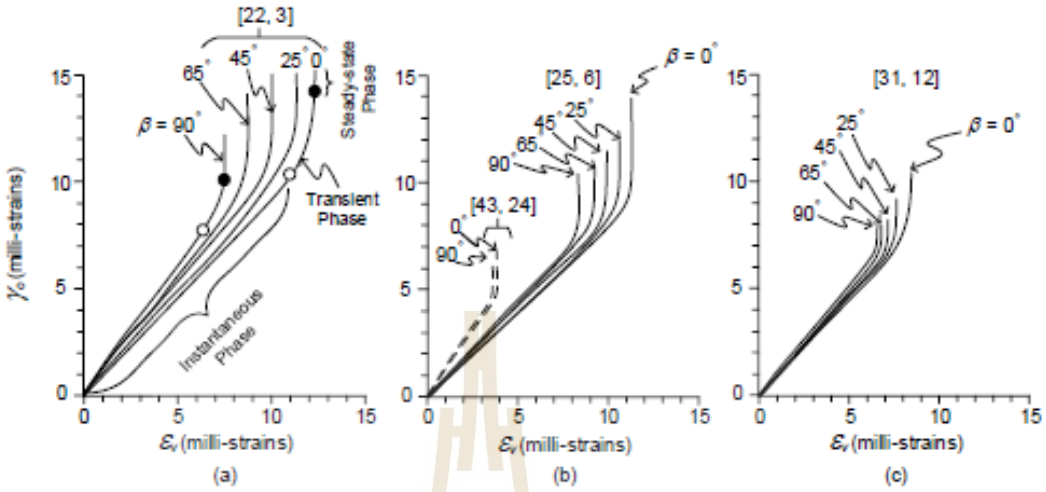

Fig. 7 Octahedral shear strains as a function of volumetric strain for confining pressures of 3 MPa (a), 6 MPa and 24 MPa (b), and 12 MPa (c). Numbers in brackets represent [σ_1, σ_3]. Open points indicate transition from instantaneous to transient phases, and solid points for transition from transient to steady-state creep phases.

Here the specimen changes shape while its volume remains constant. The γ_o -ε_v relation described above can be observed from all creep test specimens (Fig. 7). Under the same confinement, the greatest γ_o -ε_v slope in instantaneous phase is obtained from $\beta = 90°$. The slopes gradually decrease to the lowest values at $\beta = 0°$. Specimens with higher transverse isotropic angles β tend to show narrower instantaneous and transient creep phases than those with lower angle β. This means that they can reach the two transition points quicker. This behaviour can be observed for all confining pressure levels, where a higher confining pressure also results in a narrower range of transient creep phase. Diagrams suggest also that the creep test period of 10 days is sufficient to allow all specimens to reach steady-state phase. The transition points of salt deformations through different creep phases allow determining the evolution of each phase with transverse isotropic angle and confining pressure.

8. Evolution of creep phases with β and σ_3

Figure 8 shows a three-dimensional diagram of the transition points separating different phases of deformation under τ_o = 9 MPa, where γ_o at the transition points is presented as a function of angle β and σ_3. As the confining pressures increase the ranges of shear strains for the instantaneous and transient creep phases reduce. Under 24 MPa confinement, the creep strains become insensitive to the transverse isotropic (bedding plane) angle β. At this high confinement the instantaneous and transient phases become smaller, and hence the specimens reach the steady-state phase much faster, as compared to those under lower confining pressures (e.g. σ_3 = 3 or 6 MPa). Wider ranges for instantaneous and transient creep phases under low σ_3 are observed, as compared to those under high σ_3. They gradually reduce with increasing angle β.

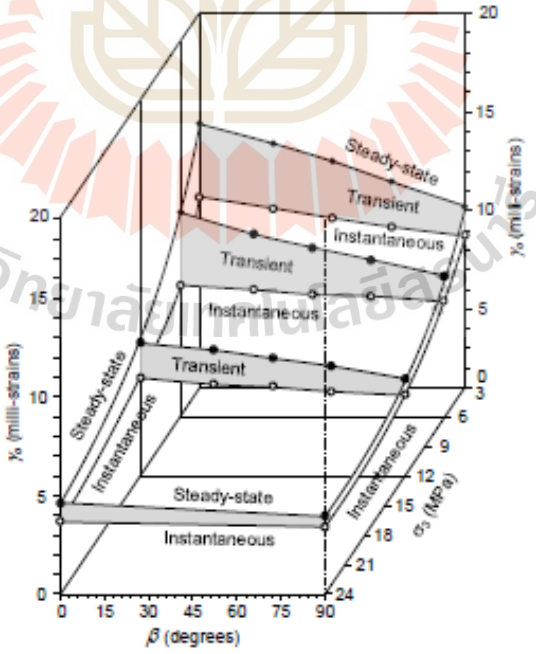

Fig. 8 Evolution of creep phases as a function of confining pressure and angle β for τ_o = 9 MPa from test results. Transient creep phases are represented by shade areas.

The range of transient creep phase in terms of octahedral shear strain can be defined by the differences of shear strains between the two transition points as follows:

$$\overline{\gamma}_o = \gamma_{o,P} - \gamma_{o,V} \tag{17}$$

where $\overline{\gamma}_o$ represents the range of transient creep strain, and $\gamma_{o,P}$ and $\gamma_{o,V}$ are creep shear strains at plastic and elastic transition points obtained from the test results, shown as examples by solid and open points in Fig. 7(a). Fig. 9 plots $\overline{\gamma}_o$ as a function of σ_3 for $\beta = 0°$ and 90°. Logarithmic equations can best describe their relationships as coefficients of correlation are greater than 0.99. Numerical values of the empirical constants are given in the figure. The diagram suggests that the range of transient creep strains for $\beta = 0°$ ($\overline{\gamma}_{o,0°}$) and $\beta = 90°$ ($\overline{\gamma}_{o,90°}$) equals to zero when the confining pressure approaches 40 MPa.

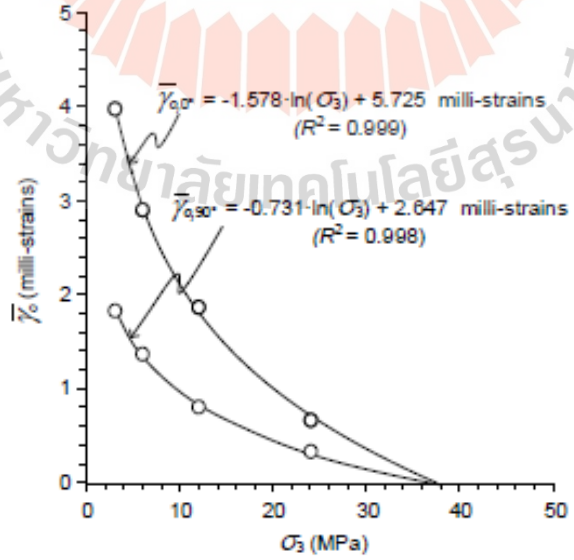

Fig. 9 Range of transient creep phase ($\overline{\gamma}_o$) as a function of σ_3 for intrinsic angles $\beta = 0°$ and 90°, under $\tau_o = 9$ MPa.

This means that under this high confinement the salt behaves as a Maxwell material where only instantaneous and steady-state creep deformations exist for all transverse isotropic angles.

9. Salt creep under various octahedral shear stresses (τ_o)

The purpose of this section is to derive governing equations for transverse isotropic creep responses under various octahedral shear stresses. From the linear visco-elastic theory (Richards 1993; Bland 2016), the octahedral shear strain (γ_o) can be presented as a function of octahedral shear stress (τ_o) for the Burgers model as:

$$\gamma_o(t) = \tau_o \left\{ 1/E_1(\beta) + t/\eta_P(\beta) + \left[(1/E_V(\beta)) \cdot \left(1 - exp\left(-E_V(\beta) \cdot t/\eta_V(\beta)\right)\right)\right]\right\} \quad (18)$$

where τ_o is constant with time and the Burger parameters are defined as a function of the transverse isotropic angle β. $E_1(\beta)$ and $\eta_P(\beta)$ can be obtained by recalling Eqs. (8) and (9). Similarly, $E_V(\beta)$ and $\eta_V(\beta)$ can be derived from the elliptic equation [Eq. (7)] as:

$$E_V(\beta) = E_{V,90^\circ} / \left\{ 1 + \left[\left(\left(E_{V,90^\circ}/E_{V,0^\circ}\right)^2 - 1 \right) \cdot cos^2\beta \right] \right\}^{1/2} \quad (19)$$

$$\eta_V(\beta) = \eta_{V,90^\circ} / \left\{ 1 + \left[\left(\left(\eta_{V,90^\circ}/\eta_{V,0^\circ}\right)^2 - 1 \right) \cdot cos^2\beta \right] \right\}^{1/2} \quad (20)$$

Burgers parameters for the intrinsic angles (β = 0° and 90°) calibrated from triaxial creep test results (Table 1) are plotted as a function of confining pressures (σ_3) in Fig. 10. The diagrams indicate that the intrinsic parameters E_1, E_V and η_P increase with σ_3, while η_V decreases as σ_3 increases. Their evolution with σ_3 can be best represented by logarithmic

equations, as shown in Fig. 10. Numerical values for their constants are given in the figure. Good correlations are obtained as indicated by $R^2 > 0.8$.

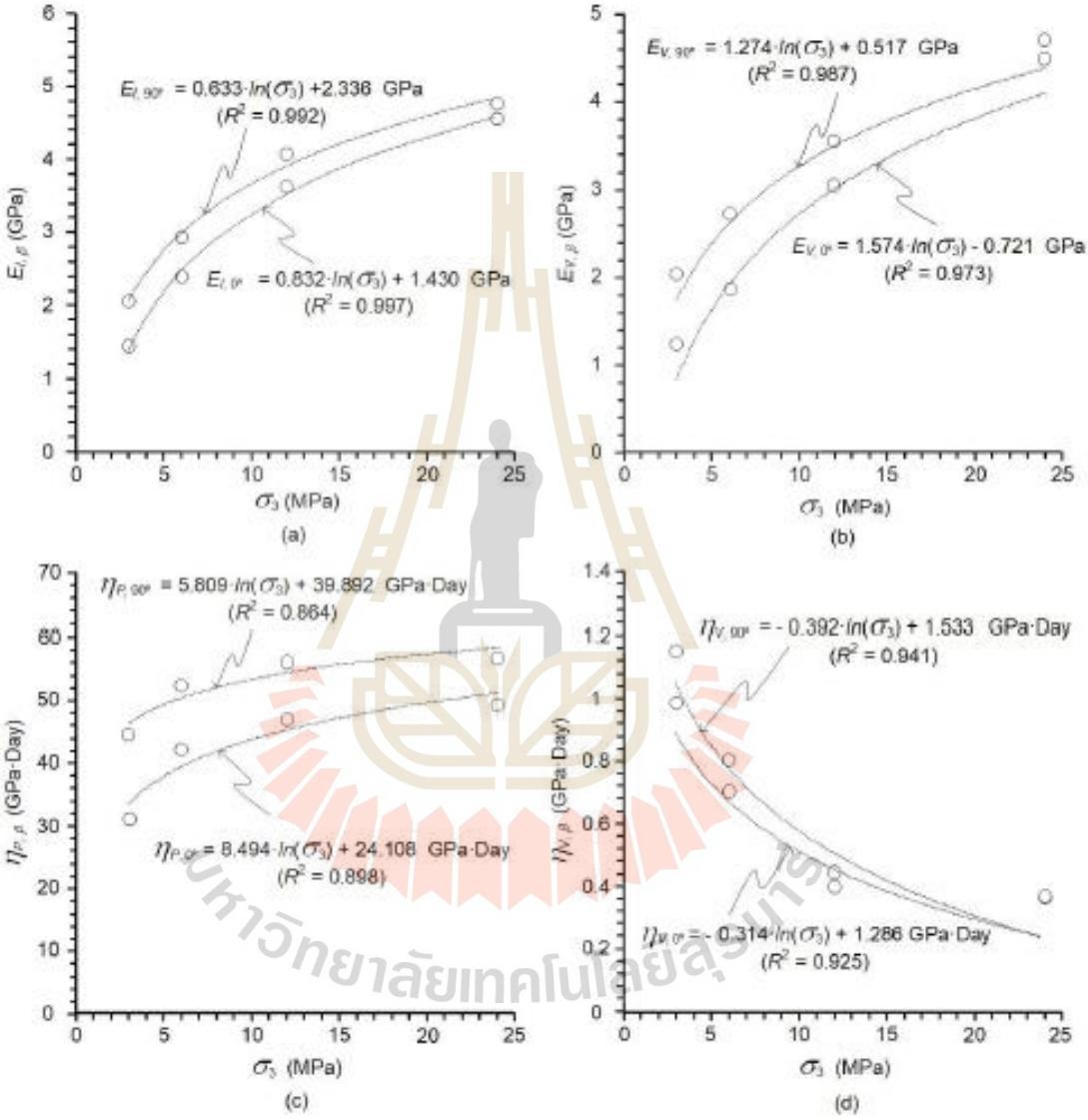

Fig. 10 Burger parameters $E_I(\beta)$ (a), $E_V(\beta)$ (b), $\eta_P(\beta)$ (c), and $\eta_V(\beta)$ (d) obtained for intrinsic angles $\beta = 0°$ and 90° as a function of confining pressure.

By substituting Eqs. (8), (9), (19) and (20) into Eq. (18), octahedral shear strains at any constant octahedral shear stress can be predicted as a function of time and transverse isotropic

angle. Examples of the predictions under confining pressures of 10 and 20 MPa are given in Fig. 11.

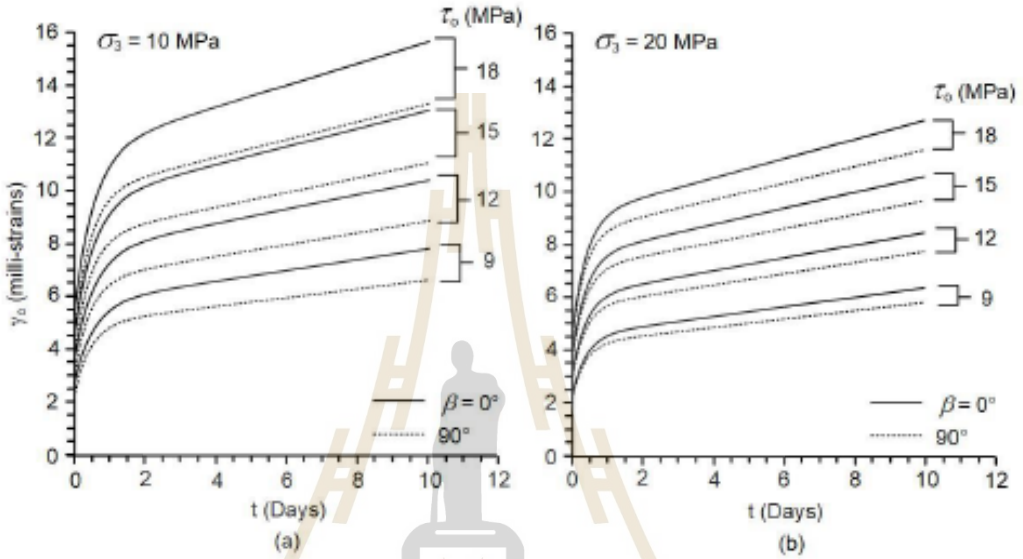

Fig. 11 Predicted octahedral shear strains – time curves under various octahedral shear stresses for σ_3 = 10 MPa (a) and 20 MPa (b).

The diagrams coincide with the test results that creep strains for $\beta = 0°$ are always greater than those under $\beta = 90°$. Their differences become larger for higher τ_o, and smaller under higher σ_3.

10. Discussions

Results from this study reveal the effects of transverse isotropy caused by bedding planes on time-dependent deformations of rock salt based on experimental and analytical investigations. Such effort has never been attempted elsewhere, in particular, on the derivation of mathematical representations to predict the salt creep as affected by bedding plane

orientations under different deviatoric and confining stresses. The same approach can be applied to salt from other source locations and other time-dependent materials posing transverse isotropic characteristics.

Larger instantaneous and creep deformations are obtained when the applied axial stress is normal to the bedding planes ($\beta = 0°$), as compared to those obtained parallel to the beds ($\beta = 90°$). This is probably caused by the alignment of inter-crystalline boundaries and the soft inclusions along bedding planes. The increases of confining pressures stiffen these soft layers and tighten the inter-crystalline boundaries, and subsequently reduce the transverse isotropic responses of the salt.

Anisotropy degrees for the instantaneous and creep deformations of Maha Sarakham salt are relatively low (less than 2;-see Fig. 6), which coincides with values for the elastic parameters and compressive strengths of the same salt experimentally obtained by Thongprapha et al. (2022). Bedded salt from other sources may however show different degrees of anisotropy depending upon their characteristics of transverse isotropic (bedding) planes.

It is recognized that the number of test specimens and test duration used here are relatively limited. Test results, nevertheless, provide sufficient and reliable trends of creep deformations under different applied stresses and bedding plane orientations (Fig. 2). All deviation strain-time curves can be well described by the Burgers model with coefficients of correlation greater than 0.9 (section 4). The apparent elastic, visco-elastic and visco-plastic deformations ($0° < \beta < 90°$) conform to the elliptic equation (Fig. 5), as indicated by their low mean misfit values. The γ_0-ε_v curves in Fig. 7 show also that all specimens reach plastic deformation in steady-state creep phase where constant ε_v is obtained while γ_0 is increasing.

Further, the γ_0-ε_v curves show the transitional shear strains from instantaneous, visco-elastic to visco-plastic creep phases more clear than do the axial and lateral strain-time curves (Fig. 2), and the strain deviation-time curves (Fig. 3). This is primarily because of the linear

relationship between γ_0 and ε_v during the elastic phase. The independency of γ_0 on ε_v during the visco-plastic phase can be easily distinguished from non-linear curves of γ_0 - ε_v during the transient creep phase. By this the transitional shear strains between them can be defined more accurately, and hence showing the evolution of each deformation phase as affected by the confining pressure σ_3 and transverse isotropic angle β.

The evolutions of transient strains with σ_3 and β allow determining the range of transient strain ($\overline{\gamma}_o$) for the two intrinsic angles ($\beta = 0°$ and 90°). They decrease logarithmically with increasing σ_3. Beyond σ_3 = 35 - 40 MPa, the transient strain no longer exists. This is however true only at τ_0 = 9 MPa.

Under the same range of confining pressures used here, and if the applied octahedral shear stress is higher than 9 MPa, there would be a wider range of shear strain values in the transient creep phase ($\overline{\gamma}_o$) under both intrinsic angles. It would also result in higher transition confining pressure at which the salt changes from a Burger to Maxwell materials. Opposite results would be obtained if τ_0 lower than 9 MPa is applied.

Even though the effect of confining pressures on the variation of transient and steady-state creep phases has long been recognized, their mathematical representation has never been developed. The decrease of $\overline{\gamma}_o$ under higher confining pressure is probably due to the predominance of dislocation glide mechanism (sliding along salt cleavages) over dislocation climb mechanism (sliding along salt crystal boundaries), as described by deformation-mechanism map developed by Senseny (1983). This enhances the visco-plastic deformation in the steady-state phase and minimizes the visco-elastic deformation in the transient phase, as shown in Fig. 8.

It is recognized that there are other factors that can affect the characteristics of transient creep strains of salt, e.g. temperature, intermediate principal stress and size of test specimens.

These factors are excluded from this study. Elevated temperatures could minimize the range of transient creep strain and enhance the steady-state strain rate, as experimentally obtained by Senseny et al. (1986), Handin et al. (1984), Moslehy and Alshibli (2023) and Dong et al. (2023). Results from series of polyaxial creep tests ($\sigma_1 \neq \sigma_2 \neq \sigma_3$) by Archeeploha et al. (2017) suggest that increasing the intermediate principal stress from $\sigma_2 = \sigma_3$ toward $\sigma_2 = \sigma_1$ notably reduces the range of transient creep strains for the Maha Sarakham salt. The transient creep strain of small specimens tends to be more sensitive to the applied stress, temperature and test duration than that of larger specimens (Senseny 1982, 1984; Linder and Brady 1984).

The Burgers creep model is used in this study because it can implicitly incorporate the effect of transverse isotropic angle β into its parameters. The analysis performed here is based on the linear visco-elastic theory from which the Burgers model has been derived. Since the applied stress-strain rate relation of salt may not be strictly linear, care should be taken when applying the results beyond the range of confining pressures from which the model parameters have been calibrated.

11. Conclusions

Experimental and analytical investigations have been performed to determine the time-dependent responses of Maha Sarakham salt as affected by varying the bedding plane orientations and confining pressures. Conclusions drawn from this study can be summarized as follows.

- Transverse isotropic creep deformations of salt due to layers of crystallization and inclusions can be clearly observed under the applied σ_3 ranging from 3 to 24 MPa with τ_0 = 9 MPa, as evidenced by the degree of anisotropy shown in Fig. 6. The salt anisotropy decreases with increasing confining pressures.

- Bedding (transverse isotropic) planes do affect the time-dependent behavior of Maha Sarakham salt. Largest instantaneous and creep deformations are obtained when the major principal stress is normal to the bedding planes ($\beta = 0°$), and the values gradually decrease to the smallest when $\beta = 90°$. Discrepancies of the deformations between the two intrinsic angles reduce as the confining pressures increase.
- Via Laplace transformation the Burgers creep model fits well to the creep test results in terms of major principal strain deviations as a function of time. Elliptic equations can describe the evolutions of the instantaneous visco-elastic and visco-plastic deformations for all apparent transverse isotropic angles ($0° < \beta < 90°$) and confining pressures.
- Anisotropy degrees for instantaneous, visco-elastic and visco-plastic deformations decrease with increasing confining pressure, where their relations can be described by power equations. Extrapolation of the equations toward higher confining pressures suggest that the instantaneous and visco-elastic responses of the salt would become isotropic at σ_3 values of 35 - 40 MPa. At σ_3 of 80 MPa and beyond the visco-plastic deformation also reaches isotropic condition.
- Octahedral shear-volumetric strain (γ_o - ε_v) curves can be used to define the transition shear strains from instantaneous, transient creep to steady-state creep phases, and hence allows determining the evolution of each deformation phase as affected by transverse isotropic angles and confining pressures.
- The ranges of transient creep strains ($\overline{\gamma}_o$) are wider under low confining pressures, as compared to those under higher confining pressures. They also become insensitive to the changes of transverse isotropic angles under high confinements.

- For both intrinsic angles ($\beta = 0°$ and 90°) $\bar{\gamma}_o$ logarithmically decrease with increasing σ_3. Under $\tau_0 = 9$ MPa they reach zero with a σ_3 value of 35 - 40 MPa, where the salt transitional changes from a Burgers to a Maxwell material, i.e. salt deforms only under instantaneous and steady-state creep phases.
- Based on the linear visco-elastic theory and the calibrated Burgers parameters under $\tau_0 = 9$ MPa with $\sigma_3 = 3$ - 24 MPa, the transverse isotropic creep of salt under different magnitudes of τ_0 and σ_3 can be calculated. This is useful for the prediction of time-dependent deformations of supported pillars and sidewalls in salt mines and around solution caverns.

Acknowledgements

This work was financially supported by Thailand Research Fund (TRF), the Thailand Science Research and Innovation (TSRI), and the National Research Council of Thailand (NRCT) through the Royal Golden Jubilee Ph. D. Program (Grant No. PHD/0215/2561)

References

Amadei, B.: Importance of anisotropy when estimating and measuring in situ stresses in rock. Int. J. Rock. Mech. Min. Sci. Geomech. Abstr. 33(3), 293- 325 (1996). https://doi.org/10.1016/0148-9062(95)00062-3

Archeeploha, S., Khamrat, S., Fuenkajorn, K.: Effects of intermediate principal stress on creep closure of storage caverns in Maha Sarakham salt. Songklanakarin J. Sci. Technol. 39(2), 143-151 (2017)

ASTM D7070-08.: Standard test methods for creep of rock core under constant stress and temperature. In Annual Book of ASTM Standards (Vol. 04.08). American Society for Testing and Materials, Philadelphia (2016)

Bland, D. R.: The Theory of Linear Viscoelasticity. Courier Dover Publications, Mineola, New York (2016)

Chan, K. S., Bodner, S. R., Fossum, A. F., Munson, D. E.: A constitutive model for inelastic flow and damage evolution in solids under triaxial compression. Mech. Mater. **14**(1), 1-14 (1992).https://doi.org/10.1016/0167-6636(92)90014-5

Chan, K. S., Brodsky, N. S., Fossum, A. F., Bodner, S. R., Munson, D. E.: Damage-induced nonassociated inelastic flow in rock salt. Int. J. Plast. **10**(6), 623-642 (1994). https://doi.org/10.1016/0749-6419(94)90026-4

Daemen, J.J.K., Fuenkajorn, K.: Design of borehole seals: process, criteria and considerations. In: Daemen, J.J.K., Fuenkajorn, K. (eds.) Sealing of boreholes and underground excavations in rock, pp. 267–279. Springer, Berlin (1996)

Dawson, P. R., Munson, D. E.: Numerical simulation of creep deformations around a room in a deep potash mine. Int. J. Rock Mech. Min. Sci. Geomech. Abstr. **20**(1), 33-42 (1983). https://doi.org/10.1016/0148-9062(83)91612-1

Dawson, P. R.: Constitutive Models Applied in the Analysis of Creep of Rock Salt (No. SAND-79-0137). Sandia Labs, United States (1979)

Dong, Z., Li, Y., Li, H., Wang, Z., Shi, X., Chen, X., Lu, Q.: Experimental study on the influence of temperature on rock salt creep. Rock Mech. Rock Eng. **56**, 3499-3518 (2023). https://doi.org/10.1007/s00603-023-03219-0

Dubey, R.K., Gairola, V.K.: Influence of structural anisotropy on creep of rock salt from Simla Himalaya, India: an experimental approach. J. Struct. Geol. **30**(6), 710–718 (2008). https://doi.org/10.1016/j.jsg.2008.01.007

Ehgartner, B. L., Sobolik, S. R.: Analysis of cavern shapes for the strategic petroleum reserve. Sandia Labs, United States (2006). https://doi.org/10.2172/888563

Fei, W., Jie, L., Quanle, Z., Cunbao, L., Jie, C., Renbo, G.: A triaxial creep model for salt rocks based on variable-order fractional derivative. Mech. Time-Depend. Mater. **25**,101-118 (2021). https://doi.org/10.1007/s11043-020-09470-0

Fereidooni, D., Khanlari, G. R., Heidari, M., Sepahigero, A. A., Kolahi-Azar, A. P.: Assessment of inherent anisotropy and confining pressure influences on mechanical behavior of anisotropic foliated rocks under triaxial compression. Rock Mech. Rock Eng. **49**, 2155-2163 (2016). https://doi.org/10.1007/s00603-015-0814-y

Findley, W. N., Lai, J. S., Onaran, K.: Creep and Relaxation of Nonlinear Viscoelastic Materials. Dover Publications, New York (1976)

Fuenkajorn, K., Sriapai, T., Samsri, P.: Effects of loading rate on strength and deformability of Maha Sarakham salt. Eng. Geol. **135–136**, 10–23 (2012). https://doi.org/10.1016/j.enggeo.2012.02.012

Gholami, R., Rasouli, V.: Mechanical and elastic properties of transversely isotropic slate. Rock Mech. Rock Eng. **47**, 1763–1773 (2014). https://doi.org/10.1007/s00603-013-0488-2

Gnirk, P. F., Johnson, R. E.: The deformational behaviour of a circular mine shaft situated in a visco-elastic medium under hydrostatic stress. In: Proceedings of the 6th Symposium on Rock Mechanics. University of Missouri, Rolla, pp.231-259 (1964)

Handin, J., Russell, J.E., Marz, D.Z.: Transient Creep of Repository Rocks. Final Report: Mechanistic Creep Laws for Rock Salts. Texas A&M Research Foundation for Office of Nuclear Waste Isolation, Battelle Memorial Institute, Columbus, Ohio (1984)

Hansen, F. D.: Reconsolidating salt: compaction, constitutive modelling, and physical processes. Int. J. Rock Mech. Min. **34**(3-4), 119.e1-119.e12 (1997). https://doi.org/10.1016/S1365-1609(97)00072-5

Hardy, H. R., Sun, X.: A nonlinear rheological model for time-dependent behavior of geologic materials. In: Proceeding of 27th US Symposium on Rock Mechanics, University of Albama, Tuscaloosa, pp. 205–212 (1986)

Holcomb, D. J., Hannum, D. W.: Consolidation of crushed-salt backfill under conditions appropriate to the WIPP facility (Report No. SAND82-0630). Sandia National Laboratories, Albuquerque, USA (1982)

Hu, S. C., Tan, Y. L., Zhou, H., Guo, W. Y., Hu, D. W., Meng, F. Z., Liu, Z. G.: Impact of bedding planes on mechanical properties of sandstone. Rock Mech. Rock Eng. **50**, 2243-2251 (2017). https://doi.org/10.1007/s00603-017-1239-6

Hunsche, U., Hampel, A.: Rock salt-the mechanical properties of the host rock material for a radioactive waste repository. J. Eng. Geol. **52**(3-4), 271-291 (1999). https://doi.org/10.1016/S0013-7952(99)00011-3

Hunter, T.O.: Technical issues of nuclear waste isolation in the Waste Isolation Pilot Plant (WIPP). SAND79-1U7C, Sandia National Laboratories. In: Proceedings of the 87th National Meeting American Institute of Chemical Engineers, Boston (1979)

Hwu, C., Ting, T. C. T.: Two-dimensional problems of the anisotropic elastic solid with an elliptic inclusion. Q. J. Mech. Appl. Math. **42**(4), 553-572 (1989). https://doi.org/10.1093/qjmam/42.4.553

Jaeger, J.C., Cook, N.G.W., Zimmerman, R.W.: Fundamentals of Rock Mechanics. Blackwell , Oxford (2007)

Jeremic, M.L.: Rock Mechanics in Salt Mining. A.A. Balkema, Netherlands (1994). https://doi.org/10.1201/9781003077589

Jiang, D.: Viscous inclusions in anisotropic materials: theoretical development and perspective applications. Tectonophysics. **693**, 116-142 (2016). https://doi.org/10.1016/j.tecto.2016.10.012

Khaledi, K., Mahmoudi, E., Datcheva, M., Schanz, T.: Stability and serviceability of underground energy storage caverns in rock salt subjected to mechanical cyclic loading. Int. J. Rock Mech. **86**, 115-131 (2016). https://doi.org/10.1016/j.ijrmms.2016.04.010

Khamrat, S., Tepnarong, P., Artkhonghan, K., Fuenkajorn, K.: Crushed salt consolidation for borehole sealing in potash mines. Geotech. Geol. Eng. **36**, 49-62 (2018). https://doi.org/10.1007/s10706-017-0301-1

Korn, G. A., Korn, T. M.: Mathematical Handbook for Scientists and Engineers. McGraw-Hill, New York (1961)

Langer, M.: Principles of geomechanical safety assessment for radioactive waste disposal in salt structures. Eng. Geol. **52**(3-4), 257-269 (1999). https://doi.org/10.1016/S0013-7952(99)00010-1

Langer, M.: The rheological behavior of rock salt. In: Hardy, H.R. J.r., Langer, M. (eds) Proceedings of the second conference on the mechanical behavior of salt, Trans Tech Publications, Clausthal, Germany, pp. 201–240 (1984)

Langer, M.: Use of solution-mined caverns in salt for oil and gas storage and toxic waste disposal in Germany. Eng. Geol. **35**(3-4), 183-190 (1993). https://doi.org/10.1016/0013-7952(93)90005-W

Lindner, E. N., Brady, B. H. G.: Memory aspects of salt creep. In: Proceedings of the first conference on the mechanics behavior of salt, Trans Tech Publications, Clausthal-Zellerfeld, pp. 241-273 (1984)

Liu, H. Z., Xie, H. Q., He, J. D., Xiao, M. L., Zhuo, L.: Nonlinear creep damage constitutive model for soft rocks. Mech. Time-Depend. Mater. **21**, 73-96 (2017). https://doi.org/10.1007/s11043-016-9319-7

Luo, G., Yang, W., Bo, C., Zhang, L., Duan, K., Jing, W., Zhao, Y.: Viscoelastic analysis of the creep characteristics of interlayered rock specimens under uniaxial compression.

Mech. Time-Depend. Mater. **25**, 37-60 (2021). https://doi.org/10.1007/s11043-019-09441-0

McLachlan, N. W.: Laplace Transforms and Their Applications to Differential Equations. Dover Publications, New York (2014)

Miller, D., Plumb, R., Boitnott, G.: Compressive strength and elastic properties of a transversely isotropic calcareous mudstone. Geophys. Prospect. **61**, 315–328 (2013). https://doi.org/10.1111/1365-2478.12031

Moslehy, A., Alshibli, K. A.: Influence of temperature and deviatoric stress on creep behavior of rock salt. In IOP Conference Series: Earth and Environmental Science, IOP Publishing, Finland. Vol. 1124, No. 1, pp. 012018 (2023). https://doi.org/10.1088/1755-1315/1124/1/012018

Motta, G. E., Pinto, C. L. L.: New constitutive equation for salt rock creep. Rev. Esc. de Minas. **67**, 397-403 (2014). https://doi.org/10.1590/0370-44672014670165

Munson, D.E.: Constitutive model of creep in rock salt applied to underground. Int. J. Rock Mech. Min. Sci. **34**(2), 233-247 (1997). https://doi.org/10.1016/S0148-9062(96)00047-2

Nair, K., Chang, C. Y., Singh, R. D., Abdullah, A. M.: Time-dependent analysis to predict closure in salt cavities. In: Proceedings of the 4th Symposium on Salt, Cleveland, Ohio, pp. 129-139 (1974)

Nasseri, M.H.B., Rao, K.S., Ramamurthy, T.: Anisotropic strength and deformational behavior of Himalayan schists. Int. J. Rock Mech. Min. Sci. **40**(1), 3–23 (2003). https://doi.org/10.1016/S1365-1609(02)00103-X

Nejati, M., Dambly, M.L.T., Saar, M.O.: A methodology to determine the elastic properties of anisotropic rocks from a single uniaxial compression test. J. Rock Mech. Geotech. Eng. **11**(6), 1166–1183 (2019). https://doi.org/10.1016/j.jrmge.2019.04.004

Nishihara, M.: Rheological properties of rocks. Doshisha Engng. Rev. **83**, 85-115 (1957)

Oksenkrug, E. S., Shafarenko, E. M.: Creep and creep strength of rock salt. Soil Mech. Found. Eng., 11(6), 387-389 (1974). https://doi.org/10.1007/BF01703810

Polyanin, A. D., Manzhirov, A. V.: Handbook of Mathematics for Engineers and Scientists. Taylor & Francis Group, New York (2006)

Reddy, J. N.: An Introduction to Continuum Mechanics. Cambridge university press, New York (2013)

Richard, J.: Plasticity and Creep Theory Example and Problems. English eds Editor. Rochester Institute of Technology, Rochester, New York (1993)

Riley, K.F., Hobson, M.P., Bence, S.J.: Mathematical Methods for Physics and Engineering. Cambridge University Press, Cambridge (1998)

Schiff, J. L.: The Laplace Transform: Theory and Applications. Springer-Verlag, New York (1999)

Senseny, P. E.: Influence of specimen size on the creep of rock salt. In: Hoftmann, P., L. (Eds.) Technology of High-Level Nuclear Waste Disposal, pp. 165-178. National Technical Information Service U. S. Department of Commerce Springfield, Virginia (1982)

Senseny, P. E.: Specimen size and history effects on creep of salt. In: Proceedings of the 1st Conference on the Mechanics Behavior of Salt, Trans Tech Publications, Clausthal-Zellerfeld, Germany. pp. 369-379 (1984).

Senseny, P.E., Hansen, F.D., Russell, J.E.: Mechanical behaviour of rock salt: phenomenology and micromechanisms. Int. J. Rock Mech. Min. Sci. Geomech. Abstr. 29, 363–378 (1992). https://doi.org/10.1016/0148-9062(92)90513-Y

Senseny, P.E., Pfeifle, T.W., Mellegard, K.D.: Exponential-time Constitutive Law for Palo Duro Unit 4 Salt from the J. Friemel No. 1 Well: Technical Report (Vol. 595). Office of Nuclear Waste Isolation, Batttelle Memorial Institute, Columbus, Ohio (1986)

Senseny, P.E.: Review of Constitutive Laws used to Describe the Creep of Salt. Office of Nuclear Waste Isolation, Batelle Memorial Institute, United States (1983)

Shen, L. J., Siritongkham, N.: The characteristics, formation and exploration progress of the potash deposits on the Khorat Plateau, Thailand and Laos, Southeast Asia. China Geol. **3**(1), 67-82 (2020). https://doi.org/10.31035/cg2020009

Sriapai, T., Walsri, C., Fuenkajorn, K.: True-triaxial compressive strength of Maha Sarakham salt. Int. J. Rock Mech. Min. Sci. **61**, 256-265 (2013). https://doi.org/10.1016/j.ijrmms.2013.03.010

Staudtmeister, K., Rokahr, R. B.: Rock mechanical design of storage caverns for natural gas in rock salt mass. Int. J. Rock Mech. Min. Sci. **34**(3-4), 300.e1-300.e13 (1997). https://doi.org/10.1016/S1365-1609(97)00199-8

Thongprapha, T., Tengpakwaen, K., Daemen, J. J. K., Fuenkajorn, K.: Effect of confining pressures on transverse isotropy of Maha Sarakham salt. Int. J. Rock Mech. Min. Sci. **152**, 105077 (2022). https://doi.org/10.1016/j.ijrmms.2022.105077

Tschoegl, N. W.: The Phenomenological Theory of Linear Viscoelastic Behavior: An Introduction. Springer-Verlag Berlin Heidelberg, New York (1989)

Wang, G.: A new constitutive creep-damage model for salt rock and its characteristics. Int. J. Rock Mech. Min. Sci. **41**, 61-67 (2004)

Wang, J. B., Liu, X. R., Guo, J. J., Huang, M.: Creep properties of salt rock and its nonlinear constitutive model. J. China Coal Soc. **39**(3), 445-451 (2014) (in Chinese)

Wang, T. T., Ma, H. L., Shi, X. L., Yang, C. H., Zhang, N., Li, J. L., Ding, S. L., Daemen, J. J. K.: Salt cavern gas storage in an ultra-deep formation in Hubei, China. Int. J. Rock Mech. Min. **102**, 57-70 (2018). https://doi.org/10.1016/j.ijrmms.2017.12.001

Wang, T., Yang, C., Ma, H., Li, Y., Shi, X.: Safety evaluation of salt cavern gas storage close to an old cavern. Int. J. Rock Mech. Min. **83**(3), 95–106 (2016). https://doi.org/10.1016/j.ijrmms.2016.01.005

Warren, J.K.: Evaporites: Their Evolution and Economics. Blackwell Science, Oxford (1999)

Wendai, L.: Regression analysis, linear regression and probit regression. In: 13 chapters Wendei, L. (eds.) SPSS for Windows: Statistical Analysis. Publishing House of Electronics, Beijing (2000)

Xu, G., He, C., Su, A., Chen, Z.: Experimental investigation of the anisotropic mechanical behavior of phyllite under triaxial compression. Int. J. Rock Mech. Min. Sci., **104**, 100-112 (2018). https://doi.org/10.1016/j.ijrmms.2018.02.017

Zhou, H. W., Wang, C. P., Mishnaevsky, L., Duan, Z. Q., Ding, J. Y.: A fractional derivative approach to full creep regions in salt rock. Mech. Time-Depend. Mater. **17**, 413-425 (2013). https://doi.org/10.1007/s11043-012-9193-x

BIOGRAPHY

Miss Kanya Kraipru was born on May 12, 1995 in Nakhon Ratchasima province, Thailand. She received her Bachelor's Degree in Engineering (Geological Engineering) from Suranaree University of Technology in 2018. For her post-graduate, she continued to study with a Doctor of Philosophy Program in the Geological Engineering Program, Institute of Engineering, Suranaree university of Technology. During graduation, 2018-2023, she was a part time worker in position of research associate at the Geomechanics Research Unit, Institute of Engineering, Suranaree University of Technology.